Investigation of fluidised bed coating: Measurement, optimisation and statistical modelling of coating layers

Dissertation zur Erlangung des Doktorgrades der Naturwissenschaften (Dr. rer. nat.)

Fakultät Naturwissenschaften
Universität Hohenheim

Institut für Lebensmittelwissenschaft und Biotechnologie
Fg. Lebensmittelverfahrenstechnik und Pulvertechnologie (150c)

vorgelegt von
Andreas van Kampen

aus *Stuttgart*

2017

Dekan:	Prof. Dr. rer. nat. Heinz Breer
1. berichtende Person:	Prof. Dr. Ing. Reinhard Kohlus
2. berichtende Person:	Prof. Dr. rer. nat. Bernd Hitzmann
Eingereicht am:	21.11.2017
Mündliche Prüfung am:	19.03.2018

Die vorliegende Arbeit wurde am 12.02.2018 von der Fakultät Naturwissenschaften der Universität Hohenheim als „Dissertation zur Erlangung des Doktorgrades der Naturwissenschaften" angenommen.

Students arrive from school confident that they know very nearly everything, and they leave years later certain that they know practically nothing. Where did the knowledge go in the meantime? Into the university, of course, where it is carefully dried and stored.

---

*Terry Pratchett (*1948 - †2015)*

Acknowledgements

This thesis was created at the *Department of Process Engineering and Food Powders* at the University of Hohenheim. I would like to express my gratitude to all the people who made the last years of work so enjoyable.

At first I would like to thank Prof. Dr.-Ing. Reinhard Kohlus for supervising this thesis and giving me the opportunity to work at his department on such an interesting topic. His advice, countless discussions and valuable insights contributed significantly to the writing of this thesis.

I would also like to thank Prof. Dr. rer. nat. Bernd Hitzmann for the second revision of this thesis.

For their good work and endless questions I would like to thank all of my students I supervised during their theses. These were: Benjamin Hartmann, Lukas Gerstweiler, Katja Zahn, Julia Zerrer, Robin Schmidt and Helena Braitmaier (Bachelor) as well as Carolin Zerweck and Heidrun Biene (Master).

My special thanks go to Peter Lang for his technical support in the pilot plant as well as Peter Sonntag who did a great job making all these modifications to the fluidised bed happen.

For good times, friendship, lots of laughs and sometimes beer I would like to thank all of my colleagues from the department: Martin Šrámek, Julia Wangler, Julia Harnacke, Annika Linke, Tobias Balke, Patrick Wilms, Nora Ruprecht, Jakob Fröhlich and Heike Teichmann as well as Peter Gschwind, Erika Denzel, Theresa Anzmann, Philipp Massar, Steffi Pavlov and Hildegard Eismann.

My parents for giving me the opportunity to go to university and their ongoing support during my studies and my PhD time.

For her love, support and just being there for me: Thank you, Franzi!

Summary

Fluidised bed coating describes a process to encapsulate particles. The coating layer is applied in order to protect the core material from chemical reactions with the environment, to control the release of drugs or to mask bad taste. Depending on the application, the coating layer must fulfil various quality requirements, such as completeness, homogeneity and minimum layer thickness.

The measurement of the coating layer thickness is therefore necessary in order to determine appropriate parameters for an optimal coating process. This, however, is difficult in the investigated core particle size range of 100 to 500 µm with a coating layer thickness of around 10 µm. Fluorescent imaging of sliced particles or imaging of optical slices using confocal laser scanning microscopy are possible ways to make the coating layer visible and to measure the coating layer thickness using image analysis techniques. This leads to detailed images of the coating layer and an accurate description of the coating layer thickness distribution, but is rather time consuming due to tedious sample preparation and long image acquisition times. Consequently only relatively few particles are measured and used to draw conclusions on the population. Other methods like measurement of the change of particle size using laser diffraction or assessment of the volume ratio of coating to core material usually only deliver the mean thickness and no information on completeness and homogeneity of the coating.

In the first part of this thesis a quick method for coating thickness measurement was developed based on a dissolution test. Sodium chloride was used as a core material and maltodextrin DE21 was used as a coating material. When dissolved in deionised water, sodium chloride raises the conductivity in contrast to maltodextrin. Therefore, the measurement of conductivity can be used to assess the dissolution curve of the core material. The coating layer delays the dissolution of the core and by comparison with the dissolution curve of pure sodium chloride the coating thickness distribution can be assessed by deconvolution.

It was shown that this method is well reproducible and delivers reliable results comparable to other methods. The method is fast, which enables the

measurement of many samples with replicates and using appropriate sample division should provide a good representation of the population. The shape of the thickness distribution allows the quantification of the three aforementioned quality parameters. The method was therefore used in the second part of this thesis in order to investigate the coating process using design of experiments.

The four factors spray rate, air temperature, air velocity and concentration of the coating solution were investigated using a central composite design of experiments. The dissolution method was used to assess the coating quality. The particle size distribution was measured in order to quantify the agglomeration rate and the mass of deposited coating material was assessed by quantifying a tracer colour in order to assess the efficiency of the process. Significant quadratic models were fitted to all response variables. These were successfully used to find a local optimum within the investigated parameter space which allowed the formation of an optimal coating layer within a short time frame.

The results of the previous investigations showed that the thickness distribution can be well described by a Weibull distribution. Furthermore, it was possible to confirm effects that were previously described in the literature, i.e. that a low concentration of the coating solution leads to more homogeneous coating layers. In order to give a general description of the coating layer, a statistical model of the coating thickness distribution was developed in the third part of this thesis and verified by a Monte-Carlo simulation.

The model reproduces the experimentally determined effect of the concentration of the coating solution qualitatively and is able to calculate the mean thickness distribution with given concentration, contact angle, sprayed mass and core particle and droplet size. Appropriate adjustments of these parameters lead to a good agreement between the model and measured thickness distributions of real experiments. It was concluded that predominant spray drying of small droplets and an increase of concentration of the remaining droplets due to pre drying negatively affects the homogeneity of the coating layer.

It was further confirmed that the Weibull distribution can be used to describe the coating layer thickness in the investigated thickness range. The

thickness distribution transitions from the Weibull distribution to a normal distribution as the coating becomes thicker. Thin coatings with defects can be described by a clinched Weibull distribution containing the uncoated area fraction as an offset.

Zusammenfassung

Das Wirbelschichtcoating ist ein Verfahren zum Umhüllen von Partikeln. Die Hüllschicht kann zum Schutz des Kernmaterials vor chemischen Reaktionen mit der Umgebung, zur Steuerung der Freisetzung von Wirkstoffen oder auch zur Geschmacksmaskierung aufgebracht werden. Abhängig vom Verwendungszweck der Hüllschicht muss diese bestimmte Qualitätskriterien wie Vollständigkeit, Gleichmäßigkeit und Mindestschichtdicke erfüllen.

Die Messung der Schichtdicke ist daher nötig, um geeignete Prozessparameter für einen optimalen Beschichtungsprozess festlegen zu können. Dies ist im untersuchten Kernpartikel Größenbereich von ca. 100 bis 500 µm mit Schichtdicken um 10 µm jedoch mit Schwierigkeiten verbunden. Fluoreszenzaufnahmen von durchschnittenen Partikeln oder die Aufnahme von optischen Schnitten mittels Konfokaler Laserscanning Mikroskopie, sind eine Möglichkeit die Hüllschicht sichtbar zu machen und mittels Bildverarbeitung zu vermessen. Dies führt zu sehr detailreichen Aufnahmen der Hüllschicht und einer genauen Beschreibung der Schichtdickenverteilung, ist jedoch durch die Probenvorbereitung und Aufnahme der optischen Schnitte sehr zeitaufwändig. Konsequenz ist die Vermessung von relativ wenigen Partikeln, anhand derer auf die Schichtdickenverteilung der Grundgesamtheit geschlossen wird. Andere Methoden wie die Messung der Partikelgrößenänderung durch Laserbeugung oder die Bestimmung des Volumenverhältnisses von Hüll- zu Kernmaterial liefern in der Regel nur mittlere Schichtdicken und keine Information über die Vollständigkeit und Gleichmäßigkeit der Schicht.

Im ersten Teil dieser Arbeit wurde daher eine Schnellmethode zur Schichtdickenmessung entwickelt, die auf einem einfach durchführbaren Auflösungstest beruht. Verwendet wurde Tafelsalz als Kernmaterial und Maltodextrin DE21 als Hüllmaterial. Tafelsalz erhöht im Gegensatz zu Maltodextrin die Leitfähigfähigkeit bei der Auflösung in entionisierten Wasser. Daher kann mit einer Leitfähigkeitsmessung die Auflösungskurve des Kernmaterials gemessen werden. Durch die Hüllschicht wird die Auflösung des Kerns verzögert und mittels Vergleich mit der Auflösungskurve von reinem Tafelsalz kann durch Rückfaltung auf die Schichtdickenverteilung geschlossen werden.

Es konnte gezeigt werden, dass die Methode gut reproduzierbar ist und im Vergleich zu anderen Methoden verlässliche Ergebnisse liefert. Die Methode ist schnell, wodurch viele Proben in Mehrfachbestimmung gemessen werden können und durch geeignete Probenteilung eine gute Übereinstimmung mit der Grundgesamtheit zu erwarten. Anhand der Form der Schichtdickenverteilung können alle drei genannten Qualitätsmerkmale quantifiziert werden. Die Methode wurde daher im zweiten Teil der Arbeit verwendet, um den Beschichtungsprozess mittels statistischer Versuchsplanung näher zu untersuchen.

Die vier Faktoren Sprührate, Lufttemperatur, Luftgeschwindigkeit und Konzentration der Sprühlösung wurden in einem Zentral Zusammengesetzen Versuchsplan untersucht. Die Auflösungsmethode wurde verwendet, um die Qualität der Schicht zu beurteilen. Die Partikelgrößenverteilung wurde gemessen, um den agglomerierten Anteil zu bestimmen, und die Masse des aufgesprühten Hüllmaterials wurde photometrisch mittels Farbstoff quantifiziert, um die Effizienz des Prozesses zu beurteilen. Für alle Antwortvariablen konnten signifikante quadratische Modelle angepasst werden. Diese konnten erfolgreich verwendet werden, um ein lokales Optimum im untersuchten Parameterraum zu bestimmen, dass es erlaubt in kurzer Zeit eine optimale Hüllschicht zu erzeugen.

Die Ergebnisse aus den vorherigen Untersuchungen zeigten, dass die Schichtdicke im untersuchten Bereich gut mit einer Weibull-Verteilung beschrieben werden kann. Des Weiteren konnten Effekte bestätigt werden, die bereits vorher in der Literatur beschrieben wurden, z.B. dass eine geringe Sprühlösungskonzentration zu gleichmäßigeren Schichten führt. Um die Schichtdicke allgemein zu beschreiben, wurde im dritten Teil der Arbeit ein statistisches Modell der Schichtdickenverteilung entwickelt und durch eine Monte-Carlo Simulation verifiziert.

Das Modell gibt den experimentell ermittelten Effekt der Sprühlösungskonzentration qualitativ wieder und kann direkt die mittlere Schichtdickenverteilung bei gegebener Konzentration, Kontaktwinkel, Aufsprühmenge sowie Kernpartikel- und Tropfengröße berechnen. Durch geeignete Anpassung der Parameter war das Modell in der Lage, gemessene Schichtdickenverteilungen realer Experimente zu beschreiben. Daraus konnte geschlossen werden, dass die bevorzugte Sprühtrocknung kleiner Tropfen und Konzentrationserhöhung

durch Vortrocknung der verbliebenen Tropfen die Gleichmäßigkeit der Hüllschicht negativ beeinflusst.

Es wurde zudem bestätigt, dass die Weibull-Verteilung die Schichtdicke im untersuchten Bereich gut beschreibt. Bei dicken Schichten geht die Weibull-Verteilung in eine Normalverteilung über. Bei dünnen Schichten mit freibleibenden Oberflächenanteilen wird die Schichtdicke gut durch eine gestauchte Weibull-Verteilung mit dem freien Oberflächenanteil als Offset beschrieben.

Contents

1 Introduction and outline

The term "coating" in general refers to the application of a thin film onto a surface. In the pharmaceutical and food industries the term refers specifically to an encapsulation process, where a continuous film is formed around a particle or tablet. This is typically done to enhance the properties of the particles or to provide an additional functionality to the product in question.

This introduction gives an overview over the equipment used in general to apply coatings to tablets or particles and describes fluid beds in more detail since this was the technology used throughout this thesis. The description of coating quality and methods to measure it will be part of the third introductory section.

1.1 Equipment for coating of particles and tablets

A classical method to apply a coating to a tablet is sugar-coating, where the coating material is a highly concentrated sugar syrup. The process consists of alternated pouring of the syrup and powder, usually icing sugar or starch, into a rotating drum which contains the tablets. The water is subsequently evaporated by heat. The mixing is assisted either by the operator who uses a scraper to mix the tablets or by baffles inside the drum. This process is repeated up to 30 times until the weight of the tablets consists of 30 to 50 % coating (Bauer-Brandl and Ritschel 2012).

An example of such a coating drum or pan is shown in figure 1.1. In this type hot air is sucked through the perforated cone and the tablets, which also removes dust formed by attrition. Dust would otherwise lead to a bumpy surface structure (Bauer-Brandl and Ritschel 2012). For a better distribution

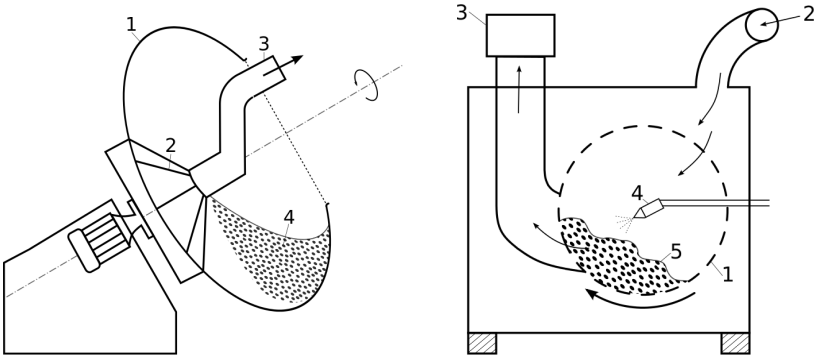

Figure 1.1: *left:* Coating pan for sugar-coating: 1. coating pan; 2. perforated cone; 3. exhaust pipe; 4. tablet bed *right:* Drum coater: 1. perforated drum; 2. conditioned inlet air; 3. filter and exhaust air; 4. two fluid nozzle; 5. tablet bed (adapted from Bauer-Brandl and Ritschel 2012)

of the coating liquid it is sometimes sprayed onto the tablets in the drum. Spraying of the coating liquid is also done in drum coaters (fig. 1.1). The tablets are placed inside a horizontally aligned perforated drum and the coating solution is sprayed by one or more nozzles onto the tablets. The drum rotates and mixing is often promoted by baffles inside the drum. Hot air is guided through the perforated drum and dries the tablets.

In pan-coaters and horizontal coating drums, agitation and mixing of the cores is realised by rotation of the drum. In fluidised beds, there are usually no rotating parts involved. Mixing is achieved by an air stream which enters the unit in the bottom and leaves it at the top, usually through filters or cyclones for fines removal. The air holds the particles in a fluidised state and simultaneously delivers the energy needed to dry the wetted particles. Typical fluidised beds are shown in figure 1.2.

Fluidised beds are distinguished by the position of the spray nozzle. In a conventional top-spray fluidised bed (fig. 1.2a) the nozzle is located in the upper part of the unit. The particles move in random trajectories and the coating solution is sprayed in a countercurrent way onto the particles. The particles are wetted in the spray zone and enter the expansion chamber and

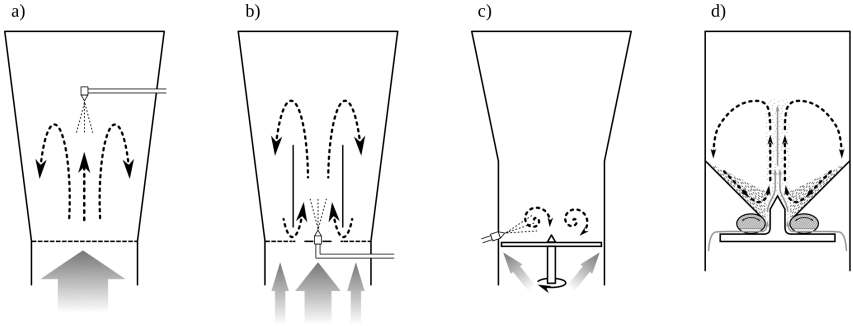

Figure 1.2: Types of fluid beds: a) top-spray; b) bottom-spray/Wurster; c) tangential-spray/rotary fluid bed; d) spouted-bed (Glatt GmbH, Germany). Solid and dotted arrows show air flow and particle trajectories (adapted from Teunou and Poncelet 2002; Dewettinck and Huyghebaert 1999; Peglow et al. 2011).

fall back down again during which drying of the particles occurs. This cycle continues in a random fashion (Dewettinck and Huyghebaert 1999).

The most common variation is the bottom-spray type. Here, the coating solution is sprayed from the bottom. A draft tube, also called Wurster tube after its inventor (Wurster and Lindlof 1966), is placed at some distance from the bottom plate centered on top of the nozzle (fig. 1.2b). The bottom plate is designed in a way, that 80 % of the air flow enters the unit at the central part below the draft tube. This sucks the particles from the outer ring into the draft tube where they are accelerated. Wetting occurs during the upward movement. The particles leave the Wurster tube at the top, enter the expansion chamber and fall down at the sides. This results in a well defined cycle time for all particles. The small distance between nozzle and particles also minimises the occurence of overspray. However, Wesdyk, Joshi, De Vincentis, et al. (1993) reported a particle size dependant film thickness which they did not observe in other fluidised bed configurations.

The tangential-spray, also called rotating or tumbling, fluidised bed (fig. 1.2c) uses a rotating disk at the bottom to accelerate the particles towards the wall of the chamber. Fluidising gas, which enters through the gap between the

disk and the chamber wall, accelerates the particles upwards. The particles eventually enter the expansion chamber and fall down at the center. The trajectory can be described as a helical path (Dewettinck and Huyghebaert 1999). The nozzle is placed at the side of the chamber and sprays the coating liquid tangentially into the particle bed.

A different approach to fluidisation is carried out in the spouted-bed type unit (fig. 1.2d). Instead of using a bottom plate, the air enters the unit through two gaps between a central profile and two cylinders placed left and right of it. These cylinders are rotatable to adjust the air velocity. In this way, very high velocities are created at the air inlet and the particles are accelerated to an upward movement in a column. As the airflow gets evened out with height, the particles eventually fall down at the sides of the unit and continue a cycle. Spraying can be realised from the top or the bottom with the bottom-spray type being more frequently used. The advantage of this type of fluidised bed is the possibility to process difficult materials, like very fine or very large particles (Geldart groups C and D, see section 1.2.1) or materials with a very broad particle size distribution (Peglow et al. 2011).

1.2 Fluid bed coating

All experimental work in this thesis was carried out in a WS-CT-L top-spray fluidised bed coater (Allgaier Process Technology GmbH, Germany). Although the Wurster type is generally considered the best equipment for coating of particles (Werner et al. 2007; Teunou and Poncelet 2002) the top-spray configuration is considered to be the better choice for most food applications due to its high versatility, relatively large batch size and relative simplicity (Dewettinck and Huyghebaert 1999).

Figure 1.3 shows the P&ID diagram of the pilot plant. The air entering the unit is divided into two streams, one of which is heated. The hot and cold air streams are mixed using two valves (K201) to regulate the temperature inside the chamber (TIC203). The coating solution is delivered to the two-fluid nozzle by means of a peristaltic pump using a mass flow controller.

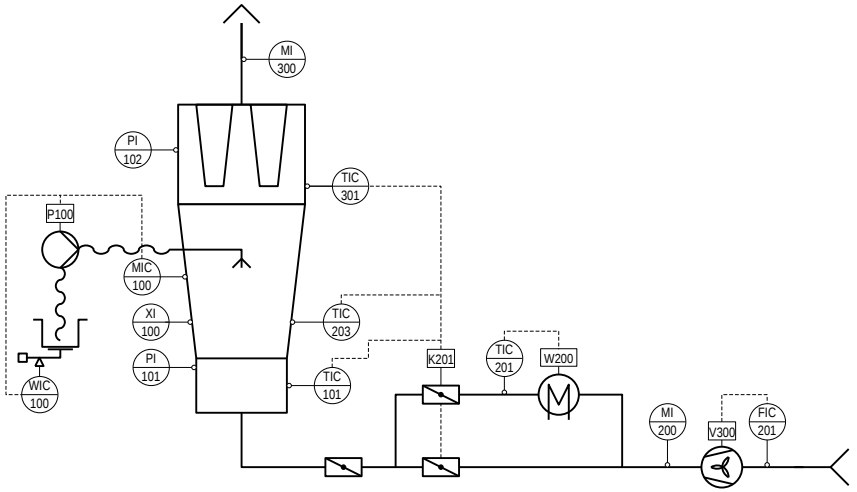

Figure 1.3: P&ID diagram of the WS-CT-L top-spray fluidised bed coater (Allgaier Process Technology GmbH, Germany) used throughout this thesis.

1.2.1 Fluidisation

An air stream that flows through a fixed particle bed experiences a pressure drop Δp proportional to the superficial gas velocity. The point of incipient fluidisation is reached when the drag force exerted on a particle is equal to its weight. The velocity at which this transition happens is called minimal fluidisation velocity u_{mf}. It is dependant on the solid and gas densities, ρ_{s} and ρ_{f} respectively, the gas' dynamic or kinematic viscosity, μ_{f} or ν_{f}, the particle diameter d and the bed porosity at minimal fluidisation $\varepsilon_{\mathrm{mf}}$.

The minimal fluidisation velocity can be predicted using the Carman-Kozeny equation 1.1 under the assumption of a laminar flow with $Re < 1$, which corresponds to particles smaller than 500 µm in diameter (Smith 2007).

$$u_{\mathrm{mf}} = \frac{\varepsilon_{\mathrm{mf}}^3(\rho_{\mathrm{s}} - \rho_{\mathrm{f}})gd^2}{180(1-\varepsilon_{\mathrm{mf}})\mu_{\mathrm{f}}} \tag{1.1}$$

For particles greater than 500 µm Ergun's equation 1.2 provides a better estimation of u_{mf} (Smith 2007; Uhlemann and Mörl 2000).

$$u_{\mathrm{mf}} = 42.9(1-\varepsilon_{\mathrm{mf}})\frac{\nu_{\mathrm{f}}}{d}\left[\sqrt{1+3.11\cdot 10^{-4}\frac{\varepsilon_{\mathrm{mf}}^3(\rho_{\mathrm{s}}-\rho_{\mathrm{f}})gd^3}{(1-\varepsilon_{\mathrm{mf}})^2\rho_{\mathrm{f}}\nu_{\mathrm{f}}^2}}-1\right] \tag{1.2}$$

It is customary to characterise the fluidisation state in dependence of the superficial gas velocity u by the fluidisation number f and the excess gas velocity u_{e} (Uhlemann and Mörl 2000).

$$f = \frac{u}{u_{\mathrm{mf}}} \tag{1.3}$$

$$u_e = u - u_{\mathrm{mf}} \tag{1.4}$$

Depending on the size and density of the particles, Geldart (1973) defined four groups of fluidisation behaviour (fig. 1.4):

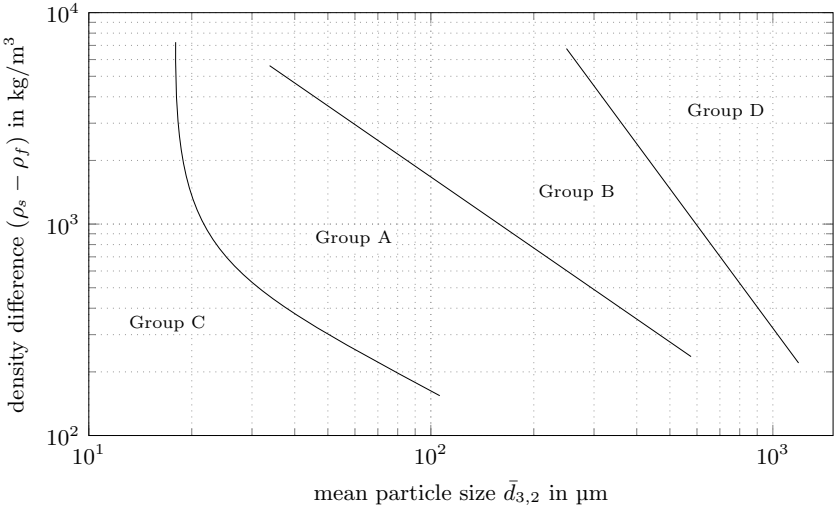

Figure 1.4: Geldart's classification of fluidisation behaviour (after Geldart 1973).

Group A (aeratable): Powders in this group are typically in the size range of 20 to 100 µm with a density less than 1400 kg m^{-3}. Beds of this kind expand considerably before any bubbles form and collapse slowly when the velocity decreases.

Group B (sand-like): Powders of this type have a diameter between 40 and 500 µm with a density between 1400 and 4000 kg m^{-3}. Bubbles already form at velocities slightly greater than the minimal fluidisation velocity and introduce a considerable amount of solids mixing into the bed.

Group C (cohesive): This group is characterised by very fine particles with a diameter below 30 µm. Powders of this kind are difficult to fluidise and tend to rise as a plug or form rat-holes. This behaviour is caused by inter particle forces which are greater than the hydrodynamic force which is exerted on the particles by the fluidising gas. Consequently particle mixing and heat transfer is much poorer than for powders of group A and B.

Group D (spoutable): Particles with a diameter larger than 600 µm and a density greater than 4000 kg m^{-3} form this group. These particles experience little bed expansion and gas bubbles grow fast in the horizontal direction. This results in poor solids mixing.

For fluidised bed coating the powders usually belong to groups A or B (Teunou and Poncelet 2002; B. Guignon et al. 2002). Larger particles of group D can be coated in spouted beds (Smith 2007; Peglow et al. 2011).

1.2.2 Growth regimes

Spraying dissolved binder material onto fluidised particles results in growth by either layering or agglomeration, depending on the process parameters and material properties. The standard growth model (Smith 2007) sees the spray as discrete droplets which come in contact with the primary particles in the bed. They can wet the surface of the particles and are dried subsequently to form a small layer of the binder material. Repeating this process of wetting and drying results finally in a layered growth of the particles, here described

as coating. When wetted particles come in contact with another particle before the surface is dried, these particles may stick together with the binder solution forming a liquid bridge which is subsequently solidified. In this way agglomeration of particles occurs. Agglomeration can also be achieved by spraying water onto amorphous water-soluble powders. Here, the water acts as a plasticiser and the particles stick to each other due to a reduced surface viscosity (Palzer 2009).

The main growth regime is controlled by the drying rate and humidity inside the bed. A high drying rate and low humidity promotes particle growth by layering. A low drying rate and consequently a high humidity promotes agglomeration of particles. In this way the growth regime can be controlled by the temperature of the fluidising gas and the concentration and spray rate of the binder solution.

According to Link and Schlünder (1997) "dry" process conditions are favourable for coating of particles. Unfortunately, this also promotes side effect spray drying, also known as overspray (Ronsse et al. 2008). This occurs mainly at high drying rates and describes the process of droplets being dried before actually wetting a particle. These particles may stay in the bed or are recirculated to form new primary particles. In coating processes these very fine dust particles are usually elutriated from the bed and thus decrease the process efficiency. At low drying rates, on the other hand, there is the risk of over wetting the particle bed. This often results in bed collapse, also called wet-quenching or flooding, which usually means the loss of the production batch.

The process window for successful operation is thus determined by material properties, process variables and the construction of the fluid bed apparatus. There have been various approaches to calculate a characteristic number describing the growth regime, which should also be scalable. One approach is the patented flux number concept from Akkermans et al. (1998). The flux number FN (eqn. 1.5) depends on the particle density ρ_p, the excess gas velocity u_e and the binder mass flow rate $\dot{q}_\mathrm{mliq}$ through the bed contact area, which itself depends on the nozzle to bed distance and the cone angle of the spray.

$$\mathrm{FN} = \log_{10}\left[\frac{\rho_\mathrm{p} u_\mathrm{e}}{\dot{q}_\mathrm{mliq}}\right] \tag{1.5}$$

According to the patent, the flux number has to be higher than 2 for most of the process time. Below that value, there is a high risk of flooding. They give a preferable maximum value of 4.5, above which the process will take too long and become economically unviable. The flux number can also be used to distinguish the growth regimes. FN < 3.5 indicates the agglomeration regime, FN > 3.5 indicates the coating regime (Boerefijn and Hounslow 2005).

Hede et al. (2008) tested this approach for the scale-up of a coating process with sodium sulfate cores. They found an overall agreement in terms of rising flux numbers decrease agglomeration tendency but, in contrast to the patent description, observed bed collapse in all cases were FN < 4.5. This illustrates the difficulty of finding a single parameter which contains all relevant parameters for successful scale-up.

1.2.3 Process control

The development of a fluid bed process is still a task which is mainly solved by trial and error approaches. Changes of the raw materials or climate changes of the inlet air, also called weather effects, often result in a reduced product quality, sometimes even in bed collapse and loss of the production batch. An a priori prediction and adjustment of the process parameters in these cases is rarely possible.

The reason for this is the highly complex nature of the process. Fluidised bed coating involves three major operations: Fluidisation, atomisation and drying (Maa et al. 1996). According to Knezevic et al. (1998) there are as many as 20 different variables involved in the process. These variables can be subdivided into system design variables, process variables, coating material properties and particle properties (Werner et al. 2007).

System design variables include the dimensions of the fluid bed chamber, bottom plate design, wall angle in conical fluidised beds, size of the expansion chamber and the design and placement of the spray nozzle (Uhlemann and Mörl 2000; Dewettinck and Huyghebaert 1999; B. Guignon et al. 2002; Teunou and Poncelet 2002; Werner et al. 2007). These variables are usually

set with any given fluidised bed unit and can not be changed easily. Since there is no general agreement on how to design a fluid bed vessel, scale-up and reproducibility across different plants is an issue (Hede et al. 2008).

Drying air temperature, gas velocity, batch-size, spray rate and atomizing conditions are process variables. These variables can be changed by the operator and optimal settings are usually determined by experimental design (for example van Kampen and Kohlus 2017; Dewettinck and Huyghebaert 1998; B. Guignon et al. 2002). Dewettinck and Huyghebaert (1998) found that changing the atomizing pressure of a two fluid nozzle not only influences the droplet size and speed, but also has a thermodynamic effect on the process which consequently influences coating efficiency. This is just one example for the inter dependency of process variables in fluid bed coating. Currently there is no model which can predict the process sufficiently and allows the extrapolation to different particles or coating formulations (B. Guignon et al. 2002).

The particle size and shape mainly influences the fluidisation behaviour (see section 1.2.1). More importantly, the wetting properties depend on the type of particles and the properties of the sprayed liquid. The binding and adhesive forces depend on the liquid surface tension and the liquid-solid contact angle. Saleh and P. Guignon (2007) found a linear relationship between the liquid-solid contact angle and coating efficiency, where an increasing contact angle led to a lower coating efficiency. Contact angles $>90°$ drastically reduced the coating efficiency due to rebound phenomena.

There have been various efforts to find control strategies for fluid bed coating and agglomeration. Watano (1995) successfully used an IR-moisture sensor to measure the granule moisture content. He used an on-off-controller and a fuzzy-logic controller to control the surface moisture content of particles by switching the spray on or off in an agitated fluidized bed. This strategy lead to reproducible granulation under varying conditions, such as temperature and humidity changes of the inlet air. Prata et al. (2012) monitored the pressure drop over the bed to successfully determine the onset of agglomeration. This enabled them to prevent batch losses and allowed for a better coating quality. In continuous operations, granule size oscillation can be an issue. This unsteady operation of the plant leads to an oscillation of the product

mass flow which in turn poses the risk of overloading or totally emptying the fluidised bed. Bück et al. (2016) successfully used model predictive control to stabilise the steady state operating point.

1.2.4 Applications of fluid bed coating

The formation of a coating layer around a particle results in a reservoir type encapsulation of the core. Aims are the increase of shelf life, masking bad flavours or odours and improvement of handling, appearance or colour. Modified release of the core during subsequent processing or consumption is another goal (Teunou and Poncelet 2002; Smith 2007; B. Guignon et al. 2002; Dewettinck and Huyghebaert 1998; Pothakamury and Barbosa-Cánovas 1995).

Solvent based coating materials are mainly natural or synthetic film forming polymers like starches, gums, maltodextrins, gelatin and polyvinyl acetate. Waxes, fatty acids, hydrogenated vegetable oils and emulsifiers are applied as hot-melt coatings (Gibbs et al. 1999; Pothakamury and Barbosa-Cánovas 1995; Dewettinck, Messens, et al. 1999).

The release of the encapsulated material can be triggered by a change in pH, Temperature, melting of the coating or through the addition of water (Pothakamury and Barbosa-Cánovas 1995). Fluidised bed coated particles can be used to separate iron from ascorbic acid in multivitamins. Sodium bicarbonate in dough leaveners, citric acid, lactic acid and salt added to pretzels and meat are other examples of encapsulated food ingredients (Gibbs et al. 1999; Pothakamury and Barbosa-Cánovas 1995).

1.3 Coating quality

According to the quality management norm DIN EN ISO 9000:2015-11, the term *quality* is defined as the "Degree to which a set of inherent characteristics fulfills requirements". A coating layer on a particle or tablet may have various requirements depending on the application of the final product. An effective encapsulation to prevent oxidation of the encapsulate or to provide a taste masking would need a complete coating layer of a certain minimum thickness. When a barrier for a controlled or delayed release application has to be formed,

the thickness needs to be well defined and homogeneous around the single particle or tablet since the release of the encapsulate would be influenced by local fluctuations of the layer thickness. A colouring application would have no special requirements other than meeting the intended intensity of the colour which should be homogeneously distributed throughout the powder batch. The same holds when the primary particles are solely used as a carrier for a drug or food ingredient which otherwise could not be blended easily into a final product.

This, not necessarily comprehensive, list gives hint on the various properties a coating layer has. The coating thickness can be described as a distributed property with a mean coating thickness and a spread, which can be regarded as a measure for the homogeneity of the coating. Both can be defined for the inter- and intra-particle coating thickness distribution respectively.

1.3.1 Parameters of a coating thickness distribution

The previous section mentioned three parameters describing a coating thickness distribution: *Completeness*, *thickness* and *homogeneity*. The *completeness* of a coating is a measure for the amount of covered surface area of the primary particles. It can be expressed as the area fraction of uncoated surface divided by the total surface area.

$$\text{Completeness} = 1 - \frac{A_{\text{uncoated}}}{A_{\text{total}}} \tag{1.6}$$

The *thickness* of a coating describes the distance between the surface of the primary particle and the surface of the coating layer. Ideally, one could measure this distance anywhere in a given particle and the measured value would always be the same. In reality, however, this distance is not always the same, so the *thickness* usually refers to the mean distance. A way to estimate the mean thickness is by considering the primary particle as a sphere with the coating layer being a concentric sphere shell around it.

$$\text{Thickness} = \frac{D_{\text{sphere}}}{2}\left(\sqrt[3]{1 + \frac{V_{\text{coating}}}{V_{\text{sphere}}}} - 1\right) \tag{1.7}$$

The *homogeneity* of a coating describes the spread of the thickness distribution. This can be calculated as the standard deviation but more often the coefficient of variation (CoV) is used.

$$\text{Homogeneity}_1 = \text{CoV} = \frac{\text{standard deviation of thickness}}{\text{Thickness}} \tag{1.8}$$

This definition provides a measure of the relative width of the thickness distribution. A similar definition is the SPAN of the distribution using the 10, 50 and 90 % quantile of the distribution.

$$\text{Homogeneity}_2 = \text{SPAN} = \frac{T_{90} - T_{10}}{T_{50}} \tag{1.9}$$

A homogeneous coating layer would have a low thickness variation in it and hence a small CoV or SPAN. A high CoV or SPAN is indicative of an inhomogeneous coating layer with a large variation of the thickness.

The coating thickness distribution can be defined in two ways. The *intra* particle coating thickness distribution describes the variation of the coating thickness within a single particle. The *inter* particle coating thickness distribution usually refers to the variation of either the mean coating thickness or coating mass within the population of particles. The coating thickness distribution of the population will be a mean distribution built from these two parts.

The intra particle coating thickness distribution depends mainly on the drying conditions, wetting properties of the film and droplet size and number. The inter particle variability on the other hand depends mainly on the mixing time in the fluidised bed and the residence time of the particles in the spray zone. According to Mörl et al. (2007), the weight gain of the particles is size dependant. Large particles will collect more droplets from the spray than small particles. The mean thickness, however, would not be particle size dependant, since the increased mass will be spread out over a larger surface area. Thus, a large inter particle coating thickness variability would be indicative of a process with poor mixing properties or a wide residence time distribution of the particles in the spray zone.

1.3.2 Coating defects

Defects within a coating layer include fissures or cracks, irregularities and uncoated parts of the surface. These errors can have various sources, that can be mainly attributed to the used process parameters, but can also be caused by the properties of the coating material or the cores (Bauer-Brandl and Ritschel 2012).

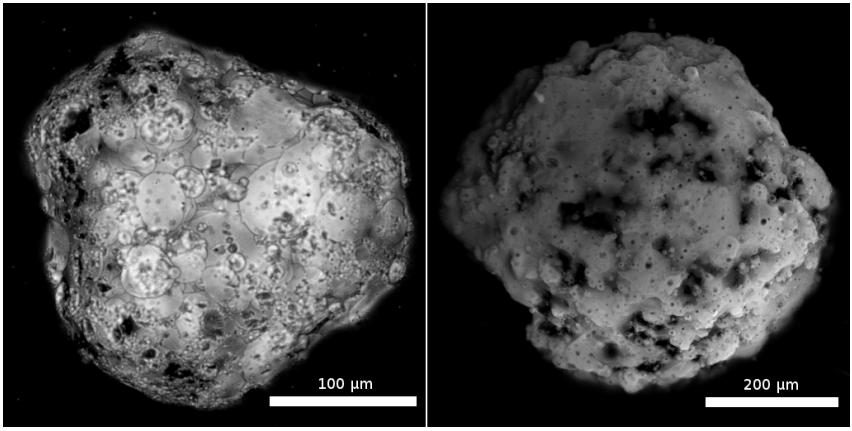

Figure 1.5: Confocal laser scanning micrographs of coated particles. *left:* Particle with uncoated areas and visible droplet structures on the surface. *right:* Particle with a very uneaven coating layer.

Holes in the coating layer will decrease its ability to protect the core material, so have to be avoided for most applications. Reasons for uncoated surface area parts include poor wetting properties of the coating solution, but also a high viscosity of the solution will decrease its ability to spread over the surface. Inefficient mixing in the coater may additionally prevent some parts of the surface to be exposed to the spray. Poor wetting and spreading are also the cause for inhomogeneous coatings with a wide thickness distribution.

For applications where the diffusion of substances through the coating layer have to be controlled, this is also undesirable. For instance Capece and Dave (2011) used fluid bed coating to encapsulate catalysts in a porous membrane

where the homogeneity and completeness of the coating was of crucial importance.

When the coating layer is stained with a fluorescent dye, the coating layer can be made visible in great detail with a confocal laser scanning microscope. Figure 1.5 shows two images of particles where some parts of the surface remained uncoated. The right particle in figure 1.5 additionally shows a very inhomogeneous coating layer, which would have very undefined diffusion properties.

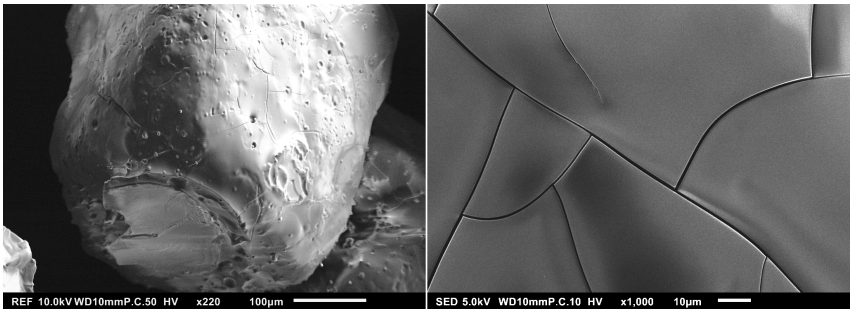

Figure 1.6: Scanning electron micrograph of coated particles. *left:* Particle with a chunk of coating layer from another particle adhered to it. *right:* Scanning electron micrograph of the surface of a coated particle which has developed cracks over the storage time.

Agglomeration that takes place during the coating operation is usually regarded as undesirable (Dewettinck, Deroo, et al. 1998; Prata et al. 2012). Besides the risk of bed collapse due to excessive agglomeration the functionality of the coating may be influenced in a negative way. Additionally, when an agglomerate breaks into its primary particles, a chunk of coating may stick to one of the particles leaving exposed surface area on the other particle. This can be seen on the left side in figure 1.6, where a chunk of coating adheres to the coating layer.

The right image in figure 1.6 shows cracks in the otherwise very smooth coating layer of another particle. These can be caused by tension due to different expansion and contraction of the core and coating material when the temperature is changed. This happens either during the process when

the material is cooled rapidly or during storage under varying temperature conditions.

1.3.3 Measurement of coating quality

There have been various reports on measuring coating thickness distributions. Depending on the size of the primary particles or tablets and the thickness, this is a task which can be difficult to achieve.

Ways to directly measure the thickness include the determination of weight gain of the primary particles, for instance by randomly taking a number of tablets and weighing them (i.e. Joglekar et al. 2007; Abe et al. 1998). The difference to the mean weight of the uncoated tablets corresponds to the coating material and the mean thickness can be calculated using equation 1.7. This method works reliably, but has practical limitations as the particles become smaller. A way to overcome these limitations is the use of other means of quantification, for instance chemical analysis of the coating material. A relatively easy way for experimental purposes is the addition of a tracer colour to the coating material and subsequent photometric quantification. Using this principal, the mean thickness of the coating layer can be relatively easily assessed. Another possibility to assess the mean thickness is by measuring the particle size distribution. Half the difference of the volume weight mean diameter before and after coating corresponds to the mean layer thickness. This straight forward technique, however, suffers from a large error. Since the absolute accuracy of laser diffraction measurement devices is around 2 % (Witt et al. 2012), the accumulated error of the difference of two measurements can be as high as 40 % depending on the size range and mean coating thickness.

The assessment of the homogeneity was previously done using the weighing technique (Abe et al. 1998). This method, however, is only capable of determining the inter particle homogeneity, which is mainly an indication for the mixing quality of the process. In order to obtain information on the layer structure and thus its ability to provide the intended function, the intra particle homogeneity is of importance. So far, this can only be determined by microscopic means.

Si-Nang et al. (1973) investigated the diffusion of eprazinone encapsulated in a gelatin and gum arabic shell. For direct measurement of the layer thickness, they sliced the microcapsules with a microtome and measured the layer thickness in various locations using a microscope. This gave a good indication of the mean thickness, but they also showed that slicing anywhere else than in the equatorial plane of the microcapsules results in an apparently larger measured thickness due to geometrical distortion.

Wesdyk, Joshi, Jain, et al. (1990) used scanning electron microscopy on sliced coated particles to measure the film thickness in three defined positions in triplicate. They reported a standard deviation of $\pm 2\,\mu m$ using this method. Although they seemingly interpreted this value as a quantification of the measurement error of the method, this should rather be treated as a measure of the intra particle homogeneity of the layer.

Fluorescence microscopy was used by Andersson, Holmquist, et al. (2000) to take images of sliced coated particles. They used an image analysis technique to measure the thickness distribution using three definitions of layer thickness. The first definition was the local minimum distance between the core and coating layer surface respectively. The second definition was to measure the distance perpendicular to the cores surface and the third definition was the measurement of the chord lengths originating in the center of gravity of the pellets. They observed that the different definitions of layer thickness did not influence the thickness distribution by a huge amount and concluded that the minimum distance approach would be the most useful because this would dominate the release rate.

Since slicing the particles is a tedious process and always poses the risk of distorting the results by damaging the coating layer, ways to asses images of the coating layer in a non invasive manner have been used more recently. One of which is confocal laser scanning microscopy, which was used (i.e. Laksmana et al. 2009; Depypere et al. 2009) to create volumetric images of coated particles, without the necessity of slicing the particles. Depth information was obtained by the laser penetrating into the translucent coating layer and core particle. With this method, the geometrical distortion reported by Si-Nang et al. (1973) is also apparent. Measurement has to be done in the equato-

rial plane or, using all of the 3d information, perpendicular to the surface. Otherwise the coating thickness would be overestimated.

More recently, micro-computed X-ray tomography has been used as a high end tool for particle and granule analysis. Perfetti et al. (2010) were one of the first to demonstrate the high potential of this method to characterise coating layers. However, like all of the microscopic methods, this has the disadvantage of being a very slow technique. Sample preparation and image acquisition can be very tedious and time consuming. And despite the high level of detail one can obtain, the statistical information on the population of particles is to be seen critically as only a few single particles can be examined. The resolution of typically between 1 and 2 µm additionally poses an issue for the measurement of thin coating layers. Ways to speed up the analysis include the work from Sondej et al. (2015), who took single images with the X-ray machine, which greatly reduces acquisition time. They showed, that the resulting thickness distributions agreed well with distributions obtained from full 3d images. However, the applicability to non spherical particles is to be questioned.

In addition to the aforementioned methods, there have been also efforts made to measure the coating thickness in-line, that should be mentioned here. Near infrared reflectance spectroscopy (NIR) has been used for instance by Kirsch and Drennen (1996) (at-line) and Andersson, Josefson, et al. (1999) (in-line). The former study calibrated the amount of material added in the process while the latter study used microscopic measured thickness data for their model. While there have been efforts to improve on the time required for calibration (i.e. Möltgen et al. 2013; Andersson, Folestad, et al. 2000) the necessity for application specific calibration remains and the quality of the model highly depends on the reference method.

Terahertz pulsed imaging (TPI) was presented by May et al. (2011) as a direct method to measure coatings on tablets in the range of 40 to 1000 µm. While this is not suitable for thin coatings on particles, this method is able to provide inter and intra tablet thickness distributions in-line. Additionally the acquisition times are rather long and the resolution is limited. Optical coherence tomography (OCT) can overcome this limitation providing a resolution of 10 µm (Markl, Hannesschläger, et al. 2014; Markl, Zettl, et al. 2015). This

method was shown to provide inter and intra tablet thickness distributions for coating layers >10 µm.

1.3.4 Dissolution of coated particles

Another approach to determine the quality of a coating is the conduction of a dissolution test. This method is used for quality assurance testing of pharmaceutical tablets after production. The liberation of the drug is measured over time under well defined conditions and, depending on the type of tablet, the liberated drug amount is measured at one or more points in time. The

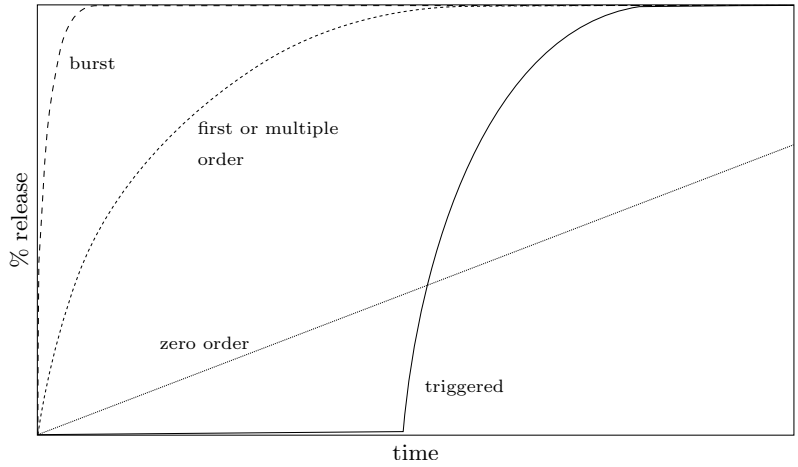

Figure 1.7: Release profiles from encapsulates (Adapted from Zhang et al. 2010).

judgement on the quality of such a tablet and therefore the coating layer in case of modified release tablets is based on predetermined criteria regarding the liberated drug amount at each measured point in time.

The form of the curve is indicative of the release type like burst or triggered release or zero, first or mutliple order release kinetics (fig. 1.7, Zhang et al. 2010). There are a variety of reaction kinetic type models which are used to describe the measured dissolution curves, but their use is limited to find-

ing reaction kinetic type constants (Bauer-Brandl and Ritschel 2012). This consequently results in the dissolution test being only suitable to determine whether the requirements on the encapsulate are met or not. Since the profile of such release curves is a direct consequence of the structure of the coating layer, one objective of this thesis was to find a way to extract this information from measured dissolution curves.

Noyes and Whitney (1897) showed that the dissolution of substances in their own solution can be described by

$$R = k(C_\mathrm{s} - C) \ , \tag{1.10}$$

where R is the rate of dissolution, C_s is the solubility of the substance, C the concentration and k is a constant. k includes the diffusion coefficient D, the thickness of the diffusion layer L and the surface area A of the solid. With the mass transfer coefficient $\beta = \frac{D}{L}$ and the test volume V, eq. 1.10 can be written as

$$\frac{dC}{dt}V = \beta A(C_\mathrm{s} - C) \ . \tag{1.11}$$

The area A may be constant throughout the dissolution process, for instance when a plate on the bottom of a cup is gradually dissolved, or it may change, which is the case for particles that shrink during dissolution. The latter case can be modelled using a shrinking sphere approach, where the particle surface area becomes smaller as the dissolution progresses (Haverkamp and Welch 1998). The surface area A at time t can be expressed using the initial area A_0 and mass M_0 of the particle.

$$A = A_0 \left(\frac{M}{M_0}\right)^{2/3} \tag{1.12}$$

Here, M is the remaining mass of the particle at time t, which can be expressed using the concentration C and the volume V of the test solution.

$$M = M_0 - CV \tag{1.13}$$

Combining equations 1.12 and 1.13 and inserting in 1.11 yields

$$\frac{dC}{dt}V = \beta A_0 \left(1 - \frac{CV}{M_0}\right)^{2/3} (C_\mathrm{s} - C) \ , \tag{1.14}$$

which can be used to model the dissolution of particles assuming a particle size independent mass transfer coefficient (Haverkamp and Welch 1998).

When a particle collective is dissolved, the concentration over time can be described by the sum of the dissolution curves of the individual particles in the case of small concentrations compared to the saturation concentration C_s. In the case of coated particles which dissolve like the triggered release type (see fig. 1.7) this principal would also apply. Different coating layer thicknesses would have different lag-times before the core dissolves. Any measured dissolution curve C of a coated sample would therefore be the sum of all responses from each thickness fraction, which can be described as the convolution of the coating layer thickness distribution x with the dissolution of an uncoated core C_{unc}.

$$C(t) = \int_0^t x(\tau) \cdot C_{\mathrm{unc}}(t - \tau)\, d\tau \tag{1.15}$$

In order to restore the coating layer thickness distribution, the dissolution curves of the coated sample and the uncoated core have to be measured. Deconvolution will then yield the coating layer thickness distribution. The development and validation of this method is subject of the first publication in section 2 of this thesis.

1.4 Thesis outline

The aim of this thesis was to gain a better understanding on the formation of coating layers in spray coating applications. This is necessary in order to improve or tailor the coating quality to meet specific requirements. Especially in food applications the profit margins are rather low so a cost effective implementation of a coating process is desirable.

The first publication *Assessment of coating quality by use of dissolution kinetics* was about the development of a bulk dissolution test and subsequent data analysis in order to measure coating thickness distributions. This technique allows us to measure coated powder samples very efficiently in a very short time – minutes instead of hours compared to microscopic methods.

Using this method, a statistical design of experiments was conducted to assess a response surface model of a top spray coating process in a pilot plant scale fluidised bed dryer. The results were published in the second article *Systematic process optimisation of fluid bed coating*. It shows the effectiveness and reliability of the dissolution method for this application. The effects of fluidisation air flow rate, spray rate, concentration of the coating solution and bed temperature on the resulting coating quality were successfully identified. Furthermore it was possible to calculate optimal process settings within the investigated design space which allowed the production of a good quality coating within a restricted time frame.

During the work on the first publication it was found, that the measured coating layer thickness was best described by a Weibull distribution. This lead to the work on the third publication *Statistical modelling of coating layer thickness distributions: Influence of overspray on coating quality*. In this contribution the formation of coating layers were simulated on the droplet level including the wetting properties, represented by the solid-liquid contact angle. Based on this simulation a statistical model was developed, which allows the direct calculation of coating thickness distributions based on the contact angle and concentration of the coating liquid, the droplet and particle size as well as the total mass ratio of coating material to the primary particles. It was found, that the coating thickness is Weibull distributed in the case of thin coating layers. The distribution evolves then rapidly into a normal distribution when the coating becomes thicker. Compared to measured coating thickness distributions, a deviation was observed, which was linked to a quality reducing effect of premature droplet drying. Taking various factors into account, the model was able to describe the measured coating thickness distribution.

2 Assessment of coating quality by use of dissolution kinetics

By Andreas van Kampen, Bernd Hitzmann and Reinhard Kohlus.
Published 2015 in *Powder Technology*, Volume 286, Pages 325–331.
Accessible under DOI: 10.1016/j.powtec.2015.08.024

Abstract

Fluid bed coating of powder is widely applied in the industry. Analysis of the production batch in terms of coating thickness and its distribution within the population cannot be performed easily. Microscopic analysis to accurately measure the shell thickness of a particle lacks the ability to give statistical information of the population within a reasonable amount of time. In this work, a novel method based on measuring the effect of the coating and solving the involved inverse problem is proposed as a fast way to measure the shell thickness distribution in the sample. The method was tested with sodium chloride particles coated with varying amounts of maltodextrin. It could be shown that coating thickness distributions between 0.2 and 20 µm can be measured with significant differences between samples.

2.1 Introduction

Encapsulation of drugs and ingredients is widely applied in the pharmaceutical and food industry in order to provide additional functionality (controlled or delayed release), protect ingredients from the environment (oxygen, other

ingredients) or to alter surface properties (flowability, colour) (B. Guignon et al. 2002).

In general, encapsulates can be divided into the reservoir and the matrix type. Where as in the matrix type capsules, the active ingredient is dispersed more or less uniformly in the encapsulation agent, the reservoir type consists of an active core, the reservoir, and a shell around it (Zuidam and Shimoni 2010). The article focuses in the following on the reservoir type or shell coating encapsulates.

The morphological requirements on these coatings depend on the application. An effective taste masking needs a complete layer of coating with a certain minimum thickness, where as a coating for a controlled release application needs a layer with a well defined thickness and/or porosity. Therefore different measures of quality can be defined for coated particles - a non comprehensive list is given below.

- mean coating thickness
- distribution of thickness on a single particle
- distribution of thickness over the whole population
- porous or non-porous
- degree of surface coverage

Some of those parameters can be assessed with ease. For instance the deposited mass of coating material can be used to determine the mean theoretical coating thickness s_{th} using the following equation.

$$s_{\mathrm{th}} = \frac{d}{2} \cdot \left[\left(1 + \frac{\rho_{\mathrm{core}} \cdot m_{\mathrm{coating}}}{\rho_{\mathrm{coating}} \cdot m_{\mathrm{core}}} \right)^{1/3} - 1 \right] \tag{2.1}$$

Here it is implied that a perfect sphere of core material with mass m_{core} and density ρ_{core} is covered with a homogeneous layer of coat with mass m_{coating} and density ρ_{coating}. The diameter of the core material d is a mean particle diameter representing the population of the particles. Accounting for the fact, that the equation basically calculates the thickness from the known volumes of

the core and coating, the mean diameter used should be the volume weighed mean diameter $\bar{d}_{4,3}$.

Other parameters are harder to assess. For instance the porosity of the shell could be measured by means of a diffusion test. Optical methods like the confocal laser scanning microscopy or micro-computed X-ray tomography are capable of producing optical slices through the particles. The thickness as well as the porosity of the shell can then be measured by image analysis techniques, as several authors reported previously (Depypere et al. 2009; Laksmana et al. 2009).

However, these methods are rather time consuming, and especially the microscopic methods are only capable to give information about single particles. Measuring enough particles to obtain statistical information about the population like the distribution of the shell thickness within the powder batch would take an unreasonable amount of time.

This article proposes a method to determine the shell thickness distribution based on the measurement of the effect of the coating, in this case the delayed dissolution of the core, accompanied by the solution of the inverse problem incorporated in the interpretation of the obtained data.

The method described in this investigation was tailored for the analysis of shell coatings produced using fluidised bed coating. Encapsulates of this type could also be formed by methods like electrostatic atomisation which can specifically form porous coatings (Nangrejo et al. 2008), coacervation, co-extrusion or by preparation of emulsions with multilayers (Zuidam and Shimoni 2010).

The studied size range was core particles with a diameter of about 400 µm and a thin coating layer of up to 10 µm thickness.

2.2 Theoretical considerations and description of the method

To address the complexity of the problem, the method proposed is based on four assumptions:

1. the population consists only of perfectly coated particles following equation 2.1, porosities within the coating layer are neglected, since they are not expected in the used model system
2. the dissolution curve of a perfectly coated particle is the same as for an uncoated particle, except for a time shift τ, which is the time needed to dissolve the shell
3. the dissolution velocity of the shell is constant, so $\tau \propto s$
4. the dissolution curve of the population is the sum of the dissolution curves of all thickness fractions

The population of coated particles consists of fractions with varying shell thickness each having a different value for the time shift τ. This results in a time shift distribution which can be expressed as a probability density function $x(t)$ in s^{-1}. The dissolution curve $c(t)$ for the coated material is then given by the convolution (indicated by the convolution operator $*$) of the dissolution curve $c_0(t)$ of the uncoated material with $x(t)$:

$$c(t) = c_0(t) * x(t) \tag{2.2}$$

This can also be written as the convolution integral:

$$c(t) = \int_0^t x(\tau) \cdot c_0(t - \tau)\, d\tau \tag{2.3}$$

The time shift distribution can thus be found by deconvolution. The dissolution curves are measured in discrete time intervals,

$$\Delta t = \frac{t_{\max}}{n} \quad , n \in \mathbb{N} \tag{2.4}$$

which leads to discretised time points:

$$t_i = \tau_i = i \cdot \Delta t \quad , i = 0, 1, \ldots, n-1, n \tag{2.5}$$

Thus the probability density function $x(t)$ is discretised as

$$x_i = x \cdot \Delta t \tag{2.6}$$

which leads to the discretised form of equation 2.3:

$$c(t) = \sum_{i=0}^{n} x_i \cdot c_0(t - \tau_i) \tag{2.7}$$

The above equation implies the following system of linear equations which can be solved for all x_i.

$$\begin{pmatrix} c(t_0) \\ c(t_1) \\ \vdots \\ c(t_n) \end{pmatrix} = \begin{pmatrix} c_0(t_0 - \tau_0) & \cdots & c_0(t_0 - \tau_n) \\ c_0(t_1 - \tau_0) & \cdots & c_0(t_1 - t_n) \\ \vdots & \ddots & \vdots \\ c_0(t_n - \tau_0) & \cdots & c_0(t_n - \tau_n) \end{pmatrix} \cdot \begin{pmatrix} x_0 \\ x_1 \\ \vdots \\ x_n \end{pmatrix} \tag{2.8}$$

Since the concentration at time t_0 is $c_0(0) = c(0) = 0$ the first row in the system above reduces to $0 = 0$. Therefore the system lacks one equation to be fully solvable. To account for this problem, the additional condition

$$\sum_{i=0}^{n} x_i = 1 \tag{2.9}$$

is introduced, which gives the missing equation. This condition makes sense, because x represents the mass fractions of coated material with different τ. The final form of the linear system, with the first row changed to the new normalising condition, then reads as follows:

$$\begin{pmatrix} 1 \\ c(t_1) \\ \vdots \\ c(t_n) \end{pmatrix} = \begin{pmatrix} 1 & \cdots & 1 \\ c_0(t_1 - \tau_0) & \cdots & c_0(t_1 - t_n) \\ \vdots & \ddots & \vdots \\ c_0(t_n - \tau_0) & \cdots & c_0(t_n - \tau_n) \end{pmatrix} \cdot \begin{pmatrix} x_0 \\ x_1 \\ \vdots \\ x_n \end{pmatrix} \tag{2.10}$$

Due to numerical instabilities of the system and the reasonable condition that all x_i should be either positive or zero, a non-negative least squares smoothing is used to solve the linear system (Lawson and Hanson 1974).

As already mentioned above, the solution of the linear system gives a time shift distribution. In order to obtain a thickness distribution, the x-axis has to be transformed from a time-axis into a thickness-axis. The condition for

that is point three in the list above. The dissolution velocity v_d is found by taking the mass balance into account. The total mass of coating deposited on the surface of the particles is divided between all time-delay fractions under the assumption of a constant dissolution velocity.

2.3 Materials and Methods

2.3.1 Materials

Table salt from the local grocery store („Gut & Günstig"-brand, EDEKA AG & Co. KG, Germany) was sieved to a fraction between 355 and 450 µm and used as core material during the coating operation. A solution of 20 % w/w maltodextrin with 21 dextrose equivalents (MD21, Roquette Frères, France) and 0.2 % w/w Ponceau 4R (Lay Gewürze OHG, Germany) in purified water was prepared and used as a coating agent. All materials used were of food grade quality.

2.3.2 Software

Unless noted otherwise, all data operations were performed using Matlab v. R2014b (The MathWorks, Inc., USA). Some of the image processing steps were performed using ImageJ (v. 1.49g, Abràmoff et al. 2004). Data logging was performed using LabView (National Instruments Corporation, USA).

2.3.3 Coating operation

The coating operation was performed in a WS-CT-L top-spray fluidized bed dryer (Allgaier Process Technology GmbH, Germany) equipped with a model 970 two-fluid nozzle (Düsen-Schlick GmbH, Germany) with a nozzle orifice diameter of 0.5 mm. The atomizing air pressure was set to 1 bar. The air distribution plate had a diameter of 100 mm.

1200 g of table salt was loaded to the device and fluidized at a volumetric air flow rate of 85 $m^3\,h^{-1}$. The inlet air temperature was maintained at 60 °C. After a bed temperature of 40 °C was reached, the coating agent was sprayed at a spray rate of 7.5 $g\,min^{-1}$. The process was interrupted four times to

remove 100 g of sample after 300, 275, 250 and 225 g of coating agent was sprayed. The material removed was not replaced, which could have had an impact on the process efficiency. This resulted in a theoretical loading of dry coating material of 5, 10, 15 and 20 % w/w on the core particles, without considering any losses due to overspray and/or attrition.

The operating conditions were chosen by the experimenters experience and were not further optimised. No aggregates were formed during the coating operation which was verified by particle size analysis.

2.3.4 Measurement of coating thickness

The measurement of the coating thickness was performed using two techniques:

1. image analysis of confocal laser scanning microscopic images
2. newly developed dissolution test as described in section 2.2

2.3.4.1 Confocal laser scanning microscopy

Image acquisition Four single particles from each sample were imaged using a Nikon C1 confocal laser scanning microscope (Nikon GmbH, Germany) equipped with a x20 PlanFluor objective and 543 nm excitation laser. The particles were placed on a cover slip suspended in immersion oil ($n = 1.543$). A z-stack was acquired. The x-y-resolution was set to 512 by 512 pixels with a 1 µm step size in z-direction. These settings resulted in an approximate voxel size of 1 μm^3.

Image enhancement Since the azo dye used gave a rather intense response to the excitation, the resulting image was blurred. In order to enhance the contrast between coated regions and non-coated regions as well as the background, a deconvolution filter was applied to the image stack. For this purpose the ImageJ plugin "PSF Generator" (Kirshner et al. 2013) was used to obtain a theoretical point spread function using the Born & Wolf model. The deconvolution filter was applied using the "Parallel Iterative Deconvolution 3D" plugin for ImageJ. The Wiener Filter Preconditioned Landweber algorithm

was used with the boundary condition set to zero, the other parameters were set to the default values.

Image analysis procedure The enhanced image stack was turned to a binary image stack by setting a threshold value which separated the coating layer from the background. A Matlab script was written to measure the thickness of the layer in three dimensional space. Three adjacent vectors were traced from the inside of the particle until an inner boundary point was detected. The normal vector $\vec{NV}$ of the plane spanned on those three points ($\vec{P_1}$, $\vec{P_2}$ and $\vec{P_3}$) was calculated using the cross-product (Equation 2.11).

$$\vec{NV} = (\vec{P_2} - \vec{P_1}) \times (\vec{P_3} - \vec{P_1}) \tag{2.11}$$

Then the thickness of the coating in this area was measured as the chord length from the inner to the outer boundary along the calculated normal vector.

The thickness was measured in 10000 random directions from which the thickness distribution on the single particle was calculated. The median of the thickness distribution was taken as the mean shell thickness s_{ia} for comparison with the other methods.

2.3.4.2 Dissolution test

Measurement The dissolution of the core particles (sodium chloride) was measured as the rise in conductivity. 400 g of purified water (weighed to 0.05 g precision) were prepared in a 600 ml beaker with a diameter of 85 mm. The water was stirred at 700 min^{-1} using an over head stirrer with a dissolver plate geometry (40 mm diameter) placed at a height of 30 mm above the bottom of the beaker.

The conductivity was measured with a conductivity meter WTW LF530 (WTW GmbH, Germany). An online photometer AvaSpec-ULS2048 (Avantes BV, Netherlands) equipped with a transmission dip probe (20 mm optical path length) was used to measure the absorption at 510 nm as well as the transmission of light. The sample rate was 10 Hz.

The data logging was started and after a few seconds, 4 g of sample material (weighed to 0.1 mg precision) were poured at once into the beaker. The first

significant transmission drop was used to trigger the starting point of the dissolution curve. The measurement was repeated three times for all samples.

Data smoothing In order to stabilize the solution algorithm the dissolution curves were first smoothed using a median filter with a window size of 40 samples, which successfully removed any outliers within the time series. Afterwards a mean filter (window size = 3) was applied. The filter replaces the value of a data point by the mean of its two neighbours when its own value is not between the values of its neighbours. This accounts for the fact, that the dissolution curve should rise monotonic.

Solving the inverse problem After the data was smoothed, the system of linear equations (equation 2.10) was built and solved using the in-built Matlab command `lsqnonneg()`, which solves non-negative least-squares constraints problems.

Determination of the amount of coat applied to the core The amount of coating material deposited on the core particles was measured using the absorption of Ponceau 4R, which was added to the coating agent as a tracer. A previously measured calibration curve ($R^2 = 0.999$, data not shown) was used to calculate the concentration of Ponceau 4R at the end of the measurement. Under the assumption that the colourant was distributed homogenously within the maltodextrin, the amount of coating added to the core particles was calculated as:

$$m_{\text{coating}} = 100 \frac{\text{g}_{\text{MD21}}}{\text{g}_{\text{E124}}} \cdot 400\,\text{g}_{\text{H}_2\text{O}} \cdot \frac{\text{Abs}_{510\,\text{nm}} + 0.0037}{72728 \frac{\text{g}_{\text{H}_2\text{O}}}{\text{g}_{\text{E124}}}} \tag{2.12}$$

Calculate thickness distribution The solution of the inverse problem yields a time delay distribution, as previously stated in chapter 2.2. Since it was assumed that the dissolution velocity v_d was constant, the thickness s can be calculated simply as follows.

$$s = t \cdot v_d \tag{2.13}$$

The unknown dissolution velocity was found using an iterative divide and conquer algorithm which searches for a value of v_d that satisfies the mass

balance, meaning that the whole amount of coating m_{coating} was distributed on the mass fractions.

Goodness of fit In order to determine the goodness of fit, the root mean square error (equation 2.14) was calculated between the measured dissolution curve c_{m} and the forward calculated dissolution curve c_{c}, which used the calculated thickness distribution, described in the next section.

$$\text{RMSE} = \sqrt{\frac{\sum_{i=1}^{n}(c_{\text{m},i} - c_{\text{c},i})^2}{n}} \tag{2.14}$$

2.3.5 Distribution fit

The obtained thickness distributions were found to be represented quite well by the Weibull distribution with shape parameter a and scale parameter b, together with an offset which represents the uncoated fraction X_{uncoated}.

$$F(x) = X_{\text{uncoated}} + (1 - X_{\text{uncoated}}) \cdot (1 - \exp(-\left(\frac{x}{b}\right)^{a})) \tag{2.15}$$

The three parameters were estimated by a best fit using Matlabs Curve Fitting Toolbox.

2.3.6 Measurement of particle size distribution

The particle size distributions of the coated and uncoated materials where measured in three fold by laser diffraction using a Mastersizer 2000 with Scirocco 2000 dry dispersion unit (Malvern Instruments Ltd, England).

The coating thickness s_{ld} was calculated as half the difference of the volume weight mean diameter $\bar{d}_{4,3}$ of the core material and the coated sample respectively.

$$s_{\text{ld}} = \frac{\bar{d}_{4,3(\text{Sample})} - \bar{d}_{4,3(\text{Core})}}{2} \tag{2.16}$$

2.4 Results and Discussion

2.4.1 Results of dissolution test

The measured dissolution curves of the core material and four coated samples are shown in Figure 2.1. The curves are shifted to the right with more amount of coating material deposited on the surface, as expected. As the coat becomes more thick and uniform, the curves become more sigmoid. This can be explained by the Noyes-Whitney equation (2.17) which describes the dissolution rates of solids in their own solutions (Noyes and Whitney 1897):

$$\frac{dm}{dt} = \beta \cdot A(t) \cdot (c_\mathrm{s} - c(t)) \tag{2.17}$$

The equation describes the change in dissolved mass per time unit with the mass transfer coefficient β in $\mathrm{m\,s^{-1}}$, surface area A in $\mathrm{m^2}$ and the difference between the solubility c_s of the solid and its concentration c at time t. In diluted systems like used in the test conducted here, the difference $c_\mathrm{s} - c(t)$ is approximately $c_\mathrm{s} = const.$ The dissolution curve is thus determined by $A(t)$ which is basically the first derivative of the measured dissolution curve. Considering an uncoated sample, which dissolves according to a shrinking sphere model, $A(t)$ will have its maximum right at the beginning and will then decrease monotonically. A coated sample, however, will have no exposed surface area at the beginning. The area is gradually exposed as the coating dissolves and therefore will have a maximum at a point when all coating is dissolved and will then decrease again, as with the shrinking sphere model. This causes a point of inflection which can be seen from the dissolution curves at higher loadings. It should be noted that the time for complete dissolution lies in between 8 and 12 s in this case, but still differences are both measurable and significant.

After performing the procedure described in section 2.3.4.2 the thickness distributions shown in figure 2.2 were obtained. The distribution fit (equation 2.15) represents the data with an RMSE < 0.012 when comparing the forward calculated dissolution curve with the measured one.

The offset X_uncoated shouldn't be misinterpreted as a fraction of particles which are really completely uncoated. It is rather a measure for the exposed

uncoated area from partially covered particles, which was verified by visual inspection (data not shown).

2.4.2 Repeatability and validation

The accurate measurement of the dissolution curve is crucial for the method. As can be seen from Figure 2.1, the measured dissolution curves are significantly different from each other. The mean absolute deviation from the mean of three repeated measurements was smaller than 0.007, which indicates a good repeatability. However, the solution parameters, namely the shape and scale parameters of the Weibull part of the distribution, the offset X_{uncoated} and the dissolution velocity, are calculated with a higher uncertainty. Figure 2.3 shows the solution parameters of the four samples, together with the

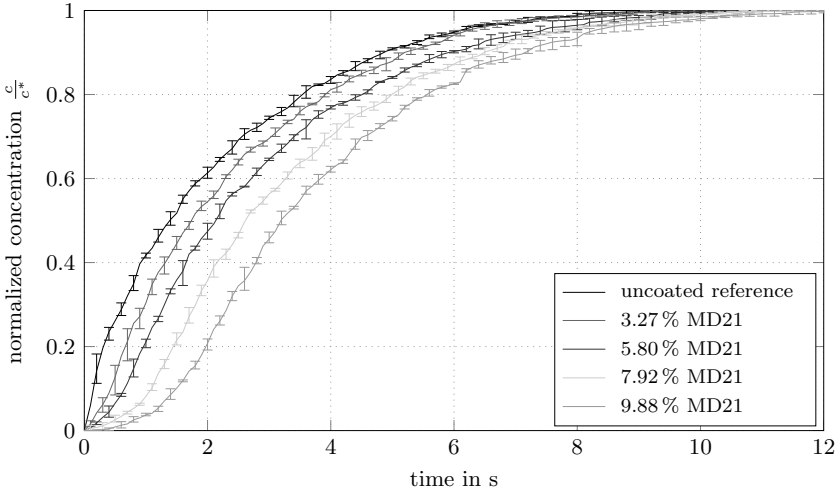

Figure 2.1: Measured dissolution curves of four MD21 coated materials, including the uncoated reference curve. Mean values from three measurements, error bars represent the maximum absolute positive and negative deviation from the mean.

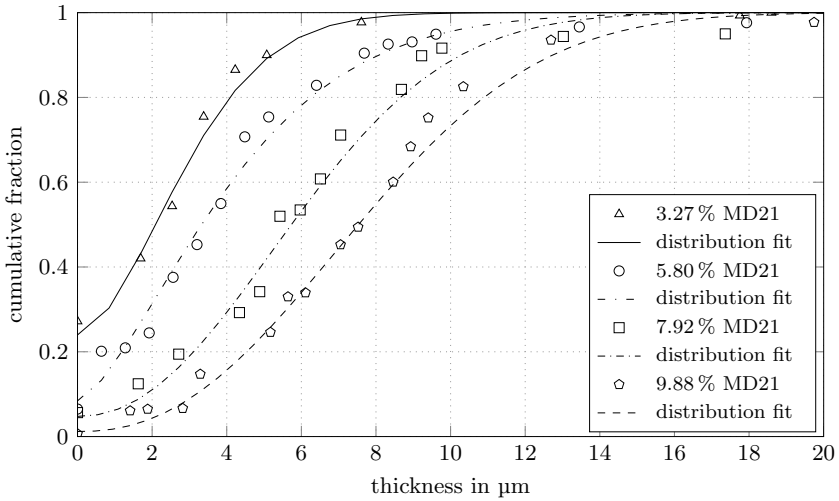

Figure 2.2: Cumulative thickness distributions obtained from the dissolution test. Symbols and lines represent the calculated values and the distribution fit, respectively.

standard deviations from nine calculations, which used all combinations of a three fold measurement of the reference curve as well as the sample curve.

As the deposited mass of coating material increases, the standard deviations of the parameters become smaller. Especially the offset value X_{uncoated} has a high uncertainty at the beginning. This could be because at this stage of the coating operation the particles aren't yet homogeneously treated, but more likely the error comes from small deviations at the beginning of the dissolution curves which have a greater impact on the solution when the overall difference of the reference curve to the sample curve is small. But still, the Weibull parameters of the distribution are calculated with a high confidence for all samples.

For further validation, the predictive capabilities of the method were investigated. Binary mixtures consisting of 10 to 90 % uncoated sodium chloride and the matching amount of sample four (9.88 % MD21) were prepared. The thickness distributions were calculated based on the measured distribution

of sample four. The dissolution curve for these mixtures were then forward calculated using this theoretical thickness distribution. The measured and forward calculated curves were then compared using the root mean square error between the two curves. The errors were in the range between 0.01 to 0.023. Two exemplary curves with the highest and lowest root mean square error are plotted in Figure 2.4. The curves with the lowest error almost fall onto one line, but also the curves with the highest error aren't that far off.

This shows, that the model is capable to predict the dissolution curve when the thickness distribution is known within a reasonable error. The assumptions made in section 2.2 are therefore valid for describing the population of coated particles.

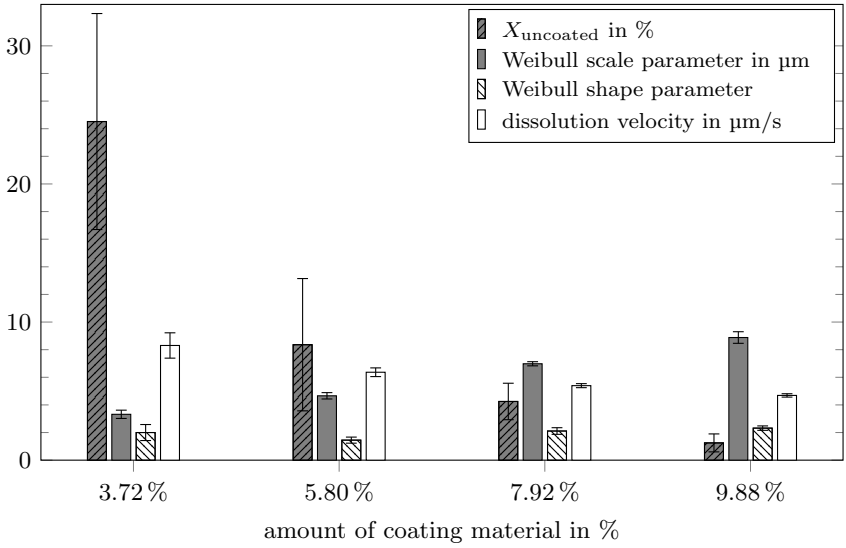

Figure 2.3: Calculated distribution parameters for the four coated samples. The mean values out of nine calculations are shown with errorbars representing the standard deviation.

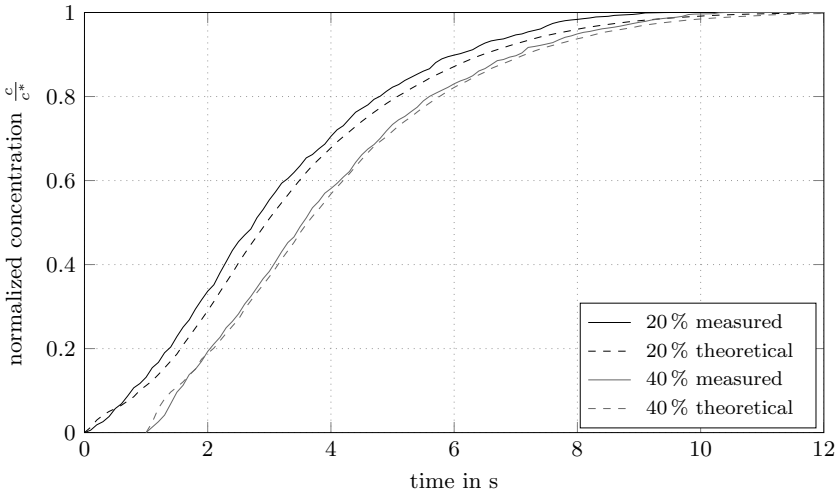

Figure 2.4: Measured and forward calculated theoretical dissolutions curves of Sample 4 mixed with 20 and 40 % uncoated sodium chloride. The curve for 40 % is shifted by one second to the right for better visualisation. ($\mathrm{RMSE}_{20\,\%} = 0.023$, $\mathrm{RMSE}_{40\,\%} = 0.010$)

2.4.3 Results of image analysis and comparison with dissolution test

Typical images from all samples made with the confocal laser scanning microscope are shown in Figure 2.5. As already suspected in the section above, the coating is still incomplete when only a low amount of coating was deposited on the surface. As the distributed mass of coating material rises, the coat becomes subsequently more complete and more homogeneous. It also becomes thicker, which can be seen from the more intense (lighter gray values) surface at high loadings.

The cumulative thickness distribution for four randomly chosen particles per sample were measured using image analysis as described in section 2.3.4.1. The results are shown in Figures 2.6a to 2.6d together with the results from the dissolution test. As the amount of deposited coating material increases the

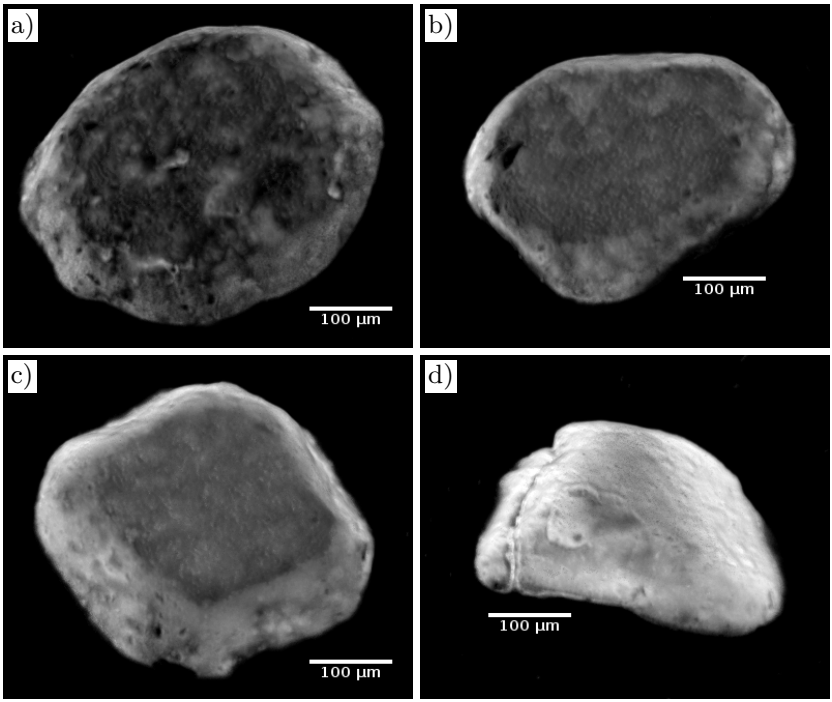

Figure 2.5: CLSM images of the four samples. a) Sample 1: 3.72 % MD21; b) Sample 2: 5.80 % MD21; c) Sample 3: 7.92 % MD21; d) Sample 4: 9.88 % MD21

distributions yielded from both methods show more agreement to each other, although the dissolution test estimates a broader distribution than the image analysis does. However, it should be kept in mind that the distributions from image analysis show the thickness distribution on one single particle, whereas the distribution from the dissolution test yields a thickness distribution of the mean thickness from all particles of the sample.

In comparison to image analysis, the dissolution test seems to underestimate the coating thickness. The difference gets smaller, the thicker the coat becomes. A reason for that could be, that the minimum thickness the image

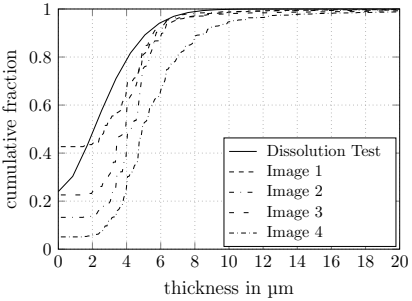

(a) Sample 1: 3.72 % MD21

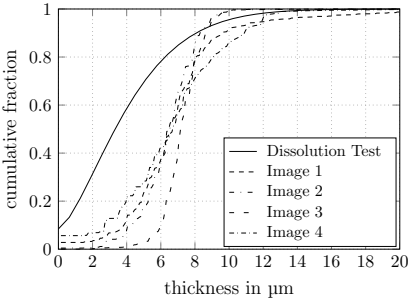

(b) Sample 2: 5.80 % MD21

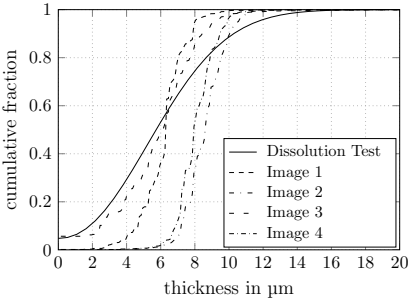

(c) Sample 3: 7.92 % MD21

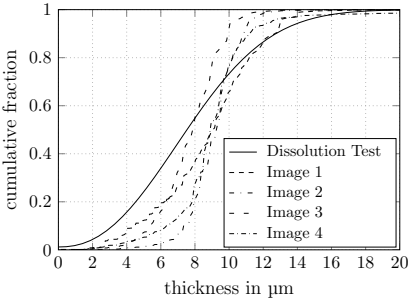

(d) Sample 4: 9.88 % MD21

Figure 2.6: Comparison of thickness distributions obtained from image analysis and the dissolution test.

analysis procedure was able to detect, was about 2 µm at the chosen acquisition settings. This is of course not the resolution limit of this technique, which in theory is well below 1 µm. The chosen settings were a trade-off between a reasonable acquisition time (in this case 15 min) and accuracy, which was found to be adequate for the purpose of this investigation. In order to double the resolution the acquisition time would increase eight fold.

2.4.4 Comparison of the mean thickness values obtained from different methods

In this work, the thickness distribution was measured using two methods. The newly proposed dissolution test and an image analysis technique using confocal laser scanning microscope images. For further comparison, the theoretical coating thickness s_{th} (equation 2.1) calculated from the measured coating amounts and the mean thickness obtained from laser diffraction measurement s_{ld} (section 2.3.6) were calculated as well. The median of the thickness distributions from image analysis and dissolution test were chosen for the comparison, which are shown in Figure 2.7.

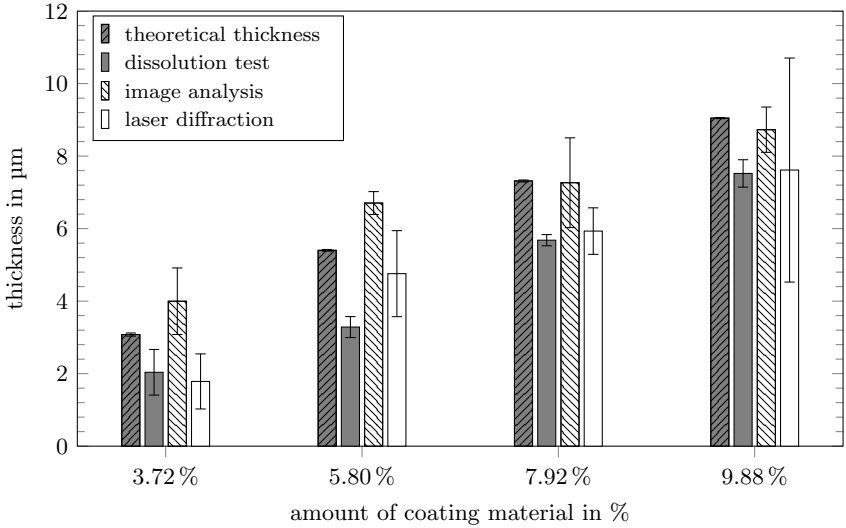

Figure 2.7: Comparison of the mean thickness values from the dissolution test with other methods.

The theoretical thickness is the measure with the highest confidence, which reflects the fact that the amount of deposited coating material can be measured very accurately. In comparison, the dissolution test underestimates the mean thickness, but correlates well with the amount of coating material. In

contrast, both the image analysis and the laser diffraction measurement suffer from higher uncertainties, which leads to not being able to significantly distinguish between the samples.

2.4.5 Limitations

Although the novel method shows promising first results, there are some limitations. The method is suitable to detect the uncoated area fraction very well, as can be seen from figure 2.6. The distribution calculated also corresponds reasonably well with the thickness distribution on single particles from image analysis. The mean thickness, however, seems to be systematically underestimated. There are two hypothesis which could explain this discrepancy.

First, the trigger for the start of the dissolution is accurate to 100 ms and detects the first particle which passes the transmission probe. This could be too late, which would result in a lower calculated thickness. The second possibility is the assumption of perfectly coated smooth spheres. In reality there is a certain amount of surface roughness present. The coating would fill the valleys and then surpasses the highest points of the core particles surface. During dissolution, these higher parts of the core are exposed before the lower parts, contributing sooner to the rise in conductivity, which results in a lower thickness calculated. The theoretical thickness calculation and the laser diffraction measurement would not account for the roughness, therefore estimating a higher thickness.

Practical limitations include the usable core and coating materials. The concentration of dissolved core material has to be measurable independently of the concentration of the dissolved coating material. The method was developed for coatings that dissolve molecule per molecule. Coatings that swell during dissolution were not yet considered. The interpretation of the obtained data may need some changes to cover those systems.

2.5 Conclusion

The use of the relatively simple measurement of dissolution curves in order to obtain information of the population of coated particles was proposed.

The results seem to underestimate the coating layer thickness compared to other methods. However, it is capable of delivering information about the distribution of the layer thickness within a reasonable amount of time, which makes the method suitable for every day quality assurance as well as process optimisation.

The method should be applicable to all systems, were the dissolution of the core material can be measured. As it was developed for coatings that dissolve molecule per molecule, its applicability to systems were the coatings swell during dissolution (biopolymers) is yet to be tested.

3 Systematic process optimisation of fluid bed coating

By Andreas van Kampen and Reinhard Kohlus.
Published 2017 in *Powder Technology*, Volume 305, Pages 426–432.
Accessible under DOI: 10.1016/j.powtec.2016.10.007

Abstract

A design of experiments approach was used to investigate the impact of bed temperature, volumetric air flow rate, spray rate and concentration of the coating solution on fluidised bed coating of particles. The process was analysed in terms of agglomeration tendency, efficiency and coating quality. Response surfaces were fitted to the experimental data from which optimal factor combinations were calculated in order to improve the coating quality. The coating quality was assessed by a previously developed method based on a dissolution test to efficiently measure the thickness, the uniformity and the completeness of the coating. It was demonstrated that the method provides a reliable way to assess the various measures for coating quality.

3.1 Introduction

Process optimisation is usually done using the rules of experimental design. These allow the systematic study of main and interaction effects of several factors, i.e. process settings or raw materials. The downside is the large

number of trial runs, usually around 16 to 32 in full-factorial designs, which also have to be analysed in terms of the product quality.

In the case of fluid bed coating, this raises the issue of the measurement of coating quality, which is essential in order to provide the intended functionality of the product. The quality of the coating layer can be looked at in terms of coating thickness, the degree of surface coverage and the homogeneity, i.e. the narrowness or broadness of the coating thickness distribution. These parameters are usually assessed using image acquisition systems, like the confocal laser scanning microscopy (Depypere et al. 2009; Laksmana et al. 2009) or micro computed X-ray tomography (Perfetti et al. 2010). Both methods are capable to produce three dimensional images of the particles, which can then be quantitatively analysed by computational image analysis procedures. This works well, providing good results and detailed information on the structure of the coating. The downside is the time consuming sample preparation and image acquisition task, which can easily take hours depending on the image quality and resolution. Especially for thin coatings in the range of a few microns, a high resolution is needed for accurate results. In order to obtain representative results one has to analyse a large number of particles, which results in a largely increased time required for the analysis.

Designed experiments were of course used previously by other workers to gather information on the fluid bed process. Two examples are the works from Dewettinck and Huyghebaert (1998) and Hede et al. (2007). While the former focuses on the impact of nozzle atomising pressure and primary particle diameter on the process efficiency, the latter focused on agglomeration tendency and stability of coated cores. Hede et al. (2007) additionally did some qualitative analysis on the structure of the coating, but to the best of our knowledge no quantitative investigation on the effect of process variables on the coating layer structure has been done so far.

A method based on dissolution kinetics was previously described and validated by the authors (van Kampen, Hitzmann, et al. 2015). It is capable to provide statistical information on the coating thickness distribution and degree of surface coverage using the simple measurement of the dissolution curve of the material. In this study, the performance of this method for the optimisation of a fluid bed coating operation was tested.

3.2 Materials and methods

3.2.1 Model system

Sodium chloride particles (Südsalz GmbH, Germany) which were sieved to a fraction of 350 to 500 µm were used as core particles for the coating operation. The salt had a volume weighted mean diameter of 395 µm and a surface weighted mean diameter of 317 µm. According to Erguns equation (eqn. 3.1, from Uhlemann and Mörl (2000)) and a measured bed porosity at minimal fluidisation of $\varepsilon_{\mathrm{mf}} = 0.45$, the minimal fluidisation velocity of the salt particles was calculated as $u_{\mathrm{mf}} = 0.126\,\mathrm{m\,s^{-1}}$.

$$u_{\mathrm{mf}} = 42.9 \cdot (1-\varepsilon_{\mathrm{mf}}) \cdot \frac{\nu_{\mathrm{F}}}{\bar{d}_{3,2}} \cdot \left[\sqrt{1 + 3.11 \cdot 10^{-4} \cdot \frac{\varepsilon_{\mathrm{mf}}^3 \cdot (\rho_{\mathrm{Ss}} - \rho_{\mathrm{F}}) \cdot g \cdot \bar{d}_{3,2}^3}{(1-\varepsilon_{\mathrm{mf}})^2 \cdot \rho_{\mathrm{F}} \cdot \nu_{\mathrm{F}}^2}} - 1 \right] \tag{3.1}$$

Maltodextrin with 21 dextrin equivalents (Roquette Frères, France) was used as a coating agent. It was dissolved in distilled water to the desired mass fraction. 2 %, with respect to the maltodextrin mass, of Ponceau 4R (Lay Gewürze OHG, Germany) was added to the solution as a tracer colour.

3.2.2 Coating operation

The coating operation was performed in a WS-CT-L top-spray fluidized bed dryer (Allgaier Process Technology GmbH, Germany) equipped with a model 970 two-fluid nozzle (Düsen-Schlick GmbH, Germany) with a nozzle orifice diameter of 0.8 mm. The atomizing air pressure was set to 1.5 bar. The air distributor plate had a diameter of 100 mm.

1 kg of primary particles was loaded into the vessel. The bed was then preheated to the desired bed temperature before the coating agent was sprayed. After 200 g of dry mass was sprayed, corresponding to a 20 % mass loading of coating material on the core, the coated particles were dried for another two minutes before the operation was completed and the product removed from the vessel.

3.2.3 Experimental design

The four factors spray rate $\dot{m}_{\mathrm{lq}}$, concentration of the bulk solution c_{lq}, volumetric air flow rate $\dot{V}_{\mathrm{Air}}$ and bed temperature T_{Bed} were investigated in a full factorial 2^4-Design with one replicate resulting in 32 trial runs, which were performed in a randomized order. See table 3.1 for the actual process variable settings. In order to investigate possible non linearities, the design was augmented using eight star points ($\alpha = 2$) and three replicates of the center point (table 3.2).

Table 3.1: Actual and coded values of the investigated factors.

		Coded Values				
Factor	Unit	$-\alpha$	-1	0	+1	$+\alpha$
S: $\dot{m}_{\mathrm{lq}}$	$\mathrm{g\,min^{-1}}$	7.5	10	12.5	15	17.5
C: c_{lq}	%	10	20	30	40	50
F: $\dot{V}_{\mathrm{Air}}$	$\mathrm{m^3\,h^{-1}}$	75	90	105	120	135
T: T_{Bed}	°C	47.5	50	52.5	55	57.5

Analysis of the responses was performed as a standard ANOVA using Design Expert (v. 9.0.6, Stat-Ease Inc., USA). A quadratic model was chosen for the analysis and subsequently reduced in order to include only effects with the largest relative impact on the response. The threshold was set to a p-value of 0.1. Effects with higher p-values were only included when it was necessary to maintain a hierarchical model. The relative impact of a factor was treated as significant when the corresponding p-value was lower than 0.05.

3.2.4 Sample division

The products from the trial runs were divided to obtain representative samples for further analysis. A riffle divider (Haver & Boecker OHG, Germany) was used to split the samples into smaller fractions (about 250 g) which were then further divided by a rotary sample splitter (Retsch GmbH, Germany) into fractions of about 30 g for particle size analysis and fractions of about 2 g for the dissolution test.

Table 3.2: 2^4-factorial design[a] augmented with star[b] and center points[c]. ([d] not included in statistical analysis)

	Factors				Responses				
No.	$\dot{m}_{\mathrm{lq}}$	c_{lq}	$\dot{V}_{\mathrm{Air}}$	T_{Bed}	x_{ag} in %	s_{c} in µm	SPAN	x_{uc} in %	w_{c} in %
1[a]	-1	-1	-1	-1	8.55	9.53	1.98	0.76	11.61
2[a]	-1	-1	-1	-1	11.36	10.25	1.62	0.38	11.54
3[a]	+1	-1	-1	-1	7.04	10.44	1.09	1.20	11.63
4[a]	+1	-1	-1	-1	11.48	11.54	1.23	0.13	12.77
5[a]	-1	+1	-1	-1	9.22	5.67	3.18	1.30	7.26
6[a]	-1	+1	-1	-1	4.77	6.76	2.08	27.12	6.23
7[a]	+1	+1	-1	-1	8.25	7.42	2.39	0	8.71
8[a]	+1	+1	-1	-1	7.03	8.78	1.64	1.44	10.09
9[a]	-1	-1	+1	-1	12.33	9.79	1.60	1.46	10.79
10[a]	-1	-1	+1	-1	30.55	10.81	2.02	2.17	11.94
11[a]	+1	-1	+1	-1	34.99	10.50	2.07	0	12.55
12[a]	+1	-1	+1	-1	26.33	10.98	1.92	0	12.62
13[a]	-1	+1	+1	-1	6.15	5.95	2.47	1.99	7.07
14[a]	-1	+1	+1	-1	6.17	7.43	2.03	4.08	8.17
15[a]	+1	+1	+1	-1	14.28	10.01	1.82	0	11.74
16[a]	+1	+1	+1	-1	9.47	10.59	1.73	4.90	11.91
17[a]	-1	-1	-1	+1	17.41	11.59	1.37	1.17	12.41
18[a]	-1	-1	-1	+1	6.59	9.77	1.01	7.58	9.55
19[a]	+1	-1	-1	+1	8.80	10.91	1.13	0.29	12.24
20[a]	+1	-1	-1	+1	7.48	10.69	1.26	0	11.66
21[a]	-1	+1	-1	+1	8.01	6.34	1.88	16.53	5.55
22[a]	-1	+1	-1	+1	7.58	7.57	1.75	15.55	7.00
23[a]	+1	+1	-1	+1	12.99	9.98	1.34	4.79	10.03
24[a]	+1	+1	-1	+1	8.17	7.66	1.94	9.44	8.35
25[a]	-1	-1	+1	+1	17.33	9.53	1.71	0	10.35
26[a]	-1	-1	+1	+1	8.57	9.59	1.47	3.64	9.85
27[a]	+1	-1	+1	+1	23.66	12.01	1.55	1.98	12.95
28[a]	+1	-1	+1	+1	19.01	10.61	1.85	1.62	12.16
29[a]	-1	+1	+1	+1	13.96	10.22	1.69	5.97	10.77
30[a]	-1	+1	+1	+1	6.50	9.02	1.82	13.48	8.50
31[a]	+1	+1	+1	+1	12.15	9.76	1.45	5.42	9.87
32[a]	+1	+1	+1	+1	8.63	8.33	1.61	7.10	8.79
33[b]	-α	0	0	0	8.92	6.29	2.07	3.67	8.15
34[b]	+α	0	0	0	8.05	12.19	1.43	1.07	12.95
35[b]	0	-α	0	0	8.33	11.44	1.28	0	12.41
36[bd]	0	+α	0	0	14.80	13.83	3.45	55.85	8.11
37[b]	0	0	-α	0	9.40	8.65	1.29	3.45	10.15
38[b]	0	0	+α	0	8.70	9.69	1.75	5.05	10.98
39[b]	0	0	0	-α	9.44	11.38	1.18	5.12	11.63
40[b]	0	0	0	+α	9.73	9.38	1.52	4.70	9.41
41[c]	0	0	0	0	8.18	10.28	1.38	0.24	12.13
42[c]	0	0	0	0	5.57	8.29	1.37	4.52	10.34
43[c]	0	0	0	0	7.53	8.98	1.08	7.70	10.31

3.2.5 Particle size analysis

The particle size distribution was measured with laser diffraction using the Mastersizer 2000 with a Scirocco 2000 dry dispersion unit (Malvern Instruments Ltd., UK). To calculate the fraction of agglomerates, the theoretical maximum coating thickness $s_{\max}$ was calculated from a mass balance by equation 3.2, which assumes the coating to be a concentric sphere around the core.

$$s_{\max} = \frac{\bar{d}_{4,3}}{2} \cdot \left[\left(1 + \frac{\rho_{\text{core}} \cdot m_{\text{coating}}}{\rho_{\text{coating}} \cdot m_{\text{core}}} \right)^{1/3} - 1 \right] \tag{3.2}$$

$s_{\max}$ was calculated as 16.7 µm so the the maximum increase of the particle diameter was assumed to be 33.4 µm. The $x_{3,90}$ of the salt particles was 573 µm, so the expected maximum diameter after coating should be around 600 µm. To account for some degree of variation, the threshold for agglomerates was set to 650 µm. The fraction above this threshold x_{ag} was calculated by the Mastersizer software.

3.2.6 Dissolution test

The dissolution of the core particles (sodium chloride) was measured as the rise in conductivity. 400 g of purified water with a temperature of 20 °C (weighed to 0.05 g precision) were prepared in a 600 ml beaker with a diameter of 85 mm. The water was stirred at 700 min^{-1} using a stirrer with a dissolver plate geometry (40 mm diameter) placed at a height of 30 mm above the bottom of the beaker.

The conductivity was measured with a conductivity meter WTW LF530 (WTW GmbH, Germany). An online photometer AvaSpec-ULS2048 (Avantes BV, Netherlands) equipped with a transmission dip probe (20 mm optical path length) was used to measure the absorption at 510 nm as well as the transmission of light. The sample rate was 10 Hz.

The data logging was started and after a few seconds, 2 g of sample material (weighed to 0.1 mg precision) were poured at once into the beaker. The first significant transmission drop was used to trigger the starting point of the dissolution curve. The measurement was repeated three times for all samples. Figure 3.1 shows a typical measured dissolution curve.

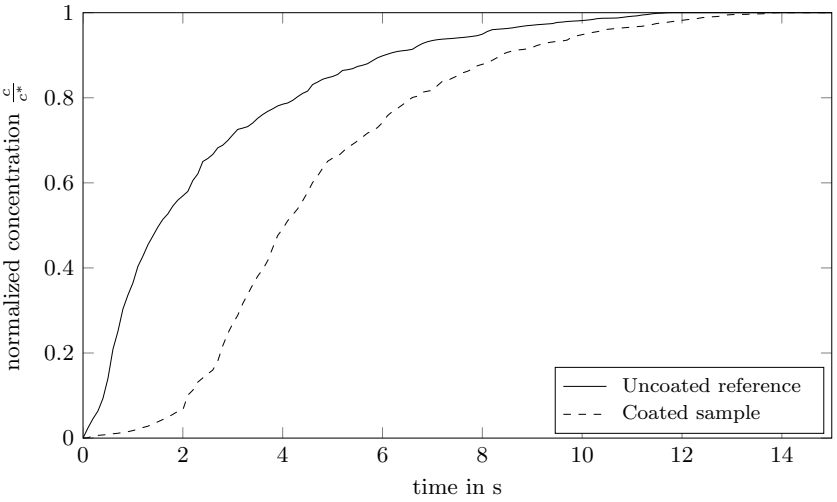

Figure 3.1: Typical dissolution curves of the uncoated reference and a coated sample.

Analysis of the sample data in terms of coating thickness distribution, uncoated surface area fraction and amount of coating material on the sample was calculated according to the method described by van Kampen, Hitzmann, et al. (2015). The Weibull scale parameter of the obtained distribution fit (eqn. 3.3) was used as the response variable for the coating thickness s_c. The offset value x_{uc} describes the uncoated area fraction.

$$F(x) = x_{uc} + (1 - x_{uc}) \cdot (1 - exp(-\left(\frac{x}{s_c}\right)^a)) \tag{3.3}$$

Since the Weibull shape parameter a is not independent from the scale parameter s_c it is not a good measure for the wideness of the distribution. Instead, the SPAN of the Weibull-part S of the distribution was calculated using the corresponding quantiles as follows:

$$S(x) = 1 - exp(-\left(\frac{x}{s_c}\right)^a) \tag{3.4}$$

$$\text{SPAN} = \frac{S_{90} - S_{10}}{S_{50}} \tag{3.5}$$

An example for a typical thickness distribution is shown in figure 3.2.

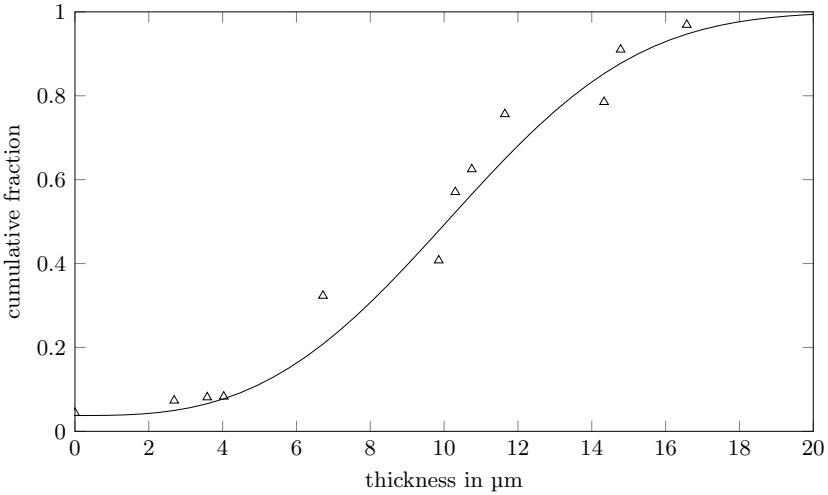

Figure 3.2: A typical thickness distribution obtained from the dissolution method. The triangles and the solid line represent the calculated values and the distribution fit, respectively.

3.2.7 Confocal laser scanning microscopy

Three single particles from selected samples were imaged using a Nikon C1 confocal laser scanning microscope (Nikon GmbH, Germany) equipped with a ×20 PlanFluor objective and 543 nm excitation laser. The particles were placed on a cover slip suspended in immersion oil (n = 1.543). A z-stack was acquired. The x–y-resolution was set to 512 by 512 pixels with a 0.43 µm step size in z-direction. To view the surface structure of the particles the z-stack was projected in a top down view using ImageJ. The software calculated the sum of all pixel values in z-direction, which was found to give a good representation of the particles surface.

3.3 Results and discussion

All trials were run successfully. Only trial number 36 (tab. 3.2), which had a high liquid concentration of 50 %, defluidised partially. Therefore this trial was left out of the statistical analysis.

The measured response values were analysed and response surfaces were calculated to describe the factor influences and interactions. All models were significant ($p < 0.001$) and of reasonable quality to navigate the investigated design space. The resulting response surfaces are discussed in the following sections.

3.3.1 Effects on agglomeration tendency and process efficiency

A coating operation is usually considered as good when the product does not form agglomerates and the losses due to overspray are minimal (Dewettinck, Deroo, et al. 1998; Prata et al. 2012). The goal for this investigation was set to a coating amount w_c of 20 % measured as the mass ratio of coating material per core particle. The highest achieved value was 12.95 % which corresponds to a process efficiency of 64.75 %. In comparison, Dewettinck, Deroo, et al. (1998) achieved 85.5 to 88.1 % when coating glass beads with various gums and 68.8 to 80.8 % when coating sodium chloride with various proteins (Dewettinck and Huyghebaert 1998).

Equations 3.6 and 3.7 show the calculated response surfaces for the amount of agglomerates x_{ag} and the amount of coating w_{c}, respectively. The parameters are normalized between -1 and 1, according to table 3.1.

$$x_{\mathrm{ag}} = 11.26 + 1.07 \cdot \mathrm{S} - 2.84 \cdot \mathrm{C} + 2.6 \cdot \mathrm{F} + 1.54 \cdot \mathrm{S} \cdot \mathrm{F} - 2.59 \cdot \mathrm{C} \cdot \mathrm{F} \qquad R^2 = 0.4888 \tag{3.6}$$

$$w_{\mathrm{c}} = 10.29 + 0.98 \cdot \mathrm{S} - 1.41 \cdot \mathrm{C} + 0.38 \cdot \mathrm{F} - 0.28 \cdot \mathrm{T} + 0.43 \cdot \mathrm{C} \cdot \mathrm{F} \qquad R^2 = 0.7800 \tag{3.7}$$

The agglomeration tendency and the process efficiency are affected by the process settings in a similar way (see fig. 3.3 and 3.4) . A high concentration

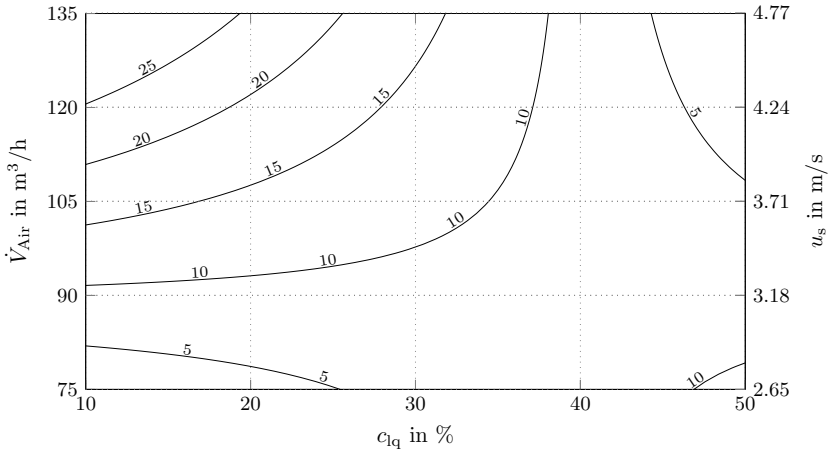

Figure 3.3: Amount of agglomerates >650 µm x_{ag} in % as a function of liquid concentration and air flow rate ($\dot{m}_{\mathrm{lq}} = 12.5\,\mathrm{g\,min^{-1}}$; $T_{\mathrm{Bed}} = 52.5\,^{\circ}\mathrm{C}$). The secondary y-axis shows the superficial gas velocity u_{s}.

of the coating solution leads to less agglomerates, but also to a lower efficiency. Since a high concentration also means less water that has to be evaporated, this leads to a higher amount of overspray, i.e. spray drying of droplets before they hit a particle. This also leads to less wetting of the particles surface, therefore leading to less agglomeration.

The volumetric air flow rate on the other hand increases both the agglomeration rate and the efficiency. The bed expands further and the distance between the nozzle and the bed surface is reduced. Consequently, the wetting is increased which favours both agglomeration and efficiency due to a reduction of overspray.

The data shows a significant interaction of the effects of liquid concentration and air flow rate. The effect of the air flow rate on the agglomeration rate was larger at low concentrations. So a low air flow rate is more favourable at low concentrations. There was little effect of the air flow rate on the efficiency at a low concentration but at a high concentration a high air flow rate increased

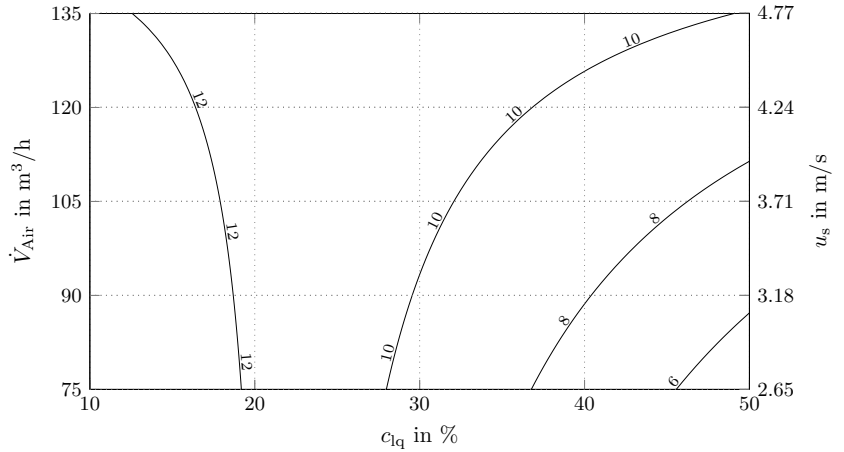

Figure 3.4: Amount of coating on the core particles w_{c} in % as a function of liquid concentration and air flow rate ($\dot{m}_{\mathrm{lq}} = 12.5\,\mathrm{g\,min^{-1}}$; $T_{\mathrm{Bed}} = 52.5\,^{\circ}\mathrm{C}$). The secondary y-axis shows the superficial gas velocity u_{s}.

the efficiency. So when one has to use a high concentrated coating agent, one can overcome overspray losses by increasing the air flow rate.

The spray rate had no significant effect on the agglomeration tendency, but a positive effect on the process efficiency. A high spray rate decreases the drying rate due to an increased humidity in the drying zone. This reduces overspray and leads to a higher efficiency.

3.3.2 Effects on coating quality

Coating quality is usually defined in terms of inter- and intra-particle variability as well as coating uniformity and the presence of coating defects (Depypere et al. 2009; Atarés et al. 2012; Werner et al. 2007). The coating quality resulting from the present experiments was investigated using the dissolution test method, which yields information on the mean thickness, uniformity (SPAN) and uncoated area fraction, i.e. presence of defects. Throughout this section

we will consider a coating with little to no defects, high thickness and good uniformity, i.e. low SPAN, as good.

It was possible to obtain empirical models which describe the relation between the process variables and the aforementioned quality measures (eqn. 3.8, 3.9 and 3.10). Figures 3.5, 3.6 and 3.7 show contour plots of the response surfaces.

$$\begin{aligned} s_{\mathrm{c}} &= 9.39 + 0.8 \cdot \mathrm{S} - 1.14 \cdot \mathrm{C} + 0.31 \cdot \mathrm{F} + 0.38 \cdot \mathrm{C} \cdot \mathrm{F} \\ R^2 &= 0.6836 \end{aligned} \tag{3.8}$$

$$\begin{aligned} \mathrm{SPAN} = 1.46 &- 0.12 \cdot \mathrm{S} + 0.21 \cdot \mathrm{C} + 0.071 \cdot \mathrm{F} - 0.13 \cdot \mathrm{T} \\ &-0.16 \cdot \mathrm{C} \cdot \mathrm{F} + 0.11 \cdot \mathrm{S}^2 + 0.13 \cdot \mathrm{C}^2 \\ R^2 &= 0.5599 \end{aligned} \tag{3.9}$$

$$\begin{aligned} x_{\mathrm{uc}} = 4.35 &- 1.75 \cdot \mathrm{S} + 2.93 \cdot \mathrm{C} - 0.77 \cdot \mathrm{F} + 1.17 \cdot \mathrm{T} \\ &-1.28 \cdot \mathrm{S} \cdot \mathrm{C} + 1.28 \cdot \mathrm{S} \cdot \mathrm{F} \\ R^2 &= 0.4999 \end{aligned} \tag{3.10}$$

A high spray rate improves the overall quality of the coating as it increases the thickness, decreases the SPAN and accounts for a more complete surface coverage. The increased humidity in the vessel leads to slower drying, thus increasing the wetting of the particles surface, which leads to a better droplet coalescence on the particle surface (B. Guignon et al. 2002). Figure 3.8 shows this trend qualitatively. The spray rate decreased from left to right and the surface gradually becomes more rough and bumpy.

A high concentration has an adverse effect compared to the spray rate. The increased overspray leads consequently to a lower thickness. The higher viscosity of the higher concentrated coating solution leads to less spreading on the particle surface resulting in a high SPAN and consequently a larger uncoated area fraction (B. Guignon et al. 2002). Again, this trend is corroborated by figure 3.8 (concentration increase from left to right). Severe defects of the coating layer were observed at high concentrations.

The temperature has a special effect on the SPAN. A higher temperature decreases the SPAN, thus improving the quality. This is somewhat counter intuitive since a higher temperature should lead to faster drying, which reduces the time for droplet spreading and coalescence on the surface. This

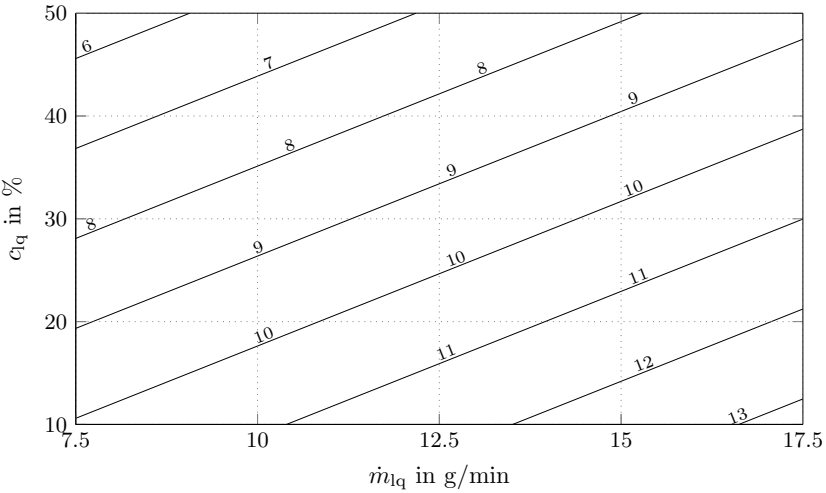

Figure 3.5: Coating thickness s_{c} in µm as a function of liquid flow rate and liquid concentration ($\dot{V}_{\mathrm{Air}} = 105\,\mathrm{m^3\,h^{-1}}$; $T_{\mathrm{Bed}} = 52.5\,^{\circ}\mathrm{C}$).

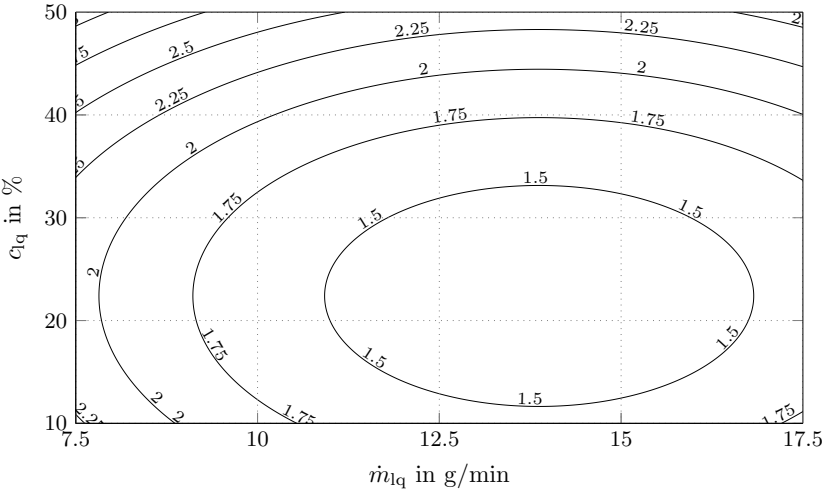

Figure 3.6: SPAN as a function of liquid flow rate and liquid concentration ($\dot{V}_{\mathrm{Air}} = 105\,\mathrm{m^3\,h^{-1}}$; $T_{\mathrm{Bed}} = 52.5\,^{\circ}\mathrm{C}$).

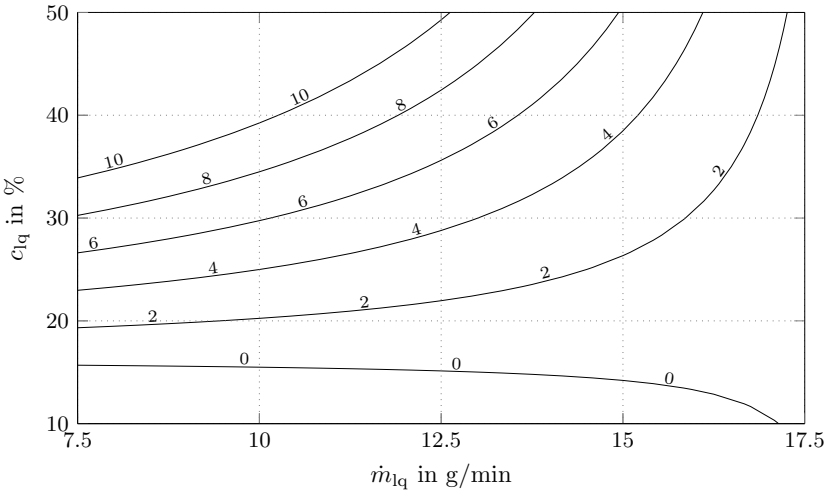

Figure 3.7: Uncoated area fraction x_{uc} in % as a function of liquid flow rate and liquid concentration ($\dot{V}_{Air} = 105\,m^3\,h^{-1}$; $T_{Bed} = 52.5\,°C$).

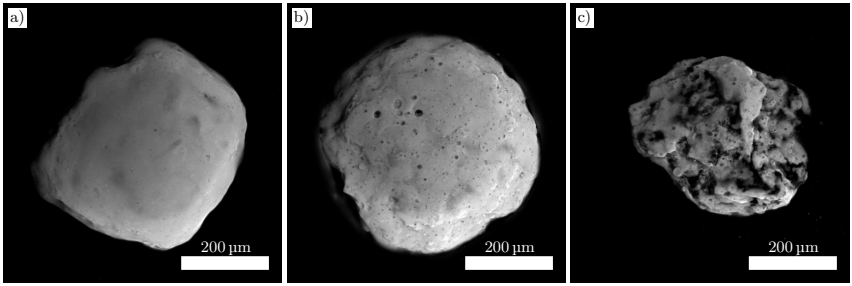

Figure 3.8: CLSM images of particles produced at a) low concentration and high spray rate (No. 3), b) medium concentration and medium spray rate (No. 41) and c) high concentration and low spray rate (No. 22).

should lead to a higher SPAN, however, the contrary was observed. Hede et al. (2007) observed a similar response on the impact resistance of coated granules. They linked the higher impact strength to a more homogeneous coating layer, which is in agreement to the results in this study.

3.3.3 Process time

Since the amount of dry coating material sprayed was fixed to 200 g, the process time needed for each trial run was dependent on the used liquid concentration and spray rate. Figure 3.9 shows a contour plot of the process time for each combination of spray rate and concentration. It can be seen that the liquid concentration has a much higher influence on the process time than the spray rate. In order to minimise the process time, it would make sense to maximise the concentration. However, this often has a negative effect in terms of coating quality as shown in the previous section.

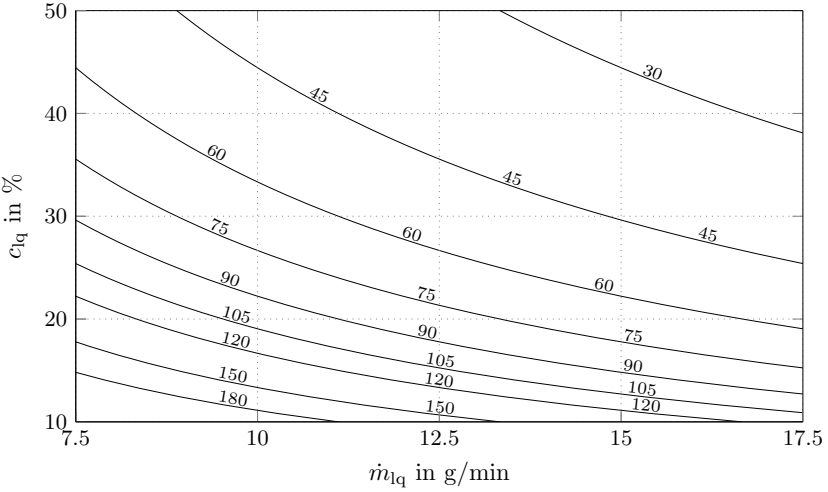

Figure 3.9: Process time in minutes needed to spray 200 g of dry coating material.

3.3.4 Optimisation

In order to verify the empirical relations discussed in the previous sections, the numerical optimisation routine from Design-Expert was used to search for optimal settings of the process variables. The algorithm is based upon a desirability function, which is constructed using the desired target values of the response variables and a given range for the process settings. Maxima of this function then represent the most desirable factor settings for the set goal.

The goal was set to an optimal structure of the coating layer, in our case to the maximum thickness s_c, the minimum SPAN and the uncoated area fraction x_{uc} should be close to or equal to zero. The other studied responses were not included in the optimisation, because they do not relate directly to the coating structure.

With the exception of c_{lq} and $\dot{V}_{Air}$ the full range of previously studied factor settings was explored for the optimal settings. $\dot{V}_{Air}$ was constrained at the lower end to $90\,m^3\,h^{-1}$, because the fluidisation at lower values was observed to be on the cusp of defluidisation. The concentration c_{lq} was also constrained at the lower end to 20 %, because the operation should be performed within a reasonable time.

Table 3.3 shows the optimisation criteria, the predicted optimal settings and the model prediction of the response variables. The high 95 % confidence bands for x_{ag} and x_{uc} result from the higher variability in these responses compared to the others, mainly due to the presence of extreme outliers which were not observed in the other responses.

Three repetitions of the optimal settings (table 3.3) were performed on the same day. The results are listed in table 3.4. First of all, it can be noted, that the deviations between the repetitions are quite low.

The samples were produced on the same day in direct sequence, so the environmental conditions did not change between the runs. The repeatability was therefore expected to be better than for the previous experiments, which were performed on different days with quite a high range of environmental conditions. Further on, the results are close to the predicted mean values for all parameters. This confirms the validity of the empirical model and demonstrates that the dissolution method is a reliable way to assess the coating quality.

Table 3.3: Goals and predicted values for the optimisation with respect to coating layer quality. Predicted response values are given as mean values with 95 % confidence interval boundarys.

Variable	Goal	Prediction
S: $\dot{m}_{\mathrm{lq}}$	in Range (7.5 to 17.5)	16.7
C: c_{lq}	in Range (20 to 40)	20
F: $\dot{V}_{\mathrm{Air}}$	in Range (90 to 135)	90
T: T_{Bed}	in Range (47.5 to 57.5)	57.5
x_{ag}	no goal set	8.14 ± 8.00
s_{c}	maximise	11.95 ± 1.46
SPAN	minimise	1.00 ± 0.55
x_{uc}	target = 0	1.57 ± 7.39
w_{c}	no goal set	12.85 ± 1.56

Table 3.4: Results from the optimisation runs (three repetitions) and their respective mean values. Process settings for these runs were $\dot{m} = 16.7\,\mathrm{g\,min^{-1}}$, $c_{\mathrm{lq}} = 20\,\%$, $\dot{V}_{\mathrm{Air}} = 90\,\mathrm{m^3\,h^{-1}}$ and $T_{\mathrm{Bed}} = 57.5\,^{\circ}\mathrm{C}$.

	Run			
Response	1	2	3	Mean
x_{ag} in %	7.45	7.87	6.77	7.36
s_{c} in µm	10.98	11.61	11.10	11.23
SPAN	1.02	0.96	1.02	1.00
x_{uc} in %	1.55	3.77	0.84	2.05
w_{c} in %	12.23	12.28	12.60	12.37

Table 3.5: Some possible optimisition goals with model predictions. The full range of possible process settings was included in the search.

Variable	Unit	Optimisation Goal			
		min. x_{uc} and max. s_c	max. w_c	max. w_c	min. x_{ag} and max. s_c
S: $\dot{m}_{lq}$	$g\,min^{-1}$	17.3	15.7	17.4	16.7
C: c_{lq}	%	17.9	12.8	21	14.3
F: $\dot{V}_{Air}$	$m^3\,h^{-1}$	116	85	92	76
T: T_{Bed}	°C	48.9	47.5	50.1	57.2
x_{ag}	%	23.12 ± 7.92	5.88 ± 9.02	9.14 ± 8.05	-0.66 ± 11.50
s_c	µm	12.20 ± 1.48	12.84 ± 1.67	12.06 ± 1.46	13.10 ± 1.92
SPAN	-	1.96 ± 0.59	1.35 ± 0.64	1.53 ± 0.60	0.70 ± 0.71
x_{uc}	%	0 ± 7.50	-3.60 ± 7.89	-2.14 ± 7.18	-0.40 ± 9.50
w_c	%	14.14 ± 1.52	15.01 ± 1.76	13.79 ± 1.47	14.24 ± 1.98
Process Time	min	65	100	55	84

Table 3.5 shows a greater variety of possible optimisation goals and resulting process settings. These settings were not verified, but the optimisation results show that, depending on the desired outcome, a great variety of optimal process settings exist. Interestingly, the predicted concentration almost never exceeds 20 %, so for most desired outcomes a high liquid concentration is undesirable, although it would reduce the needed process time drastically (see fig. 3.9).

There are almost always a variety of possible combinations of factor settings which fulfil the set goal, so one has to choose among these possibilities. One way to do this, is by looking at the time needed to run the process (see bottom row of table 3.5). This is demonstrated with the goal of maximising w_c. The best solution takes 100 min to run. If a maximum of 60 min was required, the other shown solution would be desirable. Although the predicted coating amount is lower than for the best solution, this might still be good enough considering the process time reduction by almost 50 %.

3.4 Conclusion

The present article demonstrates the use of the previously described dissolution method (van Kampen, Hitzmann, et al. 2015) as an efficient way to

analyse a high number of samples in terms of the coating quality measures thickness, uniformity and presence of defects. Using this method, top-spray fluidised-bed coating of sodium chloride particles with maltodextrin was investigated. A central composite design of experiments was used to study the relationship between the process variables (spray rate, liquid concentration, air flow rate and bed temperature) and the coating quality as well as plant performance (agglomeration tendency and process efficiency).

The observed main and interaction effects were in general agreement with results found earlier. For a stable (low agglomeration rate) and efficient process a low coating solution concentration and a low air flow rate are preferable. In terms of the quality of the coating a high spray rate, low coating solution concentration and a high temperature are desirable.

An optimisation with regard to a desirable coating quality lead to optimal settings for the process variables which were verified in three repetitions. The resulting parameters for coating quality, agglomeration rate and efficiency were close to the predicted mean values with low errors. This confirms the validity of the empirical model to predict the various coating quality measures as determined by the dissolution method.

4 Statistical modelling of coating layer thickness distributions: Influence of overspray on coating quality

By Andreas van Kampen and Reinhard Kohlus.
Published 2018 in *Powder Technology*, Volume 325, Pages 557–567.
Accessible under DOI: 10.1016/j.powtec.2017.11.031

Abstract

This paper investigates the layer formation in spray coating processes. Based on a Monte-Carlo simulation, a stochastic model of the coating layer thickness distribution was derived. It couples the stochastic process of droplet deposition on the particle surface with the droplet shape constructed from a spherical cap model and the droplets wetting properties (contact angle). The model was successfully shown to be able to replace the simulation. A parameter study revealed recommendations for designing a coating process, which were in agreement with the works from other authors. The model was then used to investigate the influence of overspray on the coating quality in comparison with experiments. It was found that the presence of overspray not only reduces the process efficiency but also increases the coefficient of variation of the resulting layer thickness distribution. This was caused by an increase in droplet size due to a predominant drying of small drops. It was also found, that a higher solid content of the spray solution increases the

coefficient of variation, not only due to a decreased number of droplets, but also due to a greater variability in the layer thickness each droplet introduces.

4.1 Introduction

Fluidised bed coating of particles is a common unit operation in various industries, such as food, pharmaceutical or agricultural industry. Generally, high quality coatings are aimed for, which usually means the formation of a homogeneous coating layer of a certain (minimum) thickness without defects. In order to keep the costs down, highly efficient processes are in demand.

The required structure of the coating layer depends on the application. Whereas an effective taste masking needs a complete layer of a certain minimum thickness, a controlled or delayed release application needs a well defined layer thickness. A colouring application in contrast, would not have a demand for a well defined layer quality, as long as the required colour intensity is achieved.

The homogeneity of the coating has been mainly studied in terms of inter particle (or tablet) coating mass variety. For instance, Abe et al. (1998) studied a tumbling fluidized bed coater and found that an increased coating time (and total mass being sprayed) lowered the coefficient of variation (CoV) of the resulting coating mass distribution. Joglekar et al. (2007) developed a mathematical model of a pan coating process and, among other relations, they found that decreasing the spray rate while increasing the coating time, thus keeping the total mass sprayed constant, also lowers the CoV. From both studies, one can conclude that an increase in droplet number leads to a reduction of CoV.

This conclusion is further strengthened by an experiment of Hemati et al. (2003), where they obtained a more homogeneous coating layer by increasing the atomizing air flow rate of the two fluid nozzle they used. This lead to the formation of smaller droplets and therefore to an increased number of droplets as well.

Furthermore Kleinbach and Riede (1995) showed that the formation of a coating layer can be modelled by a Bernoulli trial, where the probability of a surface segment being coated m-times by one droplet when a total of n

droplets are sprayed, is binomial distributed with

$$P_{m,n} = \binom{n}{m} p^m (1-p)^{n-m} \tag{4.1}$$

where p is the probability of a single surface segment being hit by a droplet. From this model they concluded that the homogeneity of the coating can be improved by either reducing the number of surface segments, which can be achieved by using a coating solution with better wetting properties, or by increasing the number of droplets, by either diluting the coating solution or spraying smaller droplets.

It should be noted that both, Kleinbach and Riede (1995) and Joglekar et al. (2007) used the binomial distribution to model the coating process but modelled the intra- and inter-particle coating variability, respectively. This leads to the conclusion, that the stochastic nature of the coating process is the same regarding inter particle coating variability, i.e. coating mass distribution, and intra particle coating variability, i.e. coating thickness distribution on single particles. Assuming a well mixed bed, large particles are likely to be hit by more spray droplets than small particles, because of their larger surface area. This would lead to a larger amount of coating mass on large particles. The mean thickness, however, would be the same as for small particles, since the coating mass is distributed on a larger area (Mörl et al. 2007). This would lead to a very low inter-particle coating thickness variability, but there is evidence that there are processes where the inter-particle coating variability is larger than what we expect from the stochastic process (Rieck, Bück, et al. 2016; Sondej et al. 2015).

Another modelling approach of Kariuki et al. (2013) should be mentioned. They derived the dimensionless particle coating number Φ_p to model the coated surface area fraction of a particle in wet granulation. They also used a Bernoulli trial to derive the probability of a certain surface segment being coated, when n droplets are deposited. They approximated their derived function by the Poisson distribution in order to have the convenience of a function relying on a single parameter, instead of having two. They reported a maximum error of 1 % in the relevant range of parameters.

Besides the coating mass or layer thickness variability, the efficiency of the coating process is of importance. Inefficiencies occur when sprayed liquid

droplets are dried prematurely before reaching a particle and are consequently elutriated from the fluidized bed (Ronsse et al. 2008). According to Link and Schlünder (1997), 'dry' process conditions are required to favour particle growth by layering. Unfortunately, the requirements for a homogeneous coating layer (small droplets) in combination with 'dry' process conditions gives rise to excessive premature droplet drying, i.e. overspray, and consequently decreases the process efficiency.

Ways to measure coating thickness distributions include microscopic methods, which can directly assess both, the inter- and intra particle coating variability separately. The downside is, that these methods are usually very tedious and time consuming, but can be sped up under certain circumstances. For example Sondej et al. (2015) used a µCT to measure coating thickness distributions on spherical pellets. The spherical nature of the investigated particles allowed them to speed up the imaging time significantly which made the investigation of the inter-particle coating variability feasible.

In our own work, we developed and used an indirect method based on the analysis of dissolution kinetics to assess the layer thickness distribution of coated salt particles efficiently (van Kampen, Hitzmann, et al. 2015). We found that our measured thickness distributions are well described by a Weibull distribution. The coating thickness distribution measured by this technique would be the mean coating thickness distribution of the sample which comprises both, the inter- and intra particle coating variability. In another series of experiments we studied the influence of the parameters of a fluid bed coating process on the resulting coating quality using the dissolution method (van Kampen and Kohlus 2017). The effects of spray rate and concentration of the coating solution regarding CoV were identical to the results from the literature discussed above.

The present study augments the current models with a more detailed stochastic model of the coating layer thickness distribution taking the droplet shape into account. This gives more insight on the formation of coating layers. The model is then used to investigate the influence of overspray on the coating quality.

4.2 Theory

In order to investigate the formation of a coating layer and the influence of the dried droplet shape, a Monte-Carlo simulation was performed as described in the next section. The validity of the Monte-Carlo method for coating thickness distributions was shown by Rieck, Bück, et al. (2016). The shape of dried deposits was modelled in three ways: A disc profile with uniform height, a spherical cap and a ring shape, which occurs when drops with dispersed solids dry on a surface (Deegan et al. 1997). Based on this simulation, a stochastic model was derived in order to replace the simulation and gain more insight in the process.

4.2.1 Description of the simulation

A simulation of the layer formation in particle coating was implemented in Matlab. A two dimensional matrix represents the particle surface without edge effects, i.e. whenever a part of a droplet would be cut off at an edge, this part is drawn on the opposite side, thus forming a flat representation of a spherical particle surface. The droplets were placed on the surface by generating two uniformly distributed random numbers representing the x- and y-coordinates respectively. The contact radius r_c was calculated from a spherical cap model, using the volume of a droplet V_drop and the contact angle θ as a parameter.

$$r_\mathrm{c} = \left(\frac{3V_\mathrm{drop} \sin^3 \theta}{\pi(2 - 3\cos\theta + \cos^3\theta)} \right)^{1/3} \tag{4.2}$$

Drying was assumed to take place with a constant contact radius, as was reported by Alsan Meric and Erbil (1998) for contact angles $\theta < 90°$. Droplet spreading was assumed to be rapid compared to drying, so the droplet reaches its final shape directly after its deposition. In order to build up the coating layer on the simulation surface, the height profiles of dry droplets were simply added to the matrix, so formation of porosity was not considered in the model.

Three different height profiles were used for the simulation, each having the same contact radius calculated from the spherical cap model.

1. a spherical cap
2. a ring shape that resembles the shapes modelled by Karlsson et al. (fig. 13a from Karlsson et al. 2011), who investigated the formation of a 'coffee ring' in single droplet drying experiments
3. a disc with uniform height, i.e. the mean height of the former two profiles

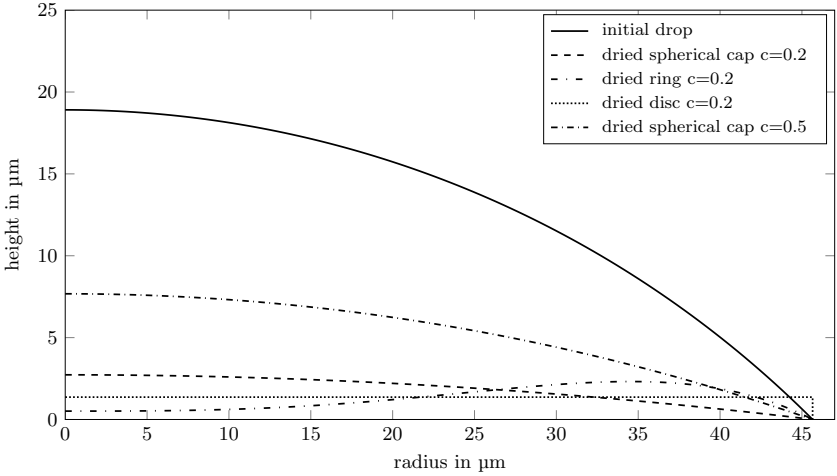

Figure 4.1: Used droplet shapes for the simulation. The contact area of the droplet was determined from the initial drop and subsequent drying of the droplet on the surface was simulated using the constant contact area mode (Alsan Meric and Erbil 1998).

The ring shape given by Karlsson et al. (2011) was approximated using a polynomial (eqn. 4.3), which was scaled to the dimensions needed.

$$h(x) = -0.3x^5 + 3x^3 + 5 \tag{4.3}$$

The droplets are dried instantly after deposition, which resembles a case of fast drying in relation to the spray rate, i.e. droplet deposition frequency. So

no smoothing of the surface occurs due to droplet coalescence. The shapes from the initial drop and the profiles after drying are shown in figure 4.1 (solid mass fraction was 20 % w/w which corresponds to a volume fraction of 13.66 % v/v).

4.2.2 Description of the model

The underlying prerequisite for most Monte-Carlo approaches regarding coating layers is the assumption of uniform distributed droplets on the surface. In most cases the droplets would be small compared to the primary particles, so the probability of any particular spot on the surface to be hit by a droplet is very small, but due to the large number of atomised droplets there is a good chance that this eventually happens. This sort of problem is typically described by the Poisson distribution with the probability density function

$$Po(m) = \frac{\lambda^m}{m!} e^{-\lambda}, m \in \mathbb{N} \tag{4.4}$$

and intensity parameter λ. It describes the probability for a specific event to happen m-times. For the description of coating layers, the methods for describing Poisson point fields seem appropriate. In the case of dots placed on a surface, the maximum-likelihood estimator for λ is the total number of dots n divided by the surface Area A_s (Stoyan et al. 1995). In case of droplets, however, the spatial extent of the drops has to be accounted for, so

$$\hat{\lambda} = \frac{nA_\mathrm{c}}{A_\mathrm{s}} \tag{4.5}$$

with A_c being the contact area of the droplet, which can be calculated according to the spherical cap geometry.

$$A_\mathrm{c} = \pi r_\mathrm{c}^2 \tag{4.6}$$

Note, that $\hat{\lambda}$ is equal to the dimensionless particle coating number Φ_p introduced by Kariuki et al. (2013), who derived this parameter using the Binomial distribution, with

$$p = \frac{A_\mathrm{c}}{A_\mathrm{s}} \tag{4.7}$$

and

$$\Phi_p = np \ . \tag{4.8}$$

This describes the probability of any part of a surface being hit by some part of a droplet. The resulting thickness at this particular spot depends on the number of times m this spot got hit and the thickness s each event adds. In the case of a disc profile with uniform height (see section above) the Poisson distribution with $\hat{\lambda}$ would just be scaled on the x-axis by the thickness of the disc, which is the case described by Kleinbach and Riede (1995). When we want to expand this description to droplets with a continuous height profile, we can consider the height profile as a probability density function sp.

sp describes the probability of a certain height in a droplet shape. Using this we can calculate the expected thickness distribution of a spot that receives m droplets by the convolution of sp m-times with itself. For example, the thickness at a spot which was hit twice is distributed with $sp * sp$ with the asterisk denoting the convolution operator. If a spot was hit three times, the thickness would be $sp * sp * sp$ distributed, and so on. This concept can be generalized to any given droplet shape. Two example probability density functions (pdf) of dried deposit profiles from a spherical cap and the simulated ring shape are shown in figure 4.2. The pdf of the spherical cap profile is very flat and can be almost approximated by an uniform distribution. This is caused by the high shrinkage compared to the initial drop (see fig. 4.1) which makes the final deposit profile very flat. The pdf of the ring shape is not a continuous line, which results from discretisation error.

Bringing it all together, the thickness distribution of the simulation case described in the previous section can be calculated using the statistical model

$$P(s) = Po(0) + \sum_{m=1}^{\infty} (sp)_m Po(m) \tag{4.9}$$

with $(sp)_m$ denoting the convolution of sp with itself m-times, with $(sp)_1 = sp$. It should be noted, that the Poisson distribution can be replaced by the binomial distribution in equation 4.9. In the relevant range of parameters both solutions are virtually identical, like in Kariuki et al. (2013), but it should be mentioned that the binomial distribution is the exact solution.

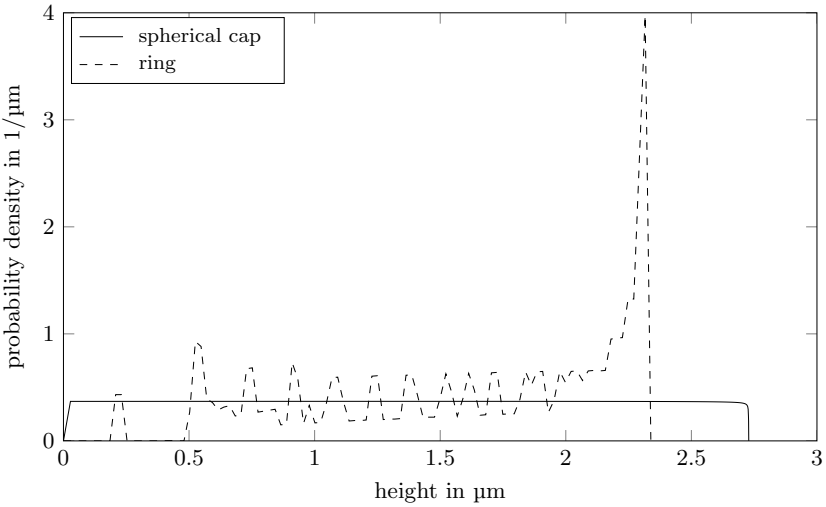

Figure 4.2: Probability density functions of the droplet height profile of a spherical cap and a ring shape (compare to fig. 4.1).

For comparison with experiments the parameters of the model have to be estimated from the experimental conditions. The droplet related parameters can be calculated when the volume mean diameter $\bar{d}_{3,0}$ of the drops is known, i.e. from laser diffraction measurement of the spray. The solid liquid contact angle θ for the used materials is also needed. The contact area A_c and can then be calculated from equations 4.2 and 4.6. The number of droplets n follows from the spray liquid mass m_lq and its density ρ_lq.

$$n = \frac{6 m_\mathrm{lq}}{\rho_\mathrm{lq} \bar{d}_{3,0}^3 \pi} \tag{4.10}$$

The surface area A_s can be estimated from the surface mean diameter $\bar{d}_{3,2}$ of the core particles and their mass and density, m_core and ρ_core respectively.

$$A_\mathrm{s} = \frac{6 m_\mathrm{core}}{\bar{d}_{3,2} \rho_\mathrm{core}} \tag{4.11}$$

4.3 Materials and methods

4.3.1 Measurement of pair correlation function and index of dispersion

1 kg of salt particles (>500 µm) were coated with 10 g of maltodextrin solution containing Ponceau 4R as a red dye. These partially coated particles were then imaged with a confocal laser scanning microscope (Nikon C1, Nikon GmbH, Germany). Ten single particles were masked out in the images and the center locations of the visible droplets were marked by hand. A Matlab script was written to determine the pair correlation function (eqn. 4.12) of the droplet locations on the particles according to Stoyan et al. (1995).

$$g(r) = \frac{\bar{n}(r)}{r^2 \pi \hat{\lambda}} \tag{4.12}$$

Where $\bar{n}$ is the mean number of drops around any given drop within the radius r and $\hat{\lambda} = \dfrac{n}{A_\mathrm{s}}$ is the estimated Poisson intensity.

The index of dispersion test is a χ^2-hypothesis test, which tests the null-hypothesis that a sample is part of a Poisson point-field. When a sample area is divided in k partial fields of equal size, the index of dispersion becomes

$$I = \frac{(k-1)s_v^2}{\bar{n}} \ , \tag{4.13}$$

with the sample variance of the point numbers within the partial areas s_v^2 and the mean point number $\bar{n}$. The Poisson hypothesis is rejected when

$$I > \chi^2_{k-1,1-\alpha} \text{ or } I < \chi^2_{k-1,\alpha} \ . \tag{4.14}$$

4.3.2 Coating operation and analysis

Table salt (Esco GmbH & Co. KG, Germany) was sieved to three fractions of <350 µm, 350 to 500 µm and >500 µm. 3 kg of each fraction were coated with a 20 % solution of maltodextrin with 21 DE and a solid density of 1580 kg m^{-3}, which was stained with 0.4 % of Ponceau 4R as a red colourant, in a WS-CT-L top-spray fluidised bed coater (Allgaier Process Technology GmbH, Germany)

with a two-fluid nozzle (Mod. 970, Düsen-Schlick GmbH, Germany) placed 0.37 m above the air distributor plate. Table 4.1 lists the settings for all three trials.

Table 4.1: Process conditions used for the coating trials. The parameters remained constant for all trials.

Parameter	Setting
Fluidising air flow rate	$200\,\mathrm{m^3\,h^{-1}}$
Air distributor plate	0.2 m diameter
Bed Temperature	55 °C
Spray rate	$30\,\mathrm{g\,min^{-1}}$
Atomizing air pressure	2 bar
Total sprayed liquid mass	3 kg
Process time	100 min

During the operation, five samples were taken over time to monitor the development of the coating. After the process, the filters were carefully removed from the pilot plant and the fines collected for particle size analysis. All samples were divided on a rotary sample splitter (PT100, Retsch GmbH, Germany) prior to analysis to ensure sample uniformity.

The particle size distributions of the samples were analysed using laser diffraction (Mastersizer 2000, Malvern Instruments Ltd, England). The efficiency η of the process in terms of coating mass was analysed photometrically by quantifying the red colourant in the coating layer. The amount of coating on the core w_c was defined as the mass ratio of coating mass and core mass.

$$w_\mathrm{c} = \frac{m_\mathrm{coating}}{m_\mathrm{core}} \tag{4.15}$$

The total sprayed coating mass in the experiment would result in a mass ratio of $w_\mathrm{c,th} = 0.2$ when all of it was successfully deposited on the cores. The efficiency of the process can then be defined as the ratio of the measured coating amount to the theoretical.

$$\eta = \frac{w_\mathrm{c}}{w_\mathrm{c,th}} \tag{4.16}$$

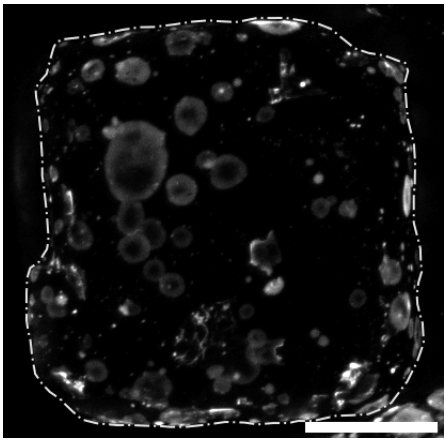

Figure 4.3: Confocal laser scanning micrograph of a partially coated salt particle. The scale bar is 100 µm and the dash-dotted line represents the approximate particle outline.

The coating thickness distribution was measured using the dissolution test method described in detail by van Kampen, Hitzmann, et al. (2015). In short, the dissolution curves of the uncoated cores and the coated samples are recorded by measuring the rise in conductivity. Using deconvolution and an axis transformation the thickness distribution of the sample can be obtained.

Furthermore, the droplet size distribution of the spray was analysed using laser diffraction (Spraytec, Malvern Instruments Ltd, England).

4.4 Results and discussion

In the first part, the model described in section 4.2.2 will be validated and compared with the simulation results. Furthermore, the parameters of the model will be discussed. The second part will then compare experimental results with the model and discuss the influence of premature drying of droplets on the resulting coating quality.

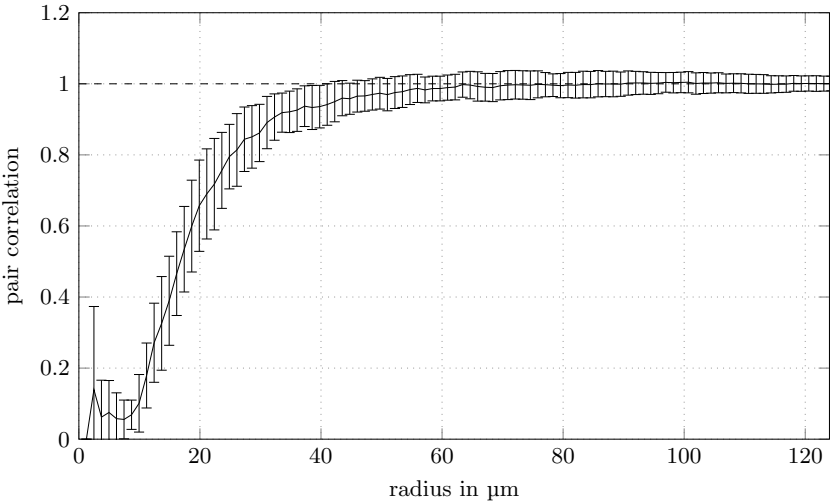

Figure 4.4: Pair correlation function of droplet positions on a primary particle surface. Mean of 10 particles with errorbars representing the standard deviation.

4.4.1 Model validation and evaluation

4.4.1.1 Test of Poisson-hypothesis

Figure 4.3 shows an example image of a partially coated salt particle obtained by confocal laser scanning microscopy. Figure 4.4 shows the mean pair correlation function of droplet locations on a salt particle surface after short coating in the fluidized bed.

According to Stoyan et al. (1995) the pair correlation function of a Poisson point-field is $g(r) = 1$. The graph in figure 4.4 approaches the value one fairly fast, which is a good indicator for the existence of a Poisson point-field. There seems to be a minimum distance of around 15 µm between two droplet centres and up to a distance of 30 µm there are less droplet centres found than expected. This can be explained with the spatial extent of the larger drops, which makes it hard to identify other smaller drops in that area.

The index of dispersion I was determined for ten pictures. The area weighed mean of I for a sub-area size of 50 by 50 µm was 52.55 with $k = 44.44$. This leads to a p-value of 0.113, so the Poisson-hypothesis is not rejected.

Both, the pair-correlation function and the index of dispersion indicate a Poisson point-field. This justifies the assumption of a Poisson-process for simulation purposes.

4.4.1.2 Comparison between simulation and model

100 simulation runs were performed for each of the three drop shapes described in section 4.2.1. 1000 drops with a diameter of 50 µm and a solid concentration of 20 % by mass were deposited on a 1024 by 1024 pixel sized area (resolution 1 px/µm). The contact angle was set to 45°, which lead to a contact radius of 45.65 µm. The intensity was equal for all simulation runs ($\lambda = 6.24$).

As expected, the simulation of the disc shape resulted in a discrete thickness distribution (fig. 4.5), since the monosized discs were of uniform height and the thickness just depends on how often one place gets hit by a droplet and not on the droplet shape itself. The other two simulations which used a cap and ring shape, respectively, resulted in continuous thickness distributions (figs. 4.6 and 4.7).

Interestingly, the shape of the thickness distributions depend mainly on the Poisson part of the model. The dry droplet profiles do change the appearance of the surface but have minor effect on the resulting thickness distribution.

Using the resulting intensity λ and the corresponding height profiles of the respective droplet shapes, the probability density function was calculated according to the model derived in section 4.2.2. Figures 4.6 and 4.7 show, that the model predicts the simulation data with low error. The error between the model and the simulation was calculated as the maximum norm $|| \; e \; ||_\infty$ of the error vector $e = pdf_\mathrm{m} - pdf_\mathrm{s}$. Figure 4.8 shows the development of the error dependant on the number of simulation runs. It can be seen that the error converges rapidly to an order of around 10^{-3}. Since the model does not cover the uniform height of the disc case, a comparison to that shape was not included.

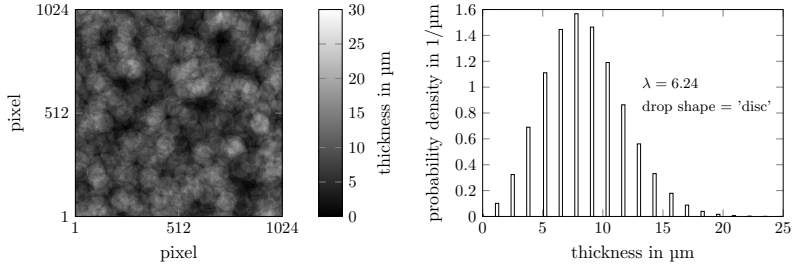

Figure 4.5: Surface plot of one simulation run using a disc shape (left) and the mean thickness distribution of 100 simulation runs (right).

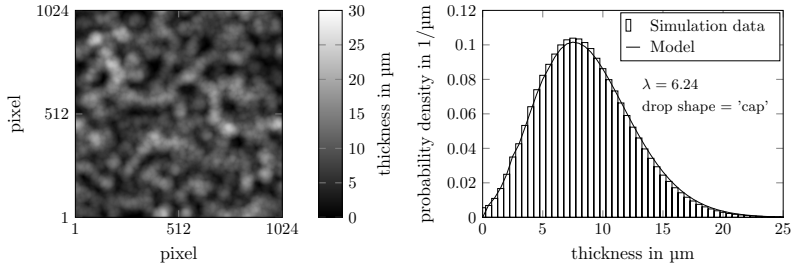

Figure 4.6: Surface plot of one simulation run using a cap shape (left) and the mean thickness distribution of 100 simulation runs together with the calculated distribution using the model (right).

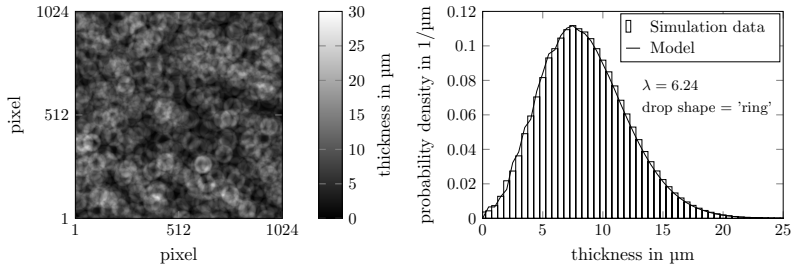

Figure 4.7: Surface plot of one simulation run using a ring shape (left) and the mean thickness distribution of 100 simulation runs together with the calculated distribution using the model (right).

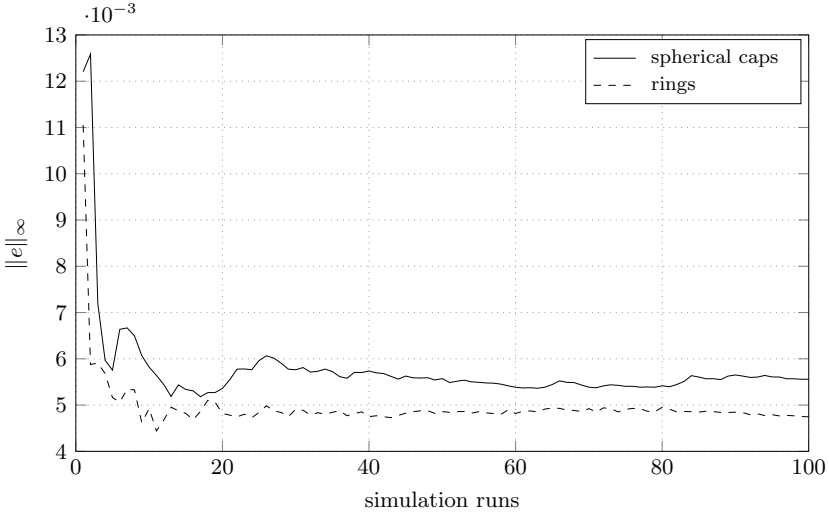

Figure 4.8: Error between the model and the mean probability density function of the simulation.

It can be concluded that the simulation approach for the instant drying case can be replaced by the statistical model. A smoothing of the surface due to coalescence of wet drops is not covered by the model at this stage but could potentially be included by a smoothing kernel depending on a coalescence probability.

4.4.1.3 Discussion on model parameters

The same simulation as discussed above was run again with log-normally distributed droplet sizes, with the mean being the same size as the fixed size from the previous simulations (results not shown). The resulting thickness distributions were virtually identical, with an equally good agreement to the described model. This leads to the conclusion, that the intensity λ can be estimated using the volume mean diameter $\bar{d}_{3,0}$ of the droplet size distribution for real world experiments. In addition to the droplet size, the wetting

characteristics of the coating solution, i.e. the contact angle between liquid and solid, does influence λ as well.

The other parameter needed for the estimation of λ is the number of droplets that are deposited on a single particle. This can be simply estimated using the mean droplet diameter and mean particle diameter for the materials used. Thus, λ can not only be influenced by varying the droplet size, but also by the spray rate and the total amount of liquid sprayed, i.e. the process time and amount of overspray.

The shape of the dried droplet seems to have little effect on the thickness distribution, so can be neglected for the estimation of the layer thickness. It does change the appearance of the layer though. This is influenced by the drying conditions and type of material, and thus can not be estimated by statistical means and is consequently left out of the further discussion.

4.4.1.4 Model parameter study

The model parameters contact angle and drop size were varied to study their influence on the homogeneity, i.e. CoV, of the coating. The particle size was constant at 400 µm and the mass of added coating material was kept constant at 20 % by adjusting the number of droplets used. Figure 4.9 shows the result as a surface plot. It can be seen, that the CoV decreases with low contact angles and small drop sizes, which was expected and is in accordance with Kleinbach and Riede (1995). Lowering the contact angle increases the contact area of the droplet and consequently increases the intensity. The same holds for decreasing the droplet diameter, as this increases the number of droplets and therefore the intensity as well.

In a second parameter study, the solid concentration of the droplets was varied in combination with the contact angle at a constant droplet diameter of 20 µm again keeping the total mass of coating material constant to a weight increase of 20 %. Figure 4.10 shows the results. The effect of the contact angle on the CoV remained the same as described in the previous paragraph. In addition, lowering the solid concentration also lowers the CoV, by increasing the number of drops. This effect, however, seems to be more pronounced, than the effect of increasing the drop number due to reducing the droplet diameter. This could be explained by an increased cap height at higher solid

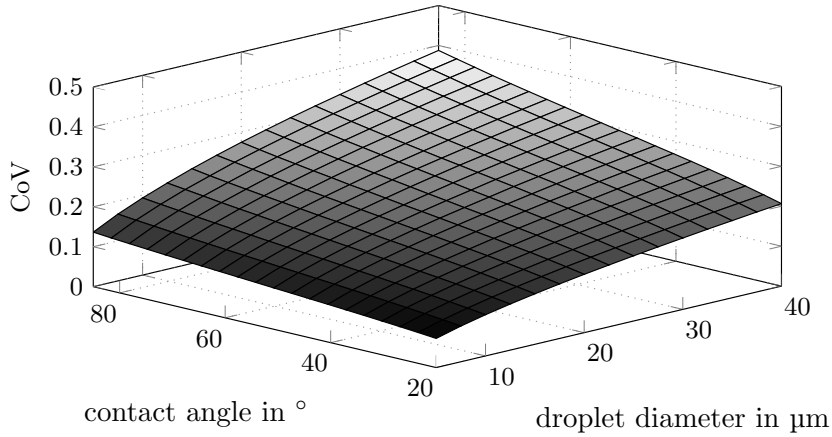

Figure 4.9: Influence of contact angle and droplet diameter on the CoV of the resulting thickness distribution. Calculation was done using the statistical model (eqn. 4.9). Concentration of the liquid coating solution was constant at 0.2 and a weight increase of 20 % was simulated.

concentrations (see fig. 4.1). The lower the solid concentration the flatter the dried drop shape becomes. Additionally the droplet shape itself introduces less variation in height at a decreased solid content, which results consequently in a lower CoV of the final coating layer.

Figure 4.11 shows the development of the surface coverage over the relative droplet number $\frac{n(t)}{n}$, equivalent to the process time t, with varying drop sizes. The volume of coating solution was kept constant and the drop numbers depend on the drop size, which could be varied by the atomizing conditions in a real experiment. The graph indicates that small droplets enable a faster coverage of the particle throughout the process. Larger drops would cover a larger area per drop, but since their deposition frequency is lower it takes a longer time to cover the whole area, see table 4.2 for the respective numbers and intensities.

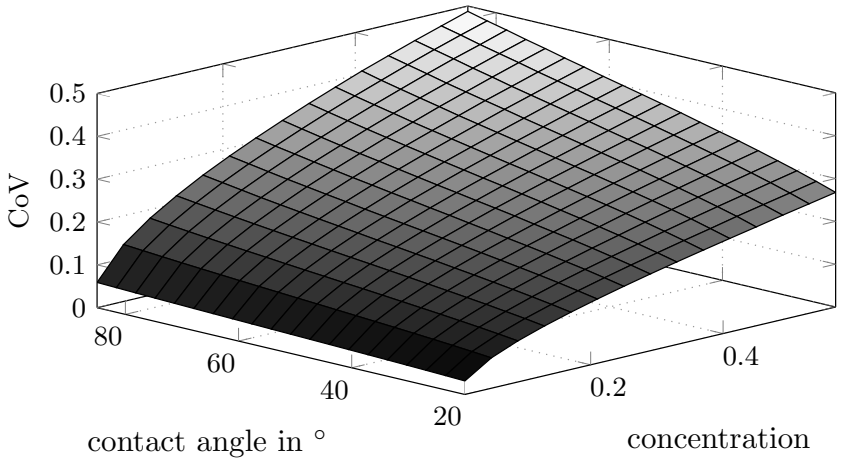

Figure 4.10: Influence of contact angle and concentration of the coating solution on the CoV of the resulting thickness distribution. Calculation was done using the statistical model (eqn. 4.9). The droplet diameter was kept constant at 20 µm and a weight increase of 20 % was simulated.

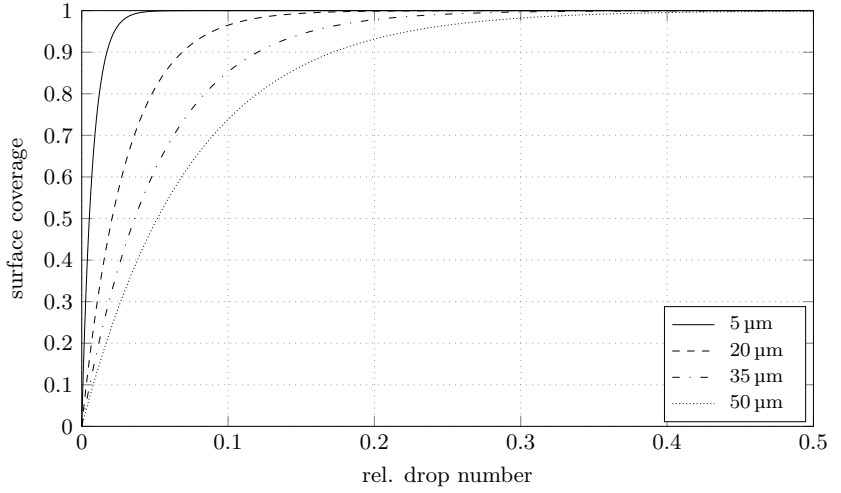

Figure 4.11: Degree of surface coverage over relative drop number.

Table 4.2: Intensity parameter $\hat{\lambda}$ and total number of drops n per particle used for the construction of fig. 4.11.

d in µm	n	$\hat{\lambda}$
5	$1.03 \cdot 10^6$	134.10
20	$1.61 \cdot 10^4$	33.53
35	$3.00 \cdot 10^3$	19.16
50	$1.03 \cdot 10^3$	13.41

4.4.1.5 Distribution parameter estimation

The uncoated surface area fraction can be modelled using the Poisson distribution. This implies that for $\lambda > 4.6$ an uncoated area fraction of $< 1\,\%$ can be expected (eqn. 4.18). We found in our previous work (van Kampen, Hitzmann, et al. 2015), that the measured thickness distribution can be well described by a Weibull distribution. When uncoated surface area is present, the cumulative distribution function can be well fitted using an off setted Weibull distribution. This is also true for the model discussed here. For $\lambda < 10$ the modelled distribution can be described by a Weibull distribution. For $\lambda > 10$ the distribution transforms relatively fast into a normal distribution. This can be explained by the central limit theorem, which states, that the sum of independent random variables tends towards a normal distribution curve.

For $\lambda < 4.6$ the cumulative distribution function

$$F(s) = F_{\text{unc}} + (1 - F_{\text{unc}}) \left(1 - e^{-\left(\frac{s}{u}\right)^k}\right) \tag{4.17}$$

with

$$F_{\text{unc}} = Po(0) = e^{-\lambda} \tag{4.18}$$

provides a good fit of the thickness distribution.

In other cases, the CoV can be used to estimate the distribution parameters. For $4.6 < \lambda < 10$ the layer thickness is Weibull distributed with the scale u

and shape k. The CoV is given in dependency of k by the following equation.

$$\mathrm{CoV} = \frac{\sigma}{\mu} = \sqrt{\frac{\Gamma\left(1+\frac{2}{k}\right)}{\Gamma^2\left(1+\frac{1}{k}\right)} - 1} \tag{4.19}$$

The inverse of this function can be fitted accurately using a power function:

$$k = 0.9804\mathrm{CoV}^{-1.105},\ R^2 = 1 \text{ for } 1 \leq k \leq 6 \tag{4.20}$$

Using a simulated design of experiments, the following empirical model for the CoV, with the parameters from the previous section, was calculated ($R^2 = 0.9958$) as a function of the volume mean diameter $\bar{d}_{3,0}$, the contact angle θ and the solid concentration c of the binder solution.

$$\begin{aligned}\mathrm{CoV}(\bar{d}_{3,0}, \theta, c) = &-1.172 \times 10^{-2} + 3.912 \times 10^{-3}\bar{d}_{3,0} \\ &+3.869 \times 10^{-4}\theta + 0.269c + 5.259 \times 10^{-5}\bar{d}_{3,0}\theta \\ &+0.012\,47 \times 10^{-2}\bar{d}_{3,0}c + 4.097 \times 10^{-3}\theta c \\ &-9.598 \times 10^{-5}\bar{d}_{3,0}^2 - 7.307 \times 10^{-6}\theta^2 - 0.402c^2\end{aligned}$$

Using this and the known mean thickness

$$\mu = \bar{s} = \frac{\bar{d}_{4,3}}{2}\left(\sqrt[3]{1 + \frac{V_{\mathrm{coating}}}{V_{\mathrm{core}}}} - 1\right) \tag{4.21}$$

with the volumes V_{core} and V_{coating} of the core and coating materials, respectively, the scale parameter u can also be calculated:

$$u = \frac{\mu}{\Gamma\left(1+\frac{1}{k}\right)} \tag{4.22}$$

For $\lambda > 10$ the parameters of the normal distribution can be estimated directly using the aforementioned mean thickness μ and $\sigma = \mathrm{CoV}\mu$.

4.4.2 Experimental results

Three fluid bed trials were conducted where the core particle size was varied from a $\bar{d}_{4,3}$ of 326 to 596 µm. The other process settings were kept constant

Table 4.3: Summary of experimental results and sets of parameters to model these results.

Experimental				Model Parameters					
Trial	$\bar{d}_{4,3}$ in µm	$\bar{d}_{3,2}$ in µm	η in %	Description	$\bar{d}_{3,0}$ in µm	n	λ	Φ in °	c_{solid}
1	326	307	79.4	Ideal	8.3	$8.21 \cdot 10^{12}$	44.95	56.4	0.2
				Overspray	14.5	$1.54 \cdot 10^{12}$	25.73	56.4	0.2
				pre-dried Overspray	10.2	$1.54 \cdot 10^{12}$	11.41	63.7	0.5
2	446	423	74.6	Ideal	8.3	$7.92 \cdot 10^{12}$	59.68	56.4	0.2
				Overspray	17.4	$8.51 \cdot 10^{11}$	28.38	56.4	0.2
				pre-dried Overspray	12.3	$8.51 \cdot 10^{11}$	12.59	63.7	0.5
3	596	562	68.3	Ideal	8.3	$7.36 \cdot 10^{12}$	73.71	56.4	0.2
				Overspray	20.2	$5.11 \cdot 10^{11}$	30.29	56.4	0.2
				pre-dried Overspray	14.2	$5.11 \cdot 10^{11}$	13.44	63.7	0.5

(see section 4.3.2), so a lower bed expansion was expected for larger particles. This should also lead to an increase in overspray. Table 4.3 summarises the results.

Increasing the particle diameter will decrease the total surface area of the core particles and consequently increases the process intensity. This could also be achieved by varying the atomisation conditions, but in practice this proved to be difficult, resulting even in total bed collapse at low atomization pressures. Dewettinck and Huyghebaert (1998) also pointed out, that the atomization pressure of the nozzle influences more than just the droplet size. So we decided to keep the spray conditions as well as the other process settings constant.

4.4.2.1 General observations

The expansion of the fluidized particle bed decreased with increasing particle size. This decreased the efficiency by 10 % (tab. 4.3) due to the increased distance to the nozzle. In addition, there was a high agglomeration rate in trial 1 (smallest particles), a moderate agglomeration rate in trial 2 and almost no agglomeration present in trial 3 which is also illustrated in figure 4.12 were the expected increase of the $\bar{d}_{4,3}$ of the particles is compared to the measured increase. It shows that the particles in trial 1 and 2 increase more in size than they would if layering was the main size enlargement process. Since this could also be explained by layer porosity (Rieck, Hoffmann, et al.

2015), scanning electron micrographs of the samples were made (fig. 4.13). They show the existence of agglomerates, that result in larger measured than calculated particles. The degree of agglomeration is strongest in trial 1 and less in trial 2. Trial 3 showed almost no agglomerates. Although porosity was generally omitted in this work, one has to keep in mind that this phenomenon is strongly dependant on coating material and droplet size and may be relevant in other coating applications.

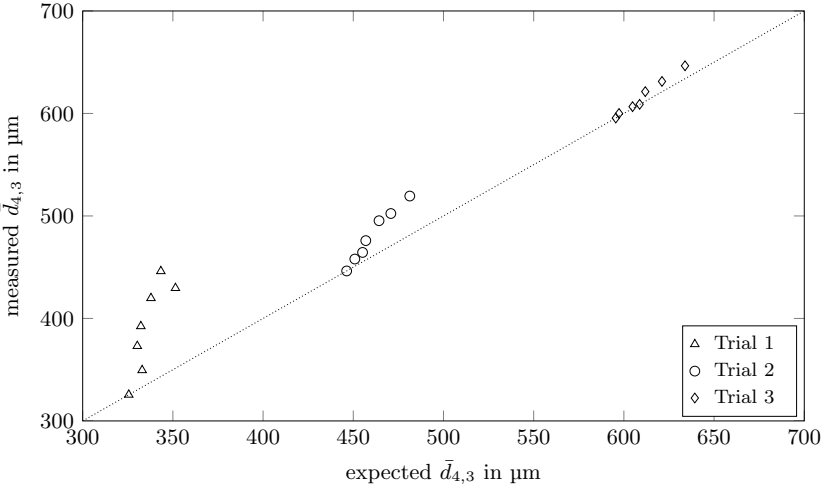

Figure 4.12: Measured and expected $\bar{d}_{4,3}$ for trials 1-3. Samples were taken over time. All points should lie on the straight line when no agglomeration took place.

4.4.2.2 Characterisation of overspray

From this experiment arises the question which droplets end up being overspray and which droplets actually reach a particles surface. From our point of view, there are two valid assumptions: First, a constant fraction of the droplets dries prematurely and independent of droplet size, and second, drying of droplets is size dependant. Under the first assumption the process

Figure 4.13: Scanning electron micrographs of the samples taken at the end of trial 1 (left), trial 2 (middle) and trial 3 (right).

intensity would only be influenced in a way, that the number of droplets n decreases ('Ideal' case in tab. 4.3). Under the second assumption, the volume mean diameter $\bar{d}_{3,0}$ of the droplets would change as well ('Overspray' case in tab. 4.3).

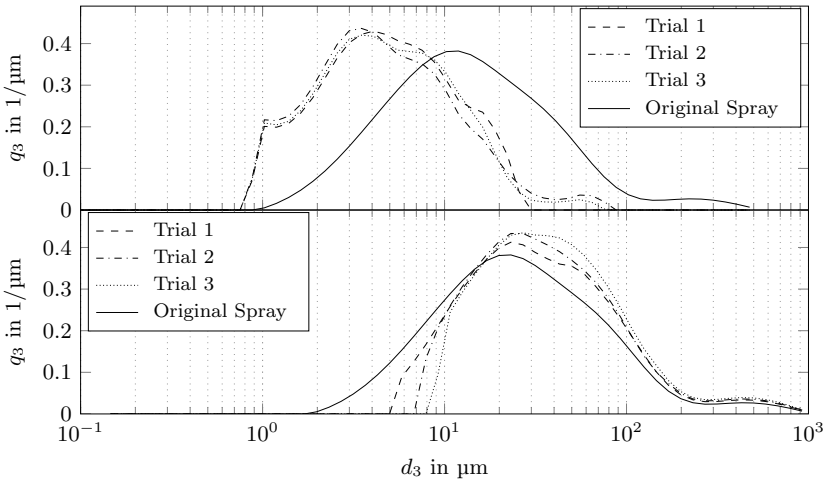

Figure 4.14: Top: Particle size distributions of fines collected from the filters in trial 1-3 and expected size distribution from spray dried particles from the original spray assuming compact particles. Bottom: Calculated droplet size distributions for trials 1-3 shown together with the original spray.

The top graph of figure 4.14 shows the expected particle size distribution of the dried spray, calculated from the volume fraction of solids in the spray assuming an ideal shrinking behaviour, and the distribution of overspray particles collected from the filters after each experiment. The bottom graph shows the distribution of original droplet sizes from the spray, and the calculated droplet size distribution (after Leschonski 1972) of the part of the spray that actually reaches and coats the particles. These graphs show that overspray is size dependant in a way that the smallest droplets are predominantly subjected to premature drying. Table 4.3 shows the calculated $\bar{d}_{3,0}$ of the droplets for each experiment ('Overspray' case). The values increase with decreasing efficiency, which would likely lead to a more inhomogeneous coating (see fig. 4.9).

4.4.2.3 Comparison with the model

The thickness distributions of the end products from the three trial runs were measured using the dissolution test method described in detail by van Kampen, Hitzmann, et al. (2015). The figures 4.15, 4.16 and 4.17 show the measured distributions together with calculated distributions using the three cases from table 4.3. The model parameters were estimated according to the description given in section 4.2.2. The change of the volume mean diameter of the droples due to overspray was used to calculate new parameter sets for the three cases of table 4.3. No parameter was obtained by fitting in this comparison. It should be noted, that by calculating the total number of droplets sprayed and the total surface area of the whole batch, the thickness distribution calculated will be a mean thickness distribution which neglects inter-particle coating variability as mentioned in the introduction.

The 'Ideal' case describes the size independent droplet evaporation case. This case results in very narrow thickness distributions, which in no case matches the measured curves. The 'Overspray' case takes the size dependent droplet evaporation into account and results in broader thickness distributions, but is still too narrow to match the measured curves. This leads to the conclusion, that correcting for the droplet size due to overspray alone is not sufficient to describe the measured data.

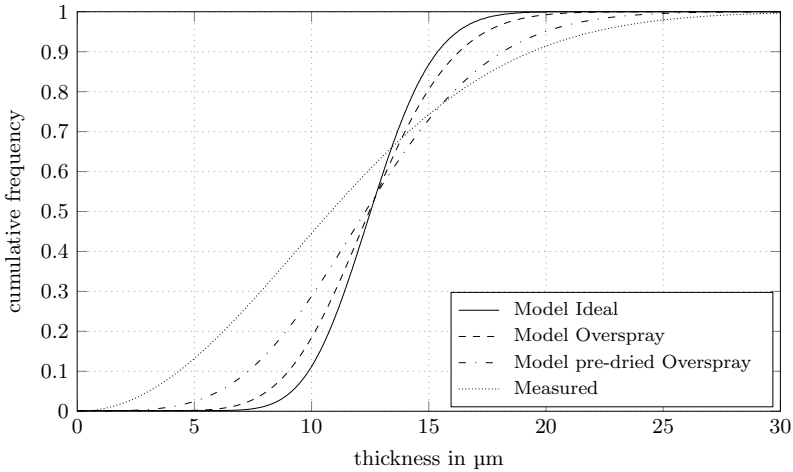

Figure 4.15: Comparison between the measured thickness distributions from trial 1 and calculated distributions from the statistical model (eqn. 4.9), with different choice of parameters (see tab. 4.3).

One reason could be that the wetting properties of the coating solution differ from the measured static contact angle we used as a parameter. Setting the contact angle as a free parameter, however, lead to unrealistically high apparent contact angles (data not shown). Since a higher apparent contact angle does not seem to explain the data, we decided to take a look at the droplet state right before deposition on the particle. We showed earlier, that a substantial amount of droplets dry prematurely so it seems reasonable to assume that the other drops are also partially dried before deposition, which has also evidence in the literature (i.e. Dernedde et al. 2011). The droplet state before deposition on a particle was successfully modelled by Dernedde et al. (2011), however, for the purpose of this article we made the reasonable assumption of a solid fraction of 0.5 in order to see whether the result agrees better with the measured distribution ('pre-dried Overspray' case in tab. 4.3). As can be seen in figures 4.15, 4.16 and 4.17, the calculated curves are now in much better agreement with the measured ones, which leads to the conclusion,

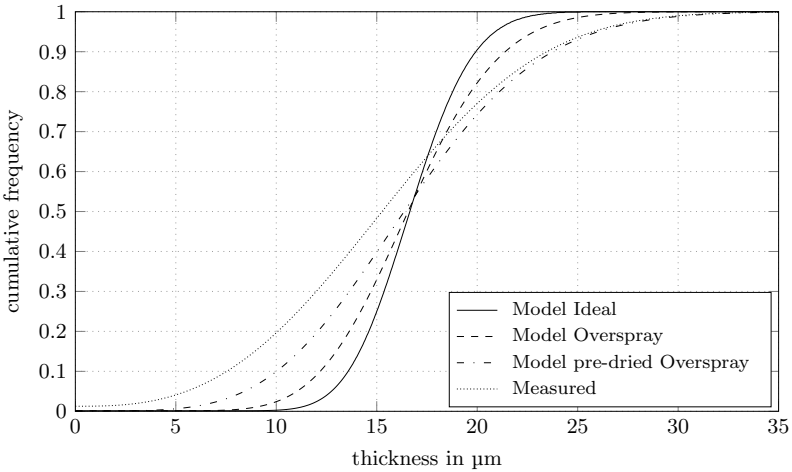

Figure 4.16: Comparison between the measured thickness distributions from trial 2 and calculated distributions from the statistical model (eqn. 4.9), with different choice of parameters (see tab. 4.3).

that a certain amount pre-drying of the droplets does influence the coating quality significantly.

The larger deviation of trial 1 and 2 from the model and the much broader size distribution compared to trial 3 can be explained by the agglomeration that took place in those experiments. The particles did agglomerate right from the beginning and thus are only connected by a very thin layer of coating material. During the dissolution test, the agglomerates disintegrated, exposing very thin layers of coating and/or uncoated surface areas. This results on the one hand in a larger intra-particle coating variability due to thinner layers on the inside of the agglomerate, but also in a larger inter-particle coating variability since the particles on the inside of an agglomerate would also receive less coating material. The dissolution test measures a mean coating layer thickness distribution, which results from both, the inter- and intra-particle coating variability, which explains the wider thickness distributions in comparison to the simulation. This effect of agglomeration on the layer thickness

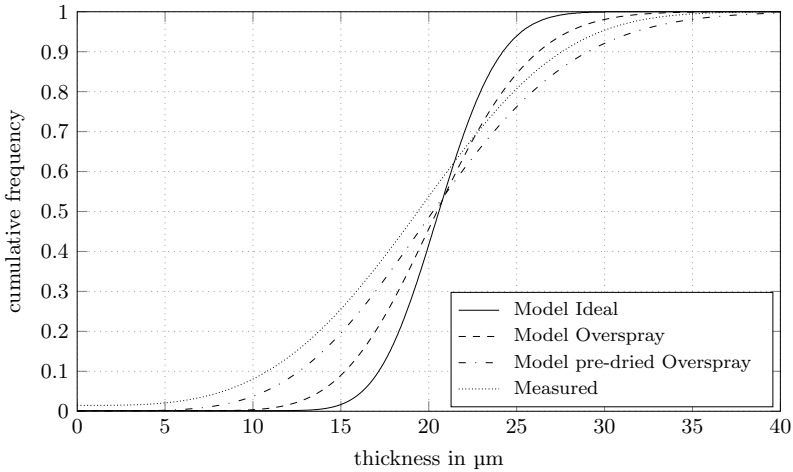

Figure 4.17: Comparison between the measured thickness distributions from trial 3 and calculated distributions from the statistical model (eqn. 4.9), with different choice of parameters (see tab. 4.3).

variability can also be seen as a non ideal mixing case, where some parts of the core particles were only exposed to the spray for a very short time. Thus, a large inter-particle coating variability could potentially also explain the wider thickness distribution measured in trial 3.

Figure 4.18 shows the development of the surface coverage over the process time for the third trial in comparison with the model using the same sets of parameters as before. The graph shows clearly that the 'Ideal' and 'Overspray' sets of parameters do not describe the measured values, but including a certain amount of pre-drying to the parameter estimation results in a better agreement with the experiment. Since the surface coverage is only dependant on λ (Kariuki et al. 2013), we can conclude that the considerations made to estimate λ are valid. This strengthens the hypothesis that a reduced number of droplets due to overspray in combination with a significant pre-drying rate explains the wider than expected thickness distribution in trial 3. However, more work is necessary to quantify the contribution of inter-particle coating

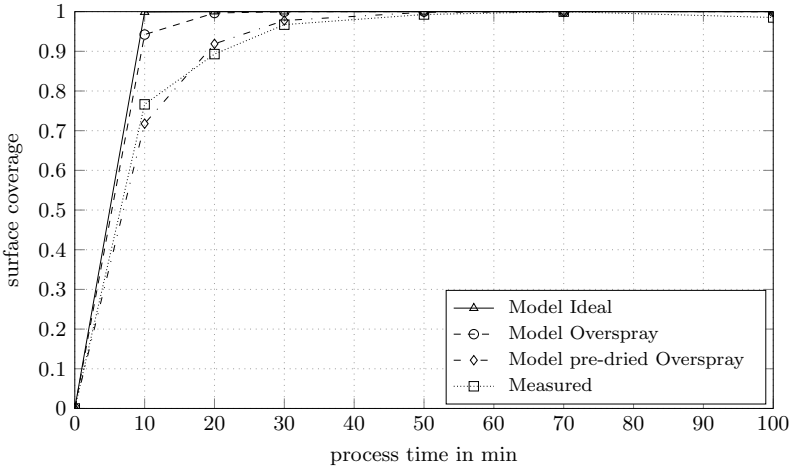

Figure 4.18: Degree of surface coverage compared between the measured values from trial 3 and calculated values from the statistical model (eqn. 4.9), with different choice of parameters (see tab. 4.3).

variability on the mean thickness distribution. The surface coverage graphs of trials 1 and 2 were not included here because the model does not hold when agglomeration is present as discussed above.

4.5 Conclusion

Using confocal laser scanning micrographs of partially coated salt particles the distribution of droplet centers on the surface was investigated. It was shown, that the droplet centers are uniformly distributed on the surface, indicating a Poisson point field.

Based on this information, a model describing the layer thickness distribution was developed comprising an alternative derivation of the particle coating number introduced by Kariuki et al. (2013). The model was built upon the Bernoulli trial approach already used by other authors but also includes the droplet shape calculated by a spherical cap model. This allows for a direct in-

vestigation of the effects of contact angle, droplet size and solid concentration on the coating layer thickness distribution.

A parameter study revealed recommendations for the choice of operating parameters, which were consistent with findings from other authors (i.e. Abe et al. 1998; Joglekar et al. 2007; Kleinbach and Riede 1995; Hemati et al. 2003) and our own work (van Kampen and Kohlus 2017).

- small droplets result in more homogeneous coating layers
- diluted coating solutions are preferable
- a large number of droplets increases homogeneity
- improving the wetting properties also improves the quality of the coating

However, these recommendations are opposed by:

- higher drying rate of small droplets which reduces the process efficiency
- longer and more energy consuming processes with diluted coating solutions

It was further shown, that the coating layer thickness can be described by a Weibull distribution for $\lambda < 10$, which justifies the use of this distribution for the description of dissolution test results in our previous work (van Kampen, Hitzmann, et al. 2015), since the samples discussed there were likely in this range. For large values of λ the coating layer thickness is normal distributed.

Experiments with varying process efficiencies showed a good agreement with the model, when appropriate adjustments to the parameters were included, such as the increased $\bar{d}_{3,0}$ due to premature drying of small droplets and increased solid concentration of the remaining droplets. These effects were shown to have a negative effect on the homogeneity of the coating.

The model did not describe coating processes where excessive agglomeration took place. This was partly due to the dissolution test, which measured the coating layer thickness around the primary particles and not the thickness around the agglomerates. In cases of non ideal mixing, the same discrepancy is likely to be observed.

5 Conclusion and final remarks

Fluidised bed coating of particles is a common unit operation in various industries like the pharmaceutical and food industry. While the process has been around for several decades it is still not fully understood, especially in terms of coating quality and its relation to process parameters. This lack of understanding is caused partly by the complexity of the process and partly by the difficulties that arise upon quantifying coating quality. The latter usually comes down to measuring the coating thickness distribution, which provides measures for the mean coating thickness, the homogeneity and the completeness of the coating.

The measurement of coating thickness distributions on coated particles is a challenging task for two main reasons. One being the usually very small coating thickness compared to the core particle size, which makes direct measurement using particle size measurement techniques difficult. The only way to accurately measure the coating thickness is by using microscopic or tomographic techniques, for example confocal laser scanning microscopy and µCT, which provide detailed insights on the structure of the coating layer, but are limited to measuring only a small number of particles. This leads to the second reason, which is that a coating thickness distribution consists of the inter- and intra-particle coating variability. The former refers to the variation within the whole particle population, which is defined either by coating mass or average coating thickness, the latter refers to the variation within a single particle. Methods to assess coating thickness distributions will have the inter- or intra-particle or the mean coating thickness distribution as a result.

In the first part of this thesis, the problem of measuring the coating thickness distribution was assessed. A method based on the measurement of dissolution curves was developed and tested. The technique relies on the assumption, that coated particles will dissolve in an equal way as the uncoated

particles once the coating layer has dissolved after a certain lag time. Deconvolution can be applied to extract the distribution of the lag time. Assuming that the mean lag time corresponds to the mean coating thickness, which can be assessed quite easily by quantifying the coating mass, the lag time axis can be transformed into a thickness axis. This yields the mean coating thickness distribution of the sample. In the first publication (chapter 2), the method was shown to provide a reliable and efficient way to assess the coating thickness distribution. It was found, that the resulting distribution can be well described by a Weibull distribution. This led to the investigation of the stochastic process which is involved during the formation of coating layers in the third publication (chapter 4). The stochastic model derived there, which takes into account the random process of droplet deposition on the particle surface and the height variation of the dry deposit, showed also a Weibull distribution in the case of thin coatings.

In a design of experiments approach, the dissolution method was used to assess the coating quality and establish a response surface model for the relation of the process parameters of a fluidised bed coating operation and the measures of the coating quality (chapter 3). A repeated 2^4-factorial design was initially chosen and subsequently expanded to a central composite design, comprising a total of 43 trial runs. This large number of trial runs was chosen instead of a more efficient reduced design, like Box-Behnken for example, in order to have a larger data basis for testing the reliability of the dissolution method. Significant response surface models of the relation between the process parameters bed temperature, spray rate, concentration of coating solution and fluidising air flow rate and the coating efficiency, agglomeration rate and coating quality were obtained. Although there were trials with poor repeatability, this was rather attributed to the process being run on different days and times of the year. Changing climate conditions, mainly changes of the inlet air humidity, are known to have a significant effect on fluidised bed processes. Three repeated trials made on the same day were characterised with low deviations using the dissolution method, which supports this conclusion.

The response surface models were used to find process parameters which allowed to produce an optimal coating quality within a restricted time frame

of one hour. The parameters air flow rate, bed temperature, solution concentration and spray rate were optimised. Three trials using the optimal settings were conducted and the samples analysed. The results were close to the predicted mean values which demonstrates the effectiveness of the dissolution method for this kind of application. Assessing the coating quality by use of a microscope would have taken hours per sample. A three fold measurement of the dissolution curve of one sample takes about 15 min including cleaning in between measurements.

The effects of the process parameters on the coating quality were in general agreement with the literature and the stochastic model that was derived in the third publication (chapter 4). The homogeneity of the coating was negatively affected by a high concentration of the coating solution. Besides the poorer ability of the droplets to spread on the particles surface due to the higher viscosity, the stochastic model revealed another possible explanation: With a higher concentrated solution, less volume has to be sprayed to achieve the same weight increase. This in addition to larger droplets leads to a significantly lower number of droplets that are distributed randomly on the surface of the particles. This leads to a larger probability that some parts of the surface remain uncoated, which is supported by the results of the second publication (chapter 3). Additionally the higher concentrated droplets will not shrink as much as diluted ones thus introducing a larger variability in coating thickness per droplet which explains the more inhomogeneous coating layers observed at a high solution concentration.

The presence of overspray is usually regarded as an issue affecting the process efficiency only. While it is true, that overspray particles do not contribute to the layer growth and thus the material is lost to the process, this work showed, that there is also a quality reducing effect which has to be considered. It was shown that premature droplet evaporation is a droplet size dependant phenomenon, where the smallest drops are more likely to be evaporated before impact on a particle. This has the effect, that the coating relevant droplet size is shifted to larger values, which results in more uneven coatings and possibly partly uncoated particles. In addition, droplets that are not lost to overspray are in a pre-dried state upon impact on a particle. The increased solid content and viscosity further reduces the coating quality

as discussed before. A possible way to overcome this limitation is to use non constant spray conditions during the coating operation. The coating material could be sprayed in intervals of high spray rates and no spray. This alternating cycle could potentially reduce overspray due to the high humidity during the spray phase and at the same time avoid agglomeration due to the drying step in between.

The model presented in this work is limited to calculating the thickness distribution according to stochastic and geometrical considerations only. These are only valid in processes with a high drying rate, which allows droplets to dry on the surface before another droplet hits the same spot. The thermodynamics of the process are only considered in the parameter estimation step before calculating the actual thickness distribution. This was only done using a reasonable assumption within this work, which nonetheless led to a good agreement between calculated and measured distribution. In future work, it would be interesting to combine this model with a thermodynamic model of the process. The model calculates the intra-particle thickness distribution, but can be used to model the mean thickness distribution by using appropriate mean values for the droplet and particle size and the number of droplets. This could be coupled to a simulation of the inter-particle thickness distribution, were only the respective number of droplets per particle, and possibly their size distribution and state, are simulated. The model parameters could then be estimated on a per particle base, without actually simulating the coating layer on these particles, which can potentially save a lot of computational time that can be used to study other effects in the simulation.

Although the dissolution method and the statistical model were developed in a fluidised bed coating context, they are also applicable to other coating methods. The dissolution method has shown its potential for research as well as process development purposes, however, there is still room for improvement, especially regarding its use for other release type coatings. The model system investigated here used maltodextrin as a coating material which dissolves quite quickly during dissolution. Other types of materials may swell during dissolution or may not dissolve at all, which would result in a different release mechanism. It would be interesting to investigate the kind of information which can be obtained using the analysis method shown here. Other

possible improvements concern mainly the data analysis algorithm. While the method was shown to be very robust, some data sets still required manual selection of outliers. More appropriate filter methods and weighting of the data points should be able to improve on that.

Bibliography

Abe, E., N. Yamada, H. Hirosue, and H. Nakamura (1998). “Coating mass distributions of seed particles in a tumbling fluidized bed coater”. In: *Powder Technol.* 97, pp. 85–90.

Abràmoff, M.D., P.J. Magalhães, and S.J. Ram (2004). “Image processing with imageJ”. In: *Biophotonics Int.* 11.7, pp. 36–41.

Akkermans, J.H.M., M.F. Edwards, A.T.J. Groot, C.P.M. Montanus, R.W.J. Van Pomeren, and K.R. Yuregir (1998). “Production of detergent granulates”. Patent WO98/58046.

Alsan Meric, R. and H.Y. Erbil (1998). “Evaporation of sessile drops on solid surfaces: Pseudospherical cap geometry”. In: *Langmuir* 14.7, pp. 1915–1920.

Andersson, M., B. Holmquist, J. Lindquist, O. Nilsson, and K.-G. Wahlund (2000). “Analysis of film coating thickness and surface area of pharmaceutical pellets using fluorescence microscopy and image analysis”. In: *J. Pharm. Biomed. Anal.* 22, pp. 325–339.

Andersson, M., S. Folestad, J. Gottfries, M.O. Johansson, M. Josefson, and K.-G. Wahlund (2000). “Quantitative analysis of film coating in a fluidized bed process by in-line NIR spectrometry and multivariate batch calibration”. In: *Anal. Chem.* 72, pp. 2099–2108.

Andersson, M., M. Josefson, F.W. Langkilde, and K.-G. Wahlund (1999). “Monitoring of a film coating process for tablets using near infrared reflectance spectrometry”. In: *J. Pharm. Biomed. Anal.* 20, pp. 27–37.

Atarés, L., F. Depypere, J.G. Pieters, and K. Dewettinck (2012). “Coating quality as affected by core particle segregation in fluidized bed processing”. In: *J. Food Eng.* 113, pp. 415–421.

Bauer-Brandl, A. and W.A. Ritschel (2012). *Die Tablette: Handbuch der Entwicklung, Herstellung und Qualitätssicherung*. 3rd ed. Editio Cantor Verlag für Medizin und Naturwissenschaften GmbH, Aulendorf. ISBN: 978-3-87193-407-0.

Boerefijn, R. and M.J. Hounslow (2005). "Studies of fluid bed granulation in an industrial R& D context". In: *Chem. Eng. Sci.* 60, pp. 3879–3890.

Bück, A., R. Dürr, M. Schmidt, and E. Tsotsas (2016). "Model predictive control of continuous layering granulation in fluidised beds with internal product classification". In: *J. Process Control* 45, pp. 65–75.

Capece, M. and R. Dave (2011). "Application of fluidized bed film coating for membrane encapsulation of catalysts". In: *Powder Technol.* 211, pp. 199–206.

Deegan, R.D., O. Bakajin, T.F. Dupont, G. Huber, S.R. Nagel, and T.A. Witten (1997). "Capillary flow as the cause of ring stains from dried liquid drops". In: *Nature* 389.6653, pp. 827–829.

Depypere, F., P. Van Oostveldt, J.G. Pieters, and K. Dewettinck (2009). "Quantification of microparticle coating quality by confocal laser scanning microscopy (CLSM)". In: *Eur. J. Pharm. Biopharm.* 73.1, pp. 179–186.

Dernedde, M., M. Peglow, and E. Tsotsas (2011). "Stochastic modeling of fluidized bed granulation: Influence of droplet pre-drying". In: *Chem. Eng. Technol.* 34.7, pp. 1177–1184.

Dewettinck, K. and A. Huyghebaert (1998). "Top-spray fluidized bed coating: Effect of process variables on coating efficiency". In: *LWT Food Sci. Technol.* 31.6, pp. 568–575.

Dewettinck, K., L. Deroo, W. Messens, and A. Huyghebaert (1998). "Agglomeration tendency during top-spray fluidized bed coating with gums". In: *LWT Food Sci. Technol.* 31.6, pp. 576–584.

Dewettinck, K. and A. Huyghebaert (1999). "Fluidized bed coating in the food industry". In: *Trends Food Sci. Technol.* 10, pp. 163–168.

Dewettinck, K., W. Messens, L. Deroo, and A. Huyghebaert (1999). "Agglomeration tendency during top-spray fluidized bed coating with gelatin and starch hydrolysate". In: *LWT Food Sci. Technol.* 32.2, pp. 102–106.

DIN EN ISO 9000:2015-11. *Quality management systems – Fundamentals and vocabulary.*

Geldart, D. (1973). "Types of gas fluidization". In: *Powder Technol.* 7, pp. 285–292.

Gibbs, B.F., S. Kermasha, I. Alli, and C.N. Mulligan (1999). "Encapsulation in the food industry: A review". In: *Int. J. Food Sci. Nutr.* 50, pp. 213–224.

Guignon, B., A. Duquenoy, and E.D. Dumoulin (2002). "Fluid bed encapsulation of particles: Principles and practice". In: *Dry. Technol.* 20.2, pp. 419–447.

Haverkamp, R.G. and B.J. Welch (1998). "Modelling the dissolution of alumina powder in cryolite". In: *Chem. Eng. Process.* 37, pp. 177–187.

Hede, P.D., P. Bach, and A.D. Jensen (2007). "Small-scale top-spray fluidised bed coating: Granule impact strength, agglomeration tendency and coating layer morphology". In: *Powder Technol.* 176, pp. 156–167.

Hede, P.D., P. Bach, and A.D. Jensen (2008). "Validation of the flux number as scaling parameter for top-spray fluidised bed systems". In: *Chem. Eng. Sci.* 63, pp. 815–828.

Hemati, M., R. Cherif, K. Saleh, and V. Pont (2003). "Fluidized bed coating and granulation: influence of process-related variables and physicochemical properties on the growth kinetics". In: *Powder Technol.* 130, pp. 18–34.

Joglekar, A., N. Joshi, Y. Song, and J. Ergun (2007). "Mathematical model to predict coat weight variability in a pan coating process". In: *Pharm. Dev. Technol.* 12, pp. 297–306.

Karlsson, S., A. Rasmuson, I.N. Björn, and S. Schantz (2011). "Characterization and mathematical modelling of single fluidised particle coating". In: *Powder Technol.* 207, pp. 245–256.

Kariuki, W.I.J., B. Freireich, R.M. Smith, M. Rhodes, and K.P. Hapgood (2013). "Distribution nucleation: Quantifying liquid distribution on the particle surface using the dimensionless particle coating number". In: *Chem. Eng. Sci.* 92, pp. 134–145.

Kirshner, H., F. Aguet, D. Sage, and M. Unser (2013). "3-D PSF Fitting for fluorescence microscopy: Implementation and localization application". In: *J. Microsc.* 249.1, pp. 13–25.

Kirsch, J.D. and J.K. Drennen (1996). "Near-infrared spectroscopic monitoring of the film coating process". In: *Pharm. Res.* 13.2, pp. 234–237.

Kleinbach, E. and Th. Riede (1995). "Coating of solids". In: *Chem. Eng. Process.* 34, pp. 329–337.

Knezevic, Z., D. Gosak, M. Hraste, and I. Jalsenjako (1998). "Fluid-bed microencapsulation of ascorbic acid". In: *J. Microencapsul.* 15.2, pp. 237–252.

Laksmana, F.L., L.J. Van Vliet, P.J.A. Hartman Kok, H. Vromans, H.W. Frijlink, and K. Van Der Voort Maarschalk (2009). "Quantitative image analysis for evaluating the coating thickness and pore distribution in coated small particles". In: *Pharm. Res.* 26.4, pp. 965–976.

Lawson, C.L. and R.J. Hanson (1974). *Solving Least Squares Problems.* Prentice-Hall.

Leschonski, K. (1972). "Characteristics of classification processes". In: *Ullmanns Encyklopädie der technischen Chemie.* Verlag Chemie, Weinheim/Bergstr.

Link, K.C. and E.-U. Schlünder (1997). "Fluidized bed spray granulation Investigation of the coating process on a single sphere". In: *Chem. Eng. Process.* 36, pp. 443–457.

Maa, Y.-F., P.-A. Nguyen, and C.C. Hsu (1996). “Spray-coating of rhDNase on lactose: effect of system design, operational parameters and protein formulation”. In: *Int. J. Pharm.* 144, pp. 47–59.

Markl, D., G. Hannesschläger, S. Sacher, M. Leitner, and J.G. Khinast (2014). “Optical coherence tomography as a novel tool for in-line monitoring of a pharmaceutical film-coating process”. In: *Eur. J. Pharm. Sci.* 55, pp. 58–67.

Markl, D., M. Zettl, G. Hannesschläger, S. Sacher, M. Leitner, A. Buchsbaum, and J.G. Khinast (2015). “Calibration-free in-line monitoring of pellet coating processes via optical coherence tomography”. In: *Chem. Eng. Sci.* 125, pp. 200–208.

May, R.K., M.J. Evans, S. Zhong, I. Warr, L.F. Gladden, Y. Shen, and J.A. Zeitler (2011). “Terahertz in-line sensor for direct coating thickness measurement of individual tablets during film coating in real-time”. In: *J. Pharm. Sci.* 100, pp. 1535–1544.

Möltgen, C.-V., T. Herdling, and G. Reich (2013). “A novel multivariate approach using science-based calibration for direct coating thickness determination in real-time NIR process monitoring”. In: *Eur. J. Pharm. Biopharm.* 85, pp. 1056–1063.

Mörl, L., S. Heinrich, and M. Peglow (2007). “Fluidized bed spray granulation”. In: *Handbook of Powder Technology: Granulation*. Ed. by A.D. Salman, M.J. Hounslow, and J.P.K. Seville. Vol. 11. Elsevier Science B.V., pp. 21–188.

Nangrejo, M., Z. Ahmad, E. Stride, M. Edirisinghe, and P. Colombo (2008). “Preparation of polymeric and ceramic porous capsules by a novel electrohydrodynamic process”. In: *Pharm. Dev. and Technol.* 13.5, pp. 425–432.

Noyes, A.A. and W.R. Whitney (1897). “The rate of solution of solid substances in their own solutions”. In: *J. Am. Chem. Soc.* 19.12, pp. 930–934.

Palzer, S. (2009). "Influence of material properties on the agglomeration of water-soluble amorphous particles". In: *Powder Technol.* 189, pp. 318–326.

Peglow, M., S. Antonyuk, M. Jacob, S. Palzer, S. Heinrich, and E. Tsotsas (2011). "Particle formulation in spray fluidized beds". In: *Modern drying technology – product quality and formulation*. Ed. by E. Tsotsas and A.S. Mujumdar. Vol. 3. Wiley-VCH Verlag & Co. KGaA. ISBN: 978-3-527-31558-1.

Perfetti, G., E. Van de Casteele, B. Rieger, W.J. Wildeboer, and G.M.H. Meesters (2010). "X-ray micro tomography and image analysis as complementary methods for morphological characterization and coating thickness measurement of coated particles". In: *Adv. Powder Technol.* 21, pp. 663–675.

Pothakamury, U.R. and G.V. Barbosa-Cánovas (1995). "Fundamental aspects of controlled release in foods". In: *Trends Food Sci. Technol.* 6, pp. 397–406.

Prata, A.S., A. Maudhuit, L. Boillereaux, and D. Poncelet (2012). "Development of a control system to anticipate agglomeration in fluidised bed coating". In: *Powder Technol.* 224, pp. 168–174.

Rieck, C., T. Hoffmann, A. Bück, M. Peglow, and E. Tsotsas (2015). "Influence of drying conditions on layer porosity in fluidized bed spray granulation". In: *Powder Technol.* 272, pp. 120–131.

Rieck, C., A. Bück, and E. Tsotsas (2016). "Monte carlo modeling of fluidized bed coating and layering processes". In: *AlChE J.* 62.8, pp. 2670–2680.

Ronsse, F., J.G. Pieters, and K. Dewettinck (2008). "Modelling side-effect spray drying in top-spray fluidised bed coating processes". In: *J. Food Eng.* 86, pp. 529–541.

Saleh, K. and P. Guignon (2007). "Influence of wetting parameters on particle growth in fluidized-bed coating and agglomeration processes". In: *Part. Part. Syst. Char.* 24, pp. 136–143.

Si-Nang, L., P.F. Carlier, P. Delort, J. Gazzola, and D. Lafont (1973). "Determination of coating thickness of microcapsules and influence upon diffusion". In: *J. Pharm. Sci.* 62.3, pp. 452–455.

Smith, P.G. (2007). *Applications of fluidization to food processing*. Blackwell Science Ltd, UK. ISBN: 978-0-6320-6456-4.

Sondej, F., A. Bück, K. Koslowsky, P. Bachmann, M. Jacob, and E. Tsotsas (2015). "Investigation of coating layer morphology by micro-computed X-ray tomography". In: *Powder Technol.* 273, pp. 165–175.

Stoyan, D., W.S. Kendall, and J. Mecke (1995). *Stochastic Geometry and its Applications, Second Edition*. John Wiley & Sons Ltd., England. ISBN: 0 471 95099 8.

Teunou, E. and D. Poncelet (2002). "Batch and continuous fluid bed coating – Review and state of the art". In: *J. Food Eng.* 53, pp. 325–340.

Uhlemann, H. and L. Mörl (2000). *Wirbelschicht-Sprühgranulation*. Springer-Verlag Berlin Heidelberg. ISBN: 3-540-66985-x.

van Kampen, A., B. Hitzmann, and R. Kohlus (2015). "Assessment of coating quality by use of dissolution kinetics". In: *Powder Technol.* 286, pp. 325–331.

van Kampen, A. and R. Kohlus (2017). "Systematic process optimisation of fluid bed coating". In: *Powder Technol.* 305, pp. 426–432.

Watano, S. (1995). "Mechanism and control of granule growth in fluidized bed granulation". Dissertation. College of Engineering, University of Osaka Prefecture.

Werner, S.R.L., J.R. Jones, A.H.J. Paterson, R.H. Archer, and D.L. Pearce (2007). "Air-suspension particle coating in the food industrie: Part I - state of the art". In: *Powder Technol.* 171, pp. 25–33.

Wesdyk, R., Y.M. Joshi, N.B. Jain, K. Morris, and A. Newman (1990). "The effect of size and mass on the film thickness of beads coated in fluidized bed equipment". In: *Int. J. Pharm.* 65, pp. 69–76.

Wesdyk, R., Y.M. Joshi, J. De Vincentis, A.W. Newman, and N.B. Jain (1993). “Factors affecting differences in film thickness of beads coated in fluidized bed units”. In: *Int. J. Pharm.* 93, pp. 101–109.

Witt, W., T. Stübinger, U. Köhler, J. List, and J. Jordan (2012). “Partikelgrößenanalyse mit absoluter Genauigkeit”. In: *Chem. Ing. Tech.* 84.3, pp. 211–222.

Wurster, D.E. and J.A. Lindlof (1966). “Particle coating apparatus”. U.S. Patent 3,241,520.

Zhang, Z., D. Law, and G. Lian (2010). “Characterization methods of encapsulates”. In: *Encapsulation technologies for active food ingredients and food processing*. Ed. by N.J. Zuidam and V.A. Nedović. Springer New York. ISBN: 978-1-4419-1007-3.

Zuidam, N.J. and E. Shimoni (2010). “Overview of microencapsulates for use in food products or processes and methods to make them”. In: *Encapsulation technologies for active food ingredients and food processing*. Ed. by N.J. Zuidam and V.A. Nedović. Springer New York. ISBN: 978-1-4419-1007-3.

Appendix

1 The spherical cap model and the distribution of height

In the third publication (chapter 4) the distribution of the height of a droplet deposited on a solid surface was calculated in a discrete way. An analytical solution will be presented here together with a description of the spherical cap model.

Description of the spherical cap model

The spherical cap model is widely used to calculate the shape of a droplet deposited on a flat surface with the liquid-solid contact angle θ. The volume of the droplet V_{drop} can be calculated from its initial diameter d.

$$V_{\mathrm{drop}} = \frac{\pi}{6} d^3 \tag{1}$$

With this information the contact radius r_{c} of the droplet on the surface can be calculated.

$$r_{\mathrm{c}} = \left(\frac{3 V_{\mathrm{drop}} \sin^3 \theta}{\pi (2 - 3\cos\theta + \cos^3\theta)} \right)^{1/3} \tag{2}$$

Two additional parameters are needed to calculate the spherical cap geometry: The height h_0 of the drop in the center and the radius r_{s} of a bigger sphere from which the cap is constructed (see fig. 1).

$$h_0 = \left(\sqrt{\frac{9 V_{\mathrm{drop}}^2}{\pi^2} + r_{\mathrm{c}}^6} + \frac{3 V_{\mathrm{drop}}}{\pi} \right)^{1/3} - r_{\mathrm{c}}^2 \left(\sqrt{\frac{9 V_{\mathrm{drop}}^2}{\pi^2} + r_{\mathrm{c}}^6} + \frac{3 V_{\mathrm{drop}}}{\pi} \right)^{-1/3} \tag{3}$$

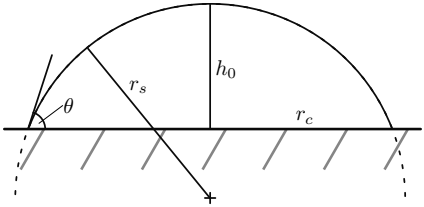

Figure 1: Schematic of the spherical cap geometry.

$$r_\mathrm{s} = \frac{V_\mathrm{drop}}{\pi h_0^2} + \frac{h_0}{3} \tag{4}$$

The shape of a dried solid deposit can be calculated under the assumption of a constant contact area drying mode, which was reported for $\theta < 90°$ (Alsan Meric and Erbil 1998), by inserting the volume of the dried deposit into equations 3 and 4.

Probability density function

The height of the cap h at a given distance r from the center can be calculated using the Pythagorean theorem:

$$h(r) = \sqrt{r_\mathrm{s}^2 - r^2} - (r_\mathrm{s} - h_0) \quad , 0 \leq r \leq r_\mathrm{c} \tag{5}$$

The inverse of this function is then given by

$$r(h) = \sqrt{r_\mathrm{s}^2 - (h + (r_\mathrm{s} - h_0))^2} \quad , 0 \leq h \leq h_0. \tag{6}$$

The area covered by a height up to h, with $0 \leq h \leq h_0$ is given by the total contact area $A_\mathrm{c} = \pi r_\mathrm{c}^2$ minus the inner circle area with radius $r(h)$.

$$A(h) = \pi r_\mathrm{c}^2 - \pi r(h)^2 = \pi r_\mathrm{c}^2 - \pi(r_\mathrm{s}^2 - (h + (r_\mathrm{s} - h_0))^2) \tag{7}$$

Dividing by A_c yields the probability of a height $h^* \leq h$.

$$P(h^* \leq h) = 1 - \frac{r_\mathrm{s}^2 - (h + (r_\mathrm{s} - h_0))^2}{r_\mathrm{c}^2} \tag{8}$$

The derivative of P with respect to h then yields the probability density function of the height in a spherical cap profile.

$$p(h) = \frac{dP}{dh} = \frac{2(r_\mathrm{s} - h_0)}{r_\mathrm{c}^2} + \frac{2}{r_\mathrm{c}^2} h \tag{9}$$

2 List of publications

Peer reviewed publications

- Sramek, M., R.M. Schweiggert, A. van Kampen, R. Carle and R. Kohlus (2015). "Preparation of High-Grade Powders from Tomato Paste Using a Vacuum Foam Drying Method". *Journal of Food Science* 80 (8), pp. E1755–E1762.

- van Kampen, A., B. Hitzmann and R. Kohlus (2015). "Assessment of coating quality by use of dissolution kinetics". *Powder Technology* 286, pp. 325–331.

- van Kampen, A. and R. Kohlus (2017). "Systematic process optimisation of fluid bed coating". *Powder Technology* 305, pp. 426–432.

- van Kampen, A. and R. Kohlus (2018). "Statistical modelling of coating layer thickness distributions: Influence of overspray on coating quality". *Powder Technology* 325, pp. 557–567.

Oral presentations

- van Kampen, A. and R. Kohlus (2014). "Coating von Lebensmittelpulvern: Qualitätsparameter und deren Quantifizierung". Presentation at the *ProcessNet Fachausschuss "Agglomerations und Schüttguttechnik"*, March 11, Magdeburg, Germany.

- van Kampen, A. and R. Kohlus (2014). "Coating of food powders: quality parameters and their quantification". Presentation at *The 7th World Congress on Particle Technology*, May 21, Beijing, China.

- van Kampen, A. and R. Kohlus (2016). "Systematic process optimization of fluid bed coating". Presentation at *PARTEC 2016*, April 19, Nuremberg, Germany.

Poster presentations

- A. van Kampen, J. Harnacke and R. Kohlus (2015). "Assessment of coating quality by use of dissolution kinetics". Poster presented at the *37th IFPRI Annual General Meeting*, June 21–25, Ithaca – New York, USA.
- A. van Kampen and R. Kohlus (2016). "Systematic Process Optimisation of Fluid Bed Coating". Poster presented at the *38th IFPRI Annual General Meeting*, June 12–16, Surrey, UK.